NASA Technical Memorandum 107154

Passive Magnetic Bearing With Ferrofluid Stabilization

Ralph Jansen
Ohio Aerospace Institute
Brook Park, Ohio

and

Eliseo DiRusso
Lewis Research Center
Cleveland, Ohio

February 1996

National Aeronautics and
Space Administration

PASSIVE MAGNETIC BEARING WITH FERROFLUID STABILIZATION

Abstract by

RALPH JANSEN

A new class of magnetic bearings is shown to exist analytically and is demonstrated experimentally. The class of magnetic bearings utilize a ferrofluid / solid magnet interaction to stabilize the axial degree of freedom of a permanent magnet radial bearing. Twenty six permanent magnet bearing designs and twenty two ferrofluid stabilizer designs are evaluated. Two types of radial bearing designs are tested to determine their force and stiffness utilizing two methods. The first method is based on the use of frequency measurements to determine stiffness by utilizing an analytical model. The second method consisted of loading the system and measuring displacement in order to measure stiffness. Two ferrofluid stabilizers are tested and force displacement curves are measured. Two experimental test fixtures are designed and constructed in order to conduct the stiffness testing. Polynomial models of the data are generated and used to design the bearing prototype. The prototype was constructed and tested and shown to be stable. Further testing shows the possibility of using this technology for vibration isolation. The project successfully demonstrated the viability of the passive magnetic bearing with ferrofluid stabilization both experimentally and analytically.

Acknowledgments

The author would like to thank Mr. Eliseo DiRusso, Dr. Gerald Brown, and Mr. Robert Fusaro of the Structural Dynamics Branch at NASA Lewis Research Center for their guidance and assistance throughout this project. Thanks also to Dr. William R. Jones, Dr. Stephen Pepper, and Dr. Mary Zeller of the Surface Science Branch for their support during undergraduate studies and Master's degree course work.

Thanks to Dr. Joseph M. Prahl of Case Western Reserve University for his support throughout my academic studies at Case Western Reserve University.

Thanks also to the numerous people at NASA Lewis who made this project a reality. Mr. Thomas Doeberling, Mr. Duane Dixon, and Mr. Thomas Toddy provided excellent technical support work. Ms. Irene Gorze, Mr. Richard Czentorycki, and Ms. Mary Grimes did excellent work providing the technical illustrations. Dr. Pilar Herrera-Fierro, Dr. Phillip Able, and Dr. Chris DellaCorte provided advise along the way.

Finally the author acknowledges the support of the National Aeronautics and Space Administration and the Ohio Aerospace Institute.

Table of Contents

List of Figures

List of Tables

Chapter 1: Introduction

1.1 Goal

The goal of this project is to develop a magnetic bearing system which is stable in all degrees of freedom, completely passive, and operational at room temperature. No previous magnetic bearing system is able to meet all of these requirements. A magnetic bearing is defined as a component consisting of a rotor and a stator in which the rotor motion is isolated from the stator through the use of a magnetic force. This magnetic force maintains the relative locations of the rotor and the stator and provides the load carrying capacity of the system.

Systems are typically referred to as stable, neutrally stable, or unstable. A stable system is one in which, when the system under goes a perturbation, there is a restoring force which returns it toward the equilibrium position. A neutrally stable system is one in which there is no resultant over some range of motion. This system does not return to equilibrium, it simply will come to rest at the new position. An unstable system is one in which, when a perturbation occurs, a force will develop which moves the system further away from the equilibrium position (Fig 1.1a). Previously all magnetic bearing systems had a least one unstable axis. The goal of this project is to build a system with no instabilities in any degree of freedom while the bearing is at rest or in motion.

A passive system is a system which does not use any control mechanism. Traditional magnetic bearings always utilize a control system in at least one axis. Typically control systems are implemented on all axes in order to increase the effective stiffness and load carrying capacity. Simple single axis control can be achieved using a mechanical system, however magnetic bearings typically utilize a electronic feedback control system. Implementation of a control system for a magnetic bearing requires the use of power and control hardware. The goal of this project is to make a system that is completely passive, thereby reducing power consumption, size, and weight while increasing reliability.

Operating temperature range is the temperature at which the system functions to specifications. Actively controlled magnetic bearing systems typically operate around room temperature. Previous attempts at passive magnetic bearings required the use of superconductive components which limited operation to temperatures below -77°C. This bearing was designed to operate at 25°C and to have an minimum operating range between 0°C and 50°C.

1.2 New Concept

A new type of magnetic bearing was developed using permanent magnets to support the rotor in four degrees of freedom (two radial and two angular) and a ferrofluid stabilizer to support the rotor in the fifth degree of freedom. A ferrofluid is

a fluid which contains chemically suspended iron oxide particles. This causes the fluid to have magnetic properties.

A typical permanent magnet system which is stable in four axes is shown in Figure (1.2a). Two magnetic disks are mounted on the rotor and two annular magnetic disks are mounted on the stator. The disks are located concentrically within the rings. The outer face of the disk and the inner face of the ring have the same magnetic polarity, resulting in a repulsive magnetic force which suspends the rotor. This type of system is stable in the radial direction and unstable axially.

The ferrofluid stabilizer is based on the interaction between a permanent magnet and a magnetic fluid. A magnet immersed in a large reservoir of magnetic fluid is shown in Figure (1.2b). The magnet will seek an equilibrium position with magnetic fluid equally distributed around it in the absence of external forces. If the magnet is displaced from equilibrium a restoring force will result. This type of system is stable in all axes, however the load capacity is minimal. The ferrofluid stabilizer will be constructed using a restricted cavity for the magnetic fluid and a optimized magnet geometry in order to increase the restoring force in one axis relative to the other two tranlational axes.

The strong axis of the stabilizer unit will then be physically coupled to the rotor of the permanent magnet system in order to stabilize the fifth (axial) degree of freedom. By combining these two systems, a single system which is stable in all five axes and based only on magnetic interactions will result.

1.3 Significance

This project was the first demonstration of a completely passive magnetic system which is stable in all degrees of freedom and can operate above cryogenic temperatures. All other magnetic bearing systems have incorporated cryogenic components, mechanical interactions, or electromagnetic control systems to stabilize the system. Cryogenic systems require that the system be maintained at a temperature below -77°C, necessitating a liquid nitrogen supply or other cryogenic cooler. Mechanically stabilized systems are prone to typical wear or fatigue failures that occur in any mechanical system. Electromagnetically controlled systems require a power source and a complex electronics package in order to maintain stability.

Since this system is completely passive none of the auxiliary hardware required by other systems is necessary. The system will not enter a failure condition due to problems such as power loss or electronic interference. The elimination of any sliding mechanical contact eliminates the friction, fracture, and wear failure modes. The system does not have mechanical noise characteristics.

This paper details the experimental and analytical work done to make this project successful. The background section covers Earnshaw's Theorem, magnetic bearing terminology and classification, and the details of magnetic solids and fluids. The concept selection of the design is covered. The next two sections cover the

design and testing of the radial bearing and ferrofluid stabilizer. The final sections cover the full prototype design and testing.

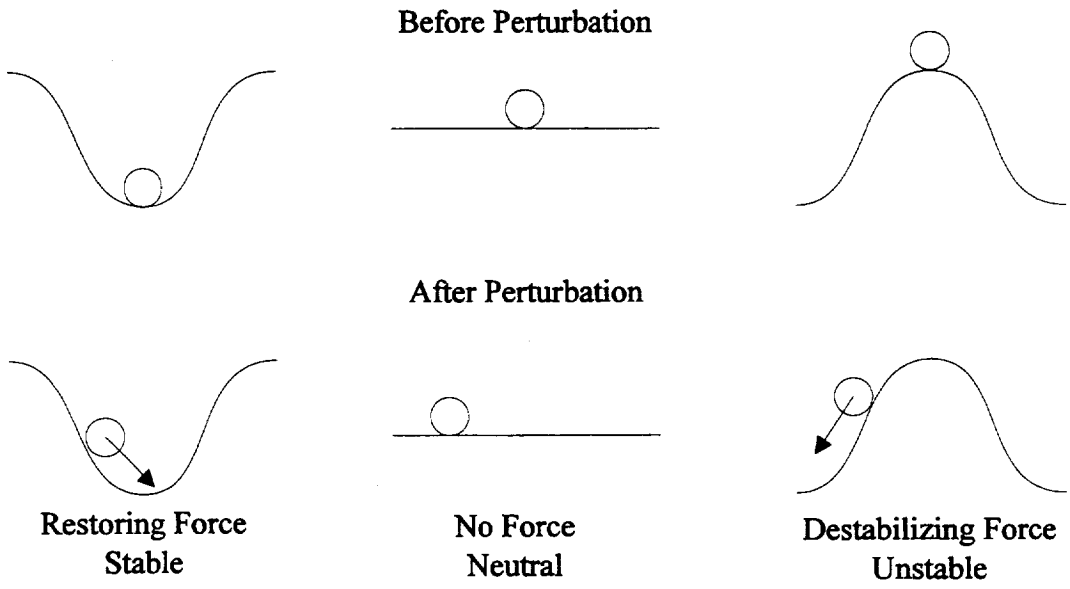

Figure 1.1a - Illustration of system stability

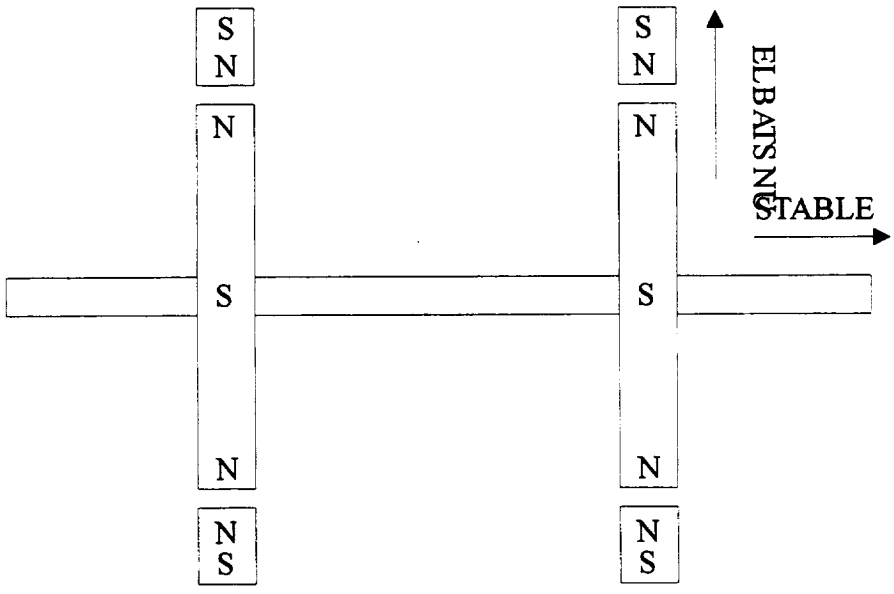

Figure 1.2a - Permanent magnet system which is stable in two axis

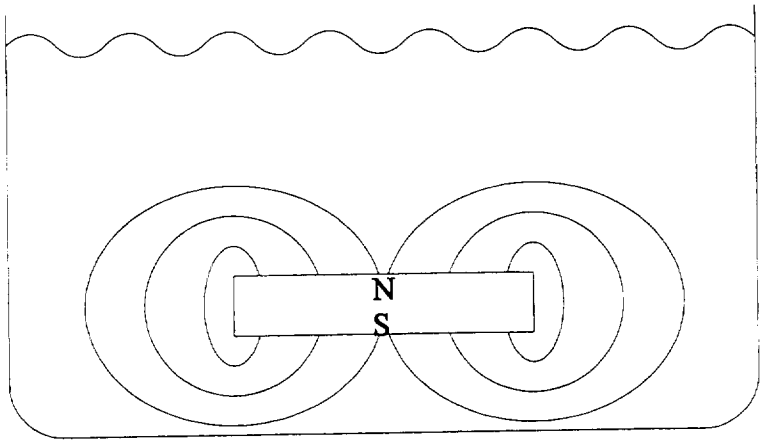

Figure 1.2b - Permanent magnet in magnetic fluid, stable in three axes

Chapter 2: Background

2.1 Earnshaw's Theorem

Earnshaw's Theorem (1842) states that a group of particles governed by inverse square law forces can not be in stable equilibrium. This theory clearly applies to charged particles and magnetic dipoles. The theorem can be extended to a solid magnet or fixed constant current circuits. Earnshaw's theorem is based on the fact that inverse square law forces follow the Laplace partial differential equation. The solution of this equation does not have any local maxima or minima, only saddle-type equilibrium points.

Five known magnetic cases exists where Earnshaw's Theorem does not apply; time varying fields, active feedback, diamagnetic systems, ferrofluids, and superconductors. Active feedback control is the most typical way to circumvent Earnshaw's Theorem in magnetic bearings. Superconductor based bearings are being explored, however they require cryogenic temperatures. Diamagnetic systems can only support extremely small loads, typically less than 1gr. Ferrofluids have not been used as a means of stabilizing a bearing.

2.2 Magnetic Bearing Terminology

Two major approaches have been used to calculate magnetic bearing forces (Schweitzer[1]), one with its basis in engineering and one based in quantum physics. The engineering, or macroscopic, approach circumvents atomic detail and assigns

magnetic materials a magnetization constant μ. Magnetic forces called reluctance forces are calculated from the change in field energy which is converted into mechanical energy based on the principle of virtual work. Magnetic forces arise between media with different relative permeability.

The physics based microscopic approach calculates forces based on a fundamental equation:

$$f = Q(E + v \times B)$$

The Lorentz force f is calculated from the charge Q in an electric field E and moving at a velocity v in a magnetic flux density of B. Typically the electrostatic E term is five orders of magnitude smaller than the magnetic term on a macroscopic scale and is neglected resulting in the equation:

$$f = i \times B$$

Resultant force is orthogonal to the flux lines and linearly dependent on the current.

2.3 Classification of Magnetic Bearings

A classification method for magnetic bearings has been proposed by H. Bleuler[2]. The classification is based on the method in which the forces are calculated, although the same fundamental principles apply to all types (Figure 2.3a). There are four subclassifications for both the reluctance and Lorentz group. Type 1 bearings are classical feedback control electromagnetic bearings. This type is by far the largest category and can be subclassified into many groups. The Type 2 bearing is based on

the use of LCR circuit which uses the magnetic bearing as the inductor. As the shaft is displaced the inductance of the electromagnet changes resulting in an increased AC current from the power source which moves the bearing back to center. This is typically referred to as a passive system although this is a misnomer since it utilizes the most primitive feedback control system. Type 3 bearings utilize permanent magnets, however are not stable in all three axis. A mechanical bearing must be introduced in the third axis. Type 4 bearings are based on the Meissner-effect and require the use of superconductors. Type 5 through Type 8 bearings are Lorentz-Force type bearings. Type 5 bearings are based on eddy current effects. A large relative velocity between the rotor and stator is required to generate a significant magnetic force. This type of bearing has been studied extensively for magnetic levitation trains. A type 6 bearing is a simple feedback system based on the interaction of the AC and induced current in the electromagnet. Type 7 bearings are similar to type 6 however an active feedback control system is used to control the interaction between the AC current in the stator windings and the induced current in the rotor. This interaction is similar to an induction motor, however the direction of the resultant force is different. Type 8 bearings utilize the same system as type 7 however the rotor is a permanent magnet.

2.4 Magnetic Solids

2.4.1 Types of magnetism

All solids exhibit magnetic characteristics, which are classified depending on the origin and order of the interaction. The most common magnetic classifications are diamagnetism, paramagnetism, ferromagnetism, ferrimagnetism, and antiferromagnetism. Diamagnetic materials only exhibit magnetic properties under an external applied field. Magnetization is extremely weak, is in the opposite direction of the applied field, and arises from atomic currents induced by the field in accordance with Lenz's law. All other types of magnetism arise from electron spin or orbital motion and are intrinsic to the atom and the structure of the molecular lattice. The intrinsic magnetic force resulting from atomic structure is referred to as the magnetic moment of the atom. Materials with an intrinsic magnetic moment are characterized by how the magnetic moments of groups of atoms interact. Figure 2.4.1a illustrates the ordering of the magnetic moments in the most common magnetic classifications (Chikazumi[3]). Atoms in paramagnetic materials only exhibit magnetism under an external field. Magnetism is in the direction of the field and results from preferential realignment of the magnetic moments of the atoms in the direction of the field. Ferromagnetism is the strongest spontaneous ordering of magnetic moments in which all magnetic moments are aligned without the influence of a external magnetic field. Antiferromagnetism results when every other pole aligns in opposite directions and the pole strengths are equal resulting in no net spontaneous magnetism despite the magnetic ordering. Ferrimagnetism has opposite pole alignment characteristic as antiferromagnetism however the pole strengths are not equal, resulting in a net

magnetism without the presence of an external field. The strength of the spontaneous magnetism in ferromagnetic and ferrimagnetic materials is a function of temperature. The maximum value of spontaneous magnetism is at absolute zero and it drops as temperature increases (Figure 2.4.1b). At the Curie point the spontaneous magnetism drops to zero and the material begins behaving like a paramagnetic material. Several more complex arrangements of magnetic moments exist in which the moments are not parallel, antiparallel, or coplanar however they can be treated as a sub case of the ferrimagnetic classification.

2.4.2 Scientific vs. Technical Magnetization.

The magnetic characteristics described in the previous section apply exactly to small regions of atoms in which the magnetic structure matches the above description. In macroscopic particles many small regions, referred to as unidomain regions, will exist each misoriented with respect to adjoining regions. Unidomain regions may correspond to grain size in some materials or single grains may have multiple unidomain regions. Domain sizes and orientations are determined during the manufacture of material, however they can be reoriented if a high external magnetic field is applied. The multidomain structure does not impact the macroscopic response of diamagnetic or paramagnetic materials. Diamagnetic materials do not have domains because no atoms have intrinsic magnetic moments. Paramagentic materials do not exhibit domains since there is not spontaneous magnetic ordering. Domain structure does have a significant impact on ferromagnetic and ferrimagnetic materials.

In these materials the random ordering of the unidomain regions result in zero net magnetization of a macroscopic material specimen. As an external field is applied the unidomain regions begin to reorient in the field direction resulting in a net magnetization. As the external field strength increases the magnetization will rise to a maximum level known as the saturation magnetization. This value is equal to the unidomain magnetic strength described in the previous section. An ideal magnetization curve is shown in Figure 2.4.2a.

2.4.3 Permanent magnets

To determine whether a material will be a good permanent magnet it is necessary to consider the complete magnetization curve (Figure 2.4.3a). This curve is generated by increasing the applied field from zero until the saturation magnetization is reached. The field is then brought through zero to the negative saturation level and then brought back to the positive saturation level. A hysteresis loop is generated, the area of which indicates the work required to completely reverse the direction of the magnetic field in the substance. The energy required is referred to as the hysteresis loss, while the crossing point of the curve on the H axis is the coercive force. Permanent magnet materials must have high a large coercive force and a high saturation magnetization. The field created by the magnet will work to demagnetize itself, therefore the magnet will operate in the second quadrant of the hysteresis loop without any external applied field. Because of this, permanent magnets are typically specified using the second quadrant properties (figure 2.4.3b). The strength of the

demagnetizing field is determined by the geometry of the magnet. For ellipsoids the demagnetization factor can be calculated, however typically it needs to be measured. Older iron based permanent magnets needed to be used with keeper pieces in order to reduce the demagnetization factor otherwise the magnetic atoms would become disordered. Modern permanent magnets have a large coercive force and do not reorder unless a strong external field is applied.

2.5 Magnetic Fluids

2.5.1 General Types

A fluid which exhibits magnetic properties is required to implement the magnetic levitation system. Three classes of fluids are candidates to meet this requirement. The first is a paramagnetic salt solution, however paramagnetic response is too weak and the mass fraction of salt molecules in solution is low. The second class consists of ferromagnetic material ground into particles on the order of 10μm diameter and mixed with a base fluid. These fluids exhibit a strong magnetic response however the mixture is not a stable colloidal suspension and the ferromagnetic particles quickly separate under the influence of a magnetic or gravitational field resulting in a distinct liquid and solid phase. The third category of fluid consists of ferromagnetic material with particle sizes on the order of 10nm coated with a stabilizer and mixed with a base fluid. With proper selection of the particle size, stabilizer, and base fluid a stable colloidal suspension results which will

not have liquid/solid phase separation under the influence of a gravitational or magnetic field. The overall response of such a fluid under a magnetic field can generally be treated as if the fluid had homogeneous magnetic properties. This third category of fluid, commonly known as ferrofluid, was chosen for this application.

2.5.2 Stability Condition of a Ferrofluid

In order for a magnetic fluid to remain a stable colloidal suspension under an external magnetic or gravitational field, the magnetic particles must not agglomerate. The simplest model of a ferrofluid is one in which a number of spherical unidomain magnetic particles are coated with a uniform layer of stabilizer and homogeneously distributed throughout the carrier liquid. Figure 2.5.2a shows a typical magnetic particle, solid diameter d_s, magnetic core diameter d_m, coating diameter d_h, with material magnetization I (Fertman[4]). The interaction between magnetic particles is dominated by three forces in this case, van der Walls, magnetic, and steric. Van der Walls forces arise from the induced electric dipole interaction between the particles, magnetic forces are a result of the magnetic moment of each particle, and steric forces are the repulsion caused by the interaction of the stabilizer coating. If the potential energy of the interaction remains below the thermal energy of the particles the mixture remains stable, otherwise the particles agglomerate. The maximum stable core size, optimum coating thickness, and resultant magnetization of the fluid can then be calculated (Fig 2.5.3b,c,d). Typical fluids use magnetite particles (I=500 kAm^{-1}) with a mean core diameter of 7nm and an oleic acid coating of 2nm.

2.5.3 Manufacture of a Ferrofluid

Three basic methods have been used to produce ferrofluids, grinding, condensation, and precipitation. The grinding method was employed to make the first magnetic fluids. Magnetite (Fe_3O_4) material was ground in a ball mill immersed in the stabilizer, oleic acid, and the base fluid, kerosene. This method can be easily implemented with many magnetic materials, stabilizers, and base fluids and results in no lost components during the process. The drawback of this system is that it has an extremely low yield, typically 200-300ml of fluid, the required long grinding time, and the magnetic saturation strength of the fluid is low (10 kA/m).

The second method is the condensation method in which the magnetic particles are formed by condensation of metal vapor. A three component system consisting of an evaporator, a reactor, and a condenser are employed in this method. A chemically bound metal, typically a metal carbonyl, is heated to its vaporization temperature. The metal vapors flow to the reaction chamber where the metal particles condense in the stabilizer / base fluid mixture, and gaseous reaction products are formed. The reaction products are removed to the condenser chamber. The reaction can also be conducted in the liquid phase using solutions of metal salts and a rotating electrode-cathode system to condense the metal particles which drift down into the stabilizer / base fluid. This method has only been employed in production of fluids with a metal particle base and requires a high ratio of stabilizer material to magnetic material to prevent agglomeration of the particles during the condensation process.

This method can be performed quickly however the limited types of fluids that can be manufactured, the high sensitivity of the product to the reaction conditions, and the low resulting magnetic strength (.5 kA/m) of the fluid have resulted in low usage.

Precipitation is the most widely used method. The original implementation of this method resulted in a fluid with magnetite (Fe_3O_4) as the magnetic particles, however many nonmagnetic particles of $mFeO \bullet nFe_2O_3$, $n \neq m$, were formed. Commercial methods typically use a reaction which forms $FeO \bullet Fe_2O_3$ magnetic particles. This commercial reaction has a low nonmagnetic byproduct yield, can be performed at a lower temperature (40°C), and particles have higher adsorption capability resulting in greater fluid stability. The particles formed are 2-20nm in diameter with a mean diameter of 7nm and exhibit the magnetic properties of $FeO \bullet Fe_2O_3$ monocrystals (Berkovsky[5]). This method limits the selection of magnetic materials used in the fluid, however due to high concentration of particles that can be suspended the fluid exhibits the highest magnetization (100 kA/m). Large amounts of fluid can be produced quickly using this method and it is applicable to a number of different stabilizer / base oil combinations resulting in its wide spread use.

2.5.4 Properties of a Ferrofluid

Seven types of properties characterize a magnetic fluid, including magnetism, viscosity, density, thermal, electrical, acoustic, and optical properties. All properties are derived from the properties of the components, the base fluid, stabilizer, and particles although the important parameter relationships are different for each

property. The focus of this section is on magnetism, viscosity, and density because these properties impact the bearing system.

Magnetization of a ferrofluid in an external field is determined by the concentration, size, and material of the suspended particles as well as the applied field strength. In general the magnetization increases with concentration, particle size and field strength. Analysis of the system is conducted as if it were a paramagnetic gas. Although each individual particle is composed of a unidirectional ferromagnetic material, the relative misorientation between particles eliminates the overall ferromagnetic effect in the fluid. The Langevin function describes the magnetization:

$$M = nm(\coth\xi - 1/\xi)$$

Where n and m are the number of the of particles and the magnetic moment of each particle. The Langevin argument is $\xi = \mu_0 mH/(kT)$ where μ_0 is the magnetic permeability in vacuum, H is the magnetic strength, k is the Boltzmann constant and T is the absolute temperature. Note the Langevin argument varies directly with applied field strength and the function approaches a maximum as $H \to \infty$ (Figure 2.5.4a) corresponding to the saturation magnetization. Actual magnetic fluids respond slightly differently due to the distributed particle size. This can be modeled using a different particle size and corresponding magnetic moment for weak and strong field interactions. A simple approximation given by Vislovich fits experimental data with great accuracy.

$$M = M_s H/(H_T + H)$$

Here M_s is the saturation magnetization and H_T is the field strength at which the magnetization is half of the saturation magnetization. Typically the magnetic properties that are used to characterize the fluid are the initial magnetic susceptibility, which is the slope of the Langevin curve at $H = 0$, and the magnetic saturation strength M_s.

Viscosity is a function of particle concentration, applied magnetic field, and temperature. The viscosity of the magnetic fluid, η_m, is a function of the viscosity of the carrier fluid, η_c, and the volume concentration of magnetic particles, φ_p. The Vand equation derived in 1940 predicts the viscosity of real magnetic fluids

$$\eta_m = \eta_c[(2.5\varphi_p + 2.7\varphi_p^2)/(1 - .609\varphi_p)]$$

based on a solid sphere / fluid model. Good agreement exists with experimental data at shear rates above 10^4 s^{-1}, however more extensive models are used in the low shear regime. The relationship between the applied magnetic field strength and the viscosity is a complex one, however it is clear that the viscosity of the magnetic fluid increases as the field increases. The primary reason for the viscosity increase is that the magnetic particles are constrained to a certain extent in their rotational degree of freedom. This rotational degree of freedom accounts for 3/5 of the viscosity in a low concentration solid sphere dispersion model. More complex particle interactions account for discrepancies between experimental results and the simple model.

Viscosity dependence upon temperature is governed by the properties of the base fluid in a low concentration magnetic fluid. High concentration magnetic fluids must be measured experimentally since the viscosity temperature dependence is affected by particle size, geometry, and chemistry. In general the viscosity is inversely proportional to the temperature, however is some special cases the viscosity actually increases with temperature.

Density and thermal expansion of a ferrofluid can be determined if the volume fractions and density of each component are known. The magnetic fluid density is:

$$\rho_m = \rho_c \varphi_c + \rho_p \varphi_p + \rho_s (1-(\varphi_c + \varphi_p))$$

Where ρ_m, ρ_c, ρ_p, and ρ_s are the densities of the magnetic fluid, carrier, magnetic particles, and the stabilizer while φ_c, and φ_p are the volume concentrations of the carrier liquid and the magnetic particles. Typically the liquid densities are similar and the formula can be reduced. The thermal expansion coefficient, β, defines volumetric expansion and follows a similar relationship.

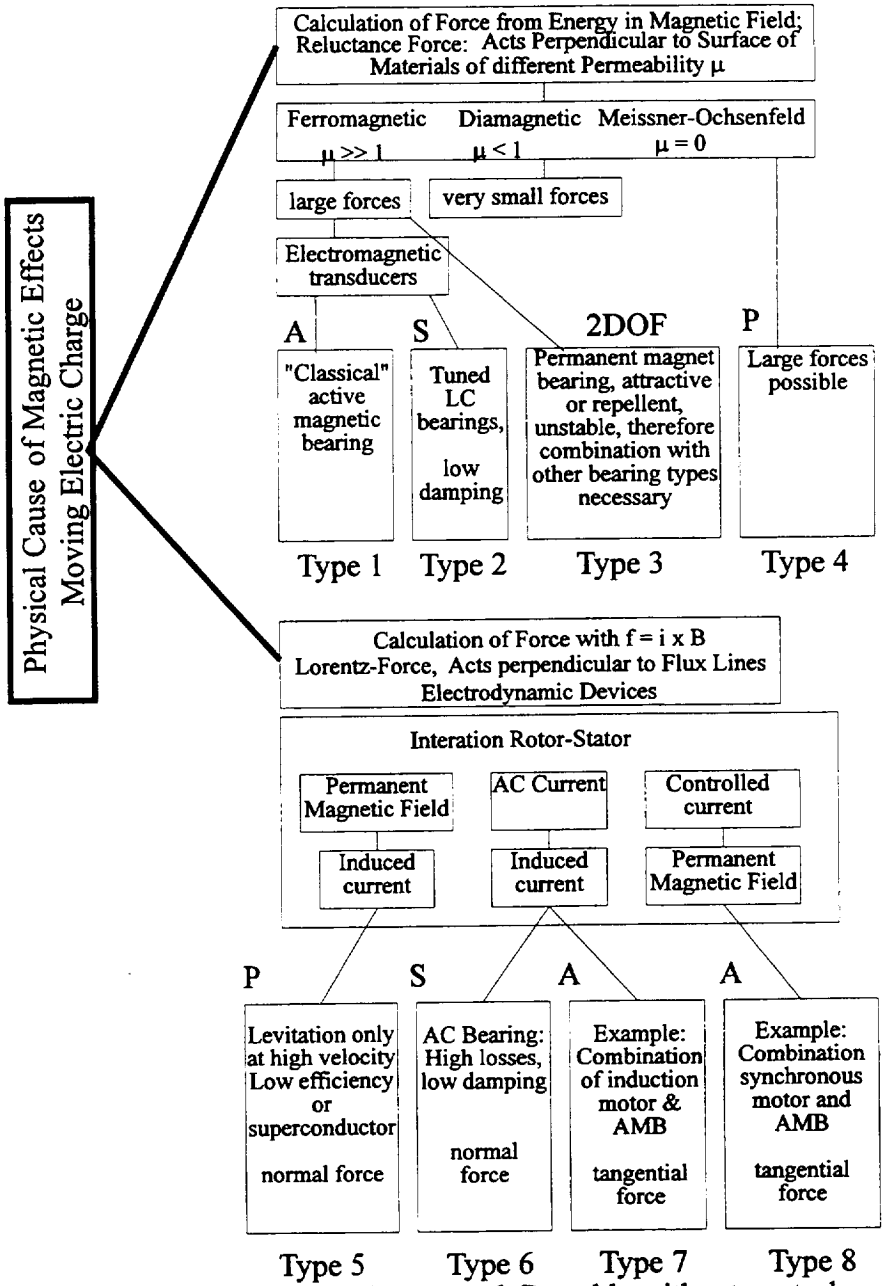

Figure 2.3a - Classification of magnetic bearings and magnetic levitation

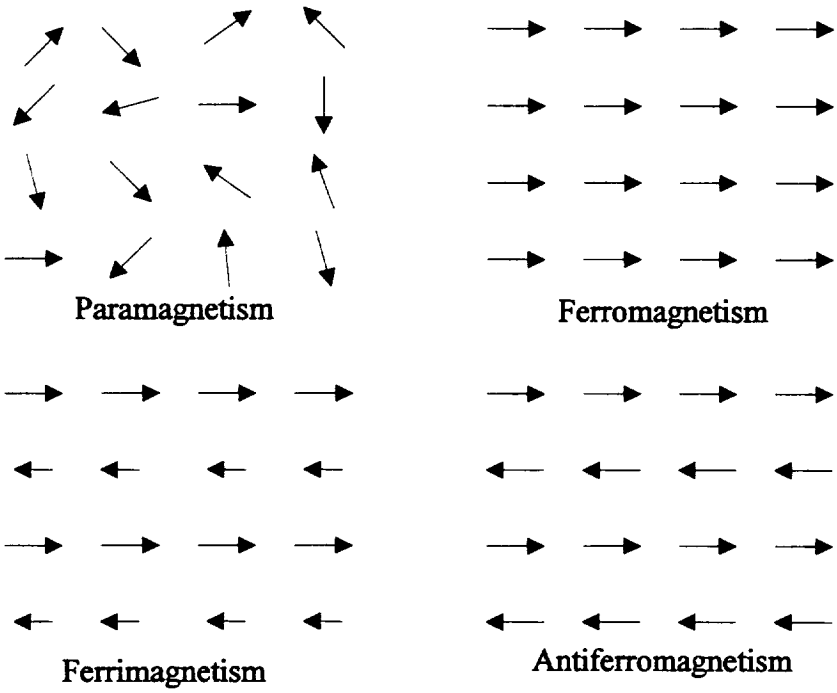

Figure 2.4.1a - Ordering of magnetic moments in solids

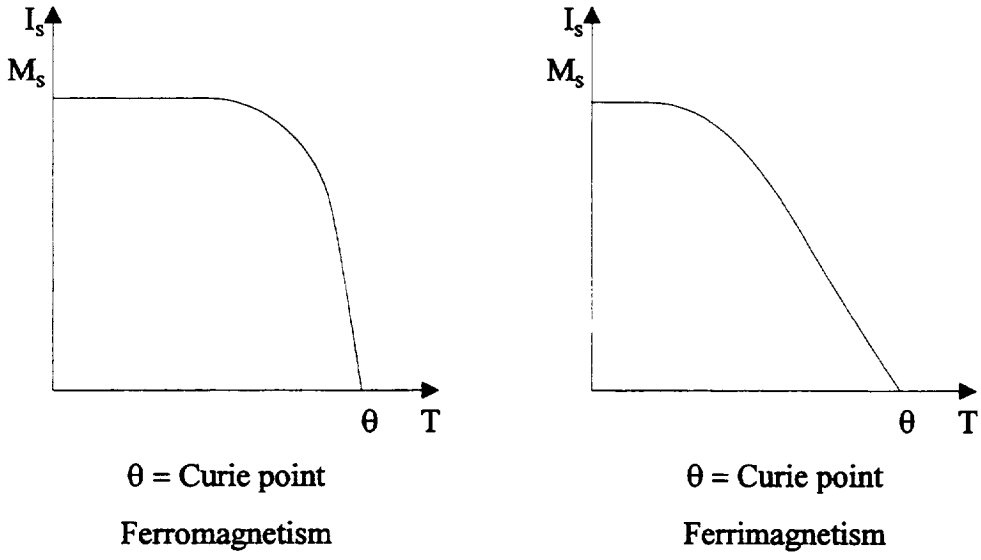

Figure 2.4.1b - Strength of spontaneous magnetization as a function of temperature

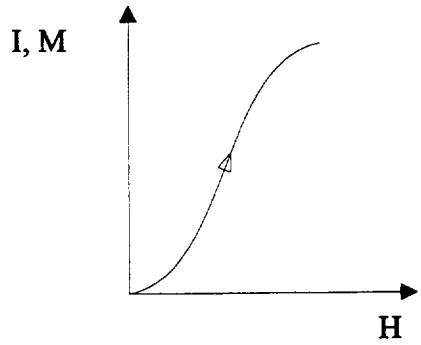

Figure 2.4.2a - Ideal magnetization curve

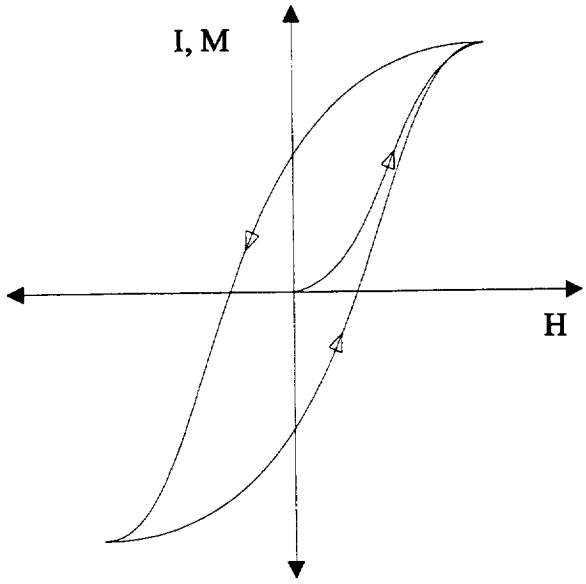

Figure 2.4.3a - Complete magnetization curve

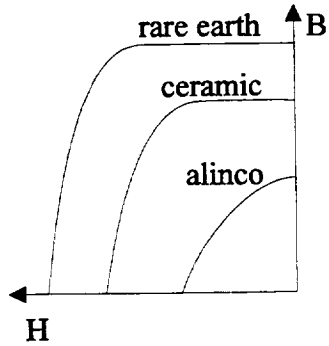

Figure 2.4.3b - Second quadrant properties of magnets

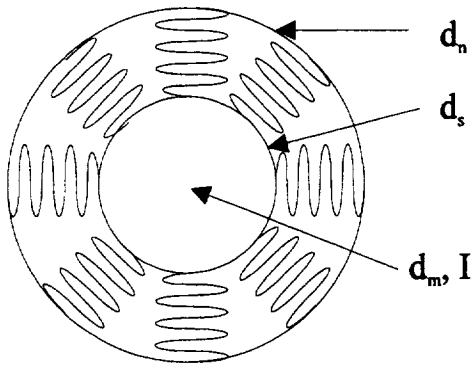

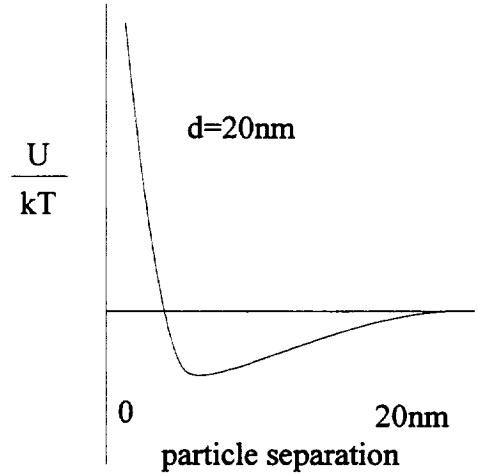

Fig. 2.5.2a-Typical magnetic particle parameters Fig. 2.5.2b-Particle potential energy

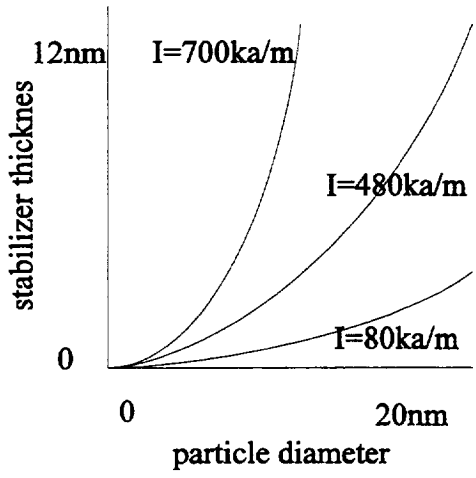

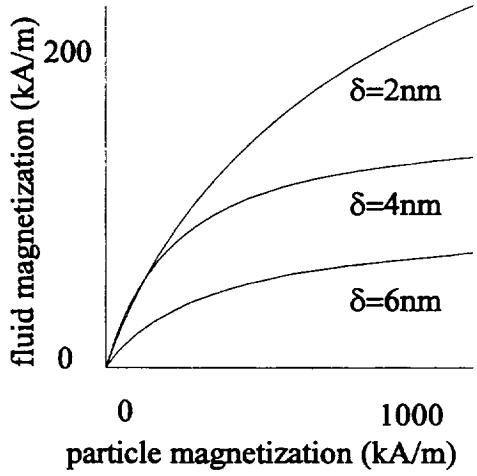

Fig. 2.5.2c - Optimum coating thickness Fig. 2.5.2d - Resultant fluid magnetization

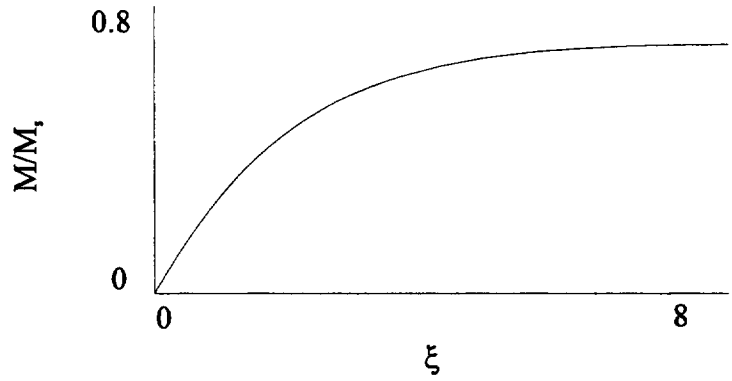

Figure 2.5.4a - Langevin function

Chapter 3: Overall System Design

A number of different system configurations are possible based on the use of a permanent magnet bearing combined with a ferrofluidic stabilizer unit. Concepts were generated using the ferrofluid stabilizer in both the axial and radial direction. A list of important system parameters was generated and each design was evaluated. A final design was chosen for implementation

3.1 Permanent Magnet Bearing Concepts

The objective of the permanent magnet bearing is to provide stability in two axes. The third axis will have an instability with a negative stiffness equal to the sum of the stiffness in each stable axis. An extensive group of permanent magnet suspension geometries was compiled by Geary[6]. These systems can be classified by suspension orientation, mode, magnetic field orientation, and geometry. Suspension orientation indicates whether stability exists in an axial, radial, or diagonal direction relative to the axis of the rotor. Bearings can be operated in attractive or repulsive modes determined by the polarity of aligned faces. Permanent magnets can be magnetized in a number of ways, however only radial and axial systems are considered herein. Radial systems have poles on interior and exterior radii, while axial systems have poles located on at each end of a cylinder or on the face of a disk. Generally a number of geometries can satisfy the suspension orientation, mode, and

magnetic field orientation constraints. Geometry impacts the load carrying capacity and size of the system.

Twenty six types of permanent magnet bearings were considered including ten axial, fourteen radial, and two diagonal suspension orientations. Table 3.1a lists each bearing and geometry. Five major classifications were derived from this list based on suspension orientation and mode. Class 1 is radial repulsion systems and includes concentric cylinder and disk geometry. Class 2 is radial attraction systems including disks, cylinders, and conical pole types. Class 3 is axial repulsion systems with disk or cylinder geometry. Class 4 is axial attraction systems based on disks or cylinders. Class 5 is diagonal repulsion systems utilizing conical geometries. Schematic representations of the bearings are shown in Figure 3.1a-e. Required restraints are indicted by arrows. A pair of arrows along an axis indicates a radial restraint, an arrow on flat indicates an axial restraint, and an arrow in cone indicates a pivot constraint.

3.2 Ferrofluid Stabilizer Concepts

The ferrofluid stabilizer is used to stabilize the third axis of the permanent magnet bearing. The ferrofluid stabilizer itself is stable in all three axes however, the magnitude of the stiffness in each axis depends on the geometry. Stabilizer designs were classified by strong axis orientation, field orientation and geometry. Strong axis

orientation means the axis on which the greatest absolute value of stiffness occurs. Field orientation and geometry are the same as the permanent magnet properties.

Twenty two types of ferrofluid stabilizers were analyzed including two non oriented, eight axially oriented, and twelve radially oriented designs. Table 3.2a lists each type of stabilizer and its geometry. Three classifications were derived from the strong axis orientation. Class 1 is non-oriented, Class 2 is axially oriented, and Class 3 is radially oriented. Each design is schematically represented in Figure 3.2a-c.

3.3 System Concepts

The system design was done in two steps. The first step was to evaluate the magnetic bearing and ferrofluid stabilizers and select the best candidates for the final design. The second step was to generate and evaluate designs using the small remaining number of components.

Five parameters were used to evaluate the components, load, size, manufacturability, ease of testing, and ease of incorporation into overall design. Load carrying capacity was based on the use of the same type of magnetic material and the same critical dimension. Sizing is based on a standard load capacity. Manufacturability is an important parameter since magnets typically come in a limited number of stock shapes. These include disk, annular disk, block, and rod. The stock magnetic orientation on disks and annular disks is typically axial. If a

stock magnet is not available a custom magnet is required which typically costs two orders of magnitude more. Ease of testing impacted the complexity of the equipment that was built for force and stiffness measurements. Certain components are difficult to incorporate with the other component due to their geometry thereby limiting usefulness.

Permanent magnet bearing concepts were evaluated in three groups based on their suspension orientation. The diagonal orientation concepts were dropped because of the difficulty in designing a diagonal ferrofluid stabilizer. Two repulsion radial bearings were selected, 4R a concentric annular disk design, and 5R a stacked concentric annular disk design. Two axial repulsion bearings were selected, 1A and 2A, based on a two disk and three disk geometry.

Ferrofluid stabilizers were evaluated in groups based on strong axis orientation. Non-oriented concepts were dropped because they did not match any permanent magnet bearing concepts. Axial stabilizers 1a, 3a, and 5a were selected. These represent the disk, concentric annular disk, and stacked disk concepts. Radial stabilizer 1r and 3r, a rod and cylinder design, were considered.

System designs were generated using the remaining components. Magnetic field orientation and concentric annular disk designs did not impact the physical features therefore eight concepts were generated. Systems were classified by unstable magnet bearing axis. Designs #1-#4 are axial systems while designs #5-#8 are radial systems. Schematics of each design are shown in Figure 3.3a,b.

3.4 Concept Selection

The eight designs were evaluated on four criteria. The first is the likelihood of producing a stable system which is the primary objective of the project. The second is the load carrying capacity which must at least be sufficient to support the rotor components. Manufacturability of the system depends on the complexity of the magnets required. Systems that can be made of stock magnets are cheaper and quicker to make. Ease of testing was the final criteria.

Preliminary work had indicated that the solid-solid magnet interaction was an order of magnitude greater than the solid-ferrofluid interaction. Since each component must have similar stiffness the decision was made to use ceramic solid magnets on the permanent magnet bearing and rare earth magnets in the ferrofluid stabilizer. The rare earth magnets have a residual magnetization ten times greater than the ceramic magnets giving each component similar force relationships.

The use of rare earth magnets in the ferrofluid stabilizer drove the design away from the use of complex magnet shapes in the stabilizer because of manufacturing difficulties. This eliminated design #7 and #8. Concern that the ferrofluid stabilizer would be the limiting factor eliminated design #5 and #6 because the stabilizer strength can not be easily enhanced if it is not sufficient. Design #2 and #4 both utilize stacked annular disk magnets to increase radial bearing strength. However it was not necessary; therefore they were eliminated. The remaining designs #1 and #3

both utilize annular disk repulsion bearing designs with a disk ferrofluid stabilizer. Design #3 incorporates a stacking scheme to increase the strength of the stabilizer. A judgment was made that by the use of the correct magnet types and sizes design #1 could be stabilized without the complexity of #3.

Selection of design #1 determined the testing work that needed to be completed. Measurements of radial bearing stiffness using an annular disk design needed to be made on a number of different size and composition magnets. Ferrofluid stabilizer force curves must be determined utilizing the disk or concentric annular disk designs.

Permanent Magnet Bearing Concepts					
Type	Class	Suspension Orientation	Mode	Field Orientation	Geometry
1r	1	Radial	Repulsion	Axial	Concentric cylinder
2r	1	Radial	Repulsion	Axial	Concentric cylinder
3r	1	Radial	Repulsion	Radial	Concentric cylinder
4r	1	Radial	Repulsion	Radial	Concentric annular disk
5r	1	Radial	Repulsion	Axial	Stacked concentric annular disk
6r	1	Radial	Repulsion	Radial	Stacked concentric annular disk
7r	1	Radial	Repulsion	Radial-U	Stacked concentric annular disk
8r	1	Radial	Repulsion	Axial	Multiple concentric cylinder
9r	2	Radial	Attraction	Axial	3 disk
10r	2	Radial	Attraction	Radial	3 disk
11r	2	Radial	Attraction	Axial	Conical pole
12r	2	Radial	Attraction	Axial	Ring ridge pole
13r	2	Radial	Attraction	Axial	Multiple ring ridge pole
14r	2	Radial	Attraction	Mixed	Cylinder / 2 annular disk
1a	3	Axial	Repulsion	Axial	2 disk
2a	3	Axial	Repulsion	Radial	2 disk
3a	3	Axial	Repulsion	Axial	3 disk
4a	3	Axial	Repulsion	Radial	Disk / annular disk
5a	3	Axial	Repulsion	Axial	Cylinder / 2 annular disk
6a	4	Axial	Attraction	Radial	Disk / annular disk
7a	4	Axial	Attraction	Axial	Concentric cylinder
8a	4	Axial	Attraction	Axial	Concentric cylinder
9a	4	Axial	Attraction	Axial	Stacked concentric cylinder
10a	4	Axial	Attraction	Mixed	Cylinder / 2 annular disk
1d	5	Diagonal	Repulsion	Radial	Concentric conical annular disk
2d	5	Diagonal	Repulsion	Axial	Concentric conical pole

Table 3.1a

Ferrofluid Stabilizer Concepts				
Type	Class	Strong Axis Orientation	Field Orientation	Geometry
1n	1	None	Axial	Sphere
2n	1	None	Radial	Sphere
1a	2	Axial	Axial	Disk
2a	2	Axial	Radial	Disk
3a	2	Axial	Axial	Concentric ring
4a	2	Axial	Radial	Concentric ring
5a	2	Axial	Axial	Stacked disk
6a	2	Axial	Radial	Stacked disk
7a	2	Axial	Axial	Stacked concentric ring
8a	2	Axial	Radial	Stacked concentric ring
1r	3	Radial	Axial	Disk
2r	3	Radial	Radial	Disk
3r	3	Radial	Axial	Cylinder
4r	3	Radial	Radial	Cylinder
5r	3	Radial	Axial	Concentric cylinder
6r	3	Radial	Radial	Concentric cylinder
7r	3	Radial	Axial	Stacked disk
8r	3	Radial	Radial	Stacked disk
9r	3	Radial	Axial	Stacked cylinder
10r	3	Radial	Radial	Stacked cylinder
11r	3	Radial	Axial	Stacked concentric cylinder
12r	3	Radial	Radial	Stacked concentric cylinder

Table 3.2a

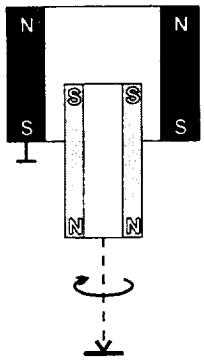

1r - offset concentric cylinder
axial field orientation

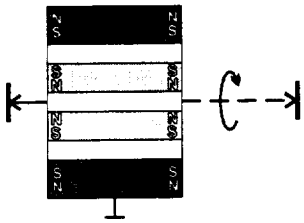

3r - concentric cylinder
radial field orientation

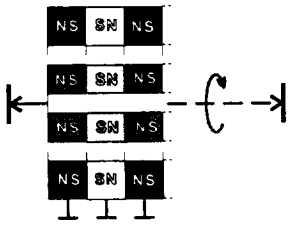

5r - stacked concentric disk
axial field orientation

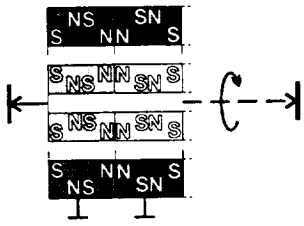

7r - stacked concentric disk
radial - U field orientation

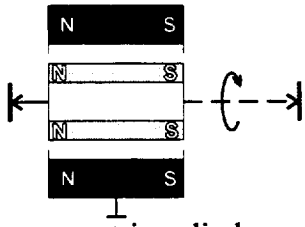

2r - concentric cylinder
axial field orientation

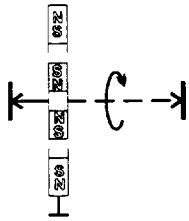

4r - concentric disk
radial field orientation

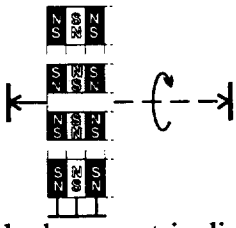

6r - stacked concentric disk
radial field orientation

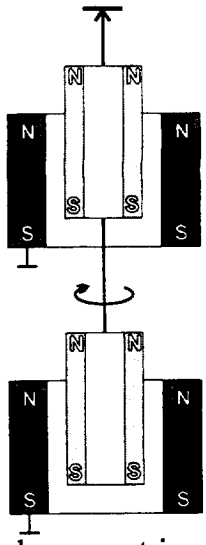

8r - multiple concentric cylinder
axial field orientation

Figure 3.1a - Class 1 radial repulsion permanent magnet bearings

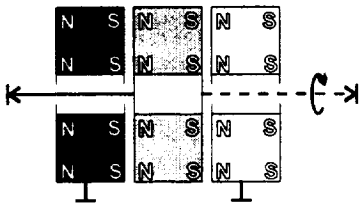

9r - three disk
axial field orientation

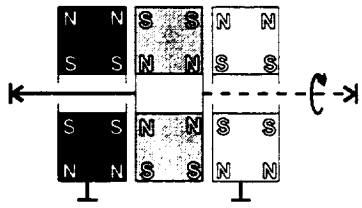

10r - three disk
radial field orientation

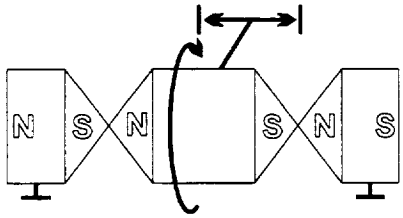

11r - conical pole
axial field orientation

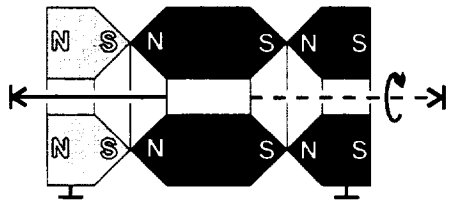

12r - ring ridge pole
axial field orientation

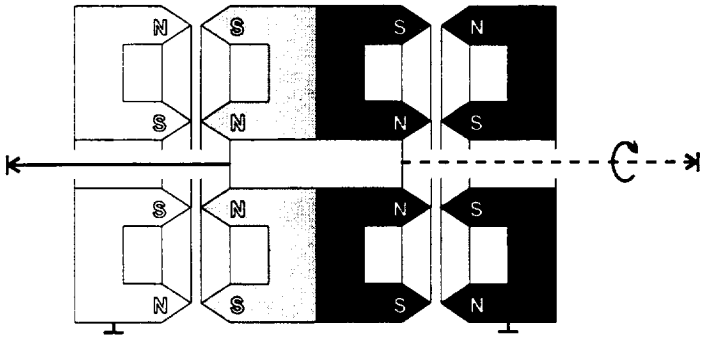

13r - multiple ridge pole
axial field orientation

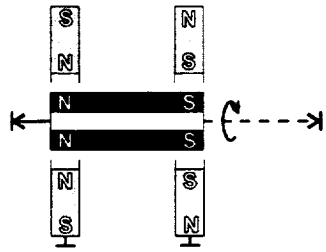

14r - cylinder /annular disk
mixed field orientation

Figure 3.1b - Class 2 radial attraction permanent magnet bearings

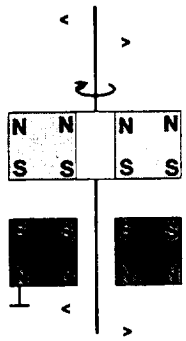

1a - two disk
axial magnetic field

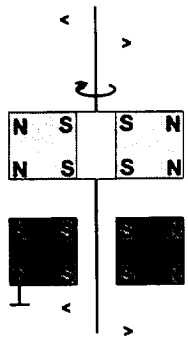

2a - two disk
radial magnetic field

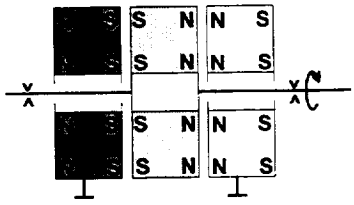

3a - three disk
axial magnetic field

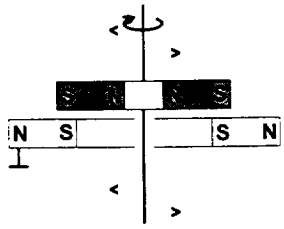

4a - disk / annular disk
radial magnetic field

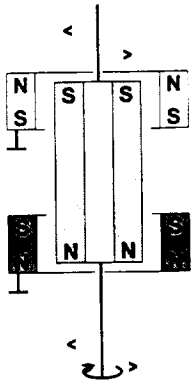

5a - cylinder / two annular disks
axial magnetic field

Figure 3.1c - Class 3 axial repulsion permanent magnet bearings

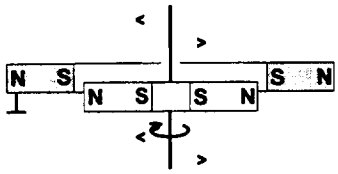

6a - disk / annular disk
radial magnetic field

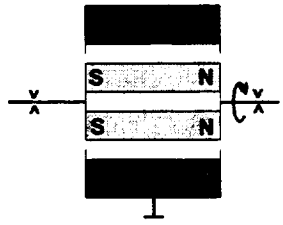

7a - concentric cylinder
axial magnetic field

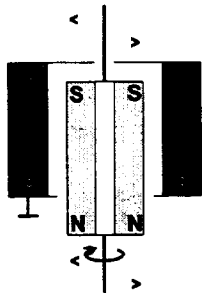

8a - concentric cylinder
axial magnetic field

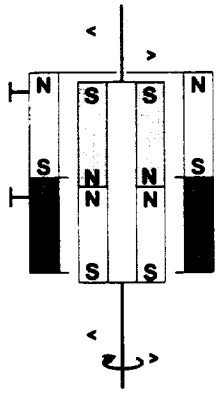

9a - stacked concentric cylinder
axial magnetic field

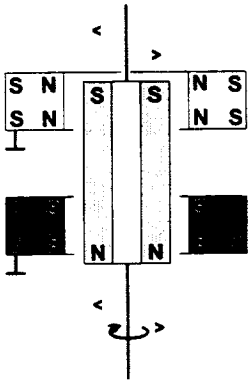

10a - cylinder / two annular disk
mixed magnetic field

Figure 3.1d - Class 4 axial attraction permanent magnet bearings

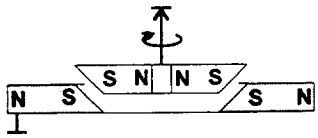

1d - concentric conical annular disk
radial magnetic field

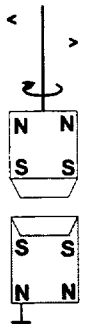

2d - concentric conical pole
axial magnetic field

Figure 3.1e - Class 5 diagonal repulsion permanent magnet bearings

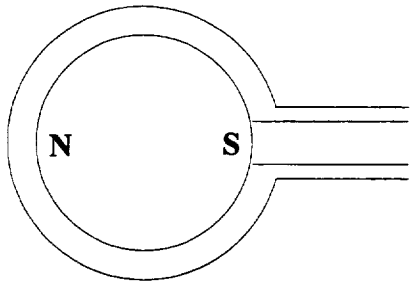

1n - axial magnetic field orientation

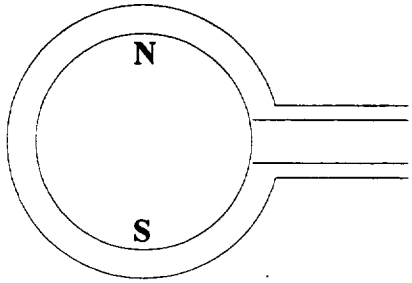

Figure 3.2a - Class 1 non-oriented ferrofluid stabilizer

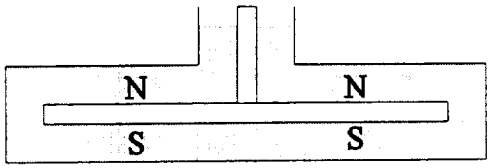

1a - axial field orientation

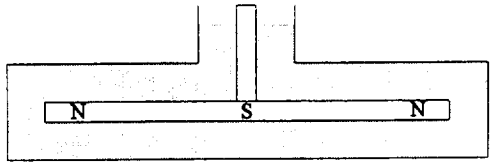

2a - radial field orientation

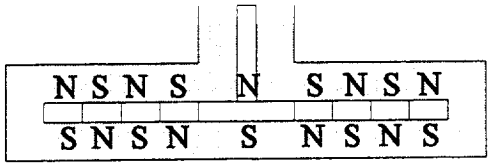

3a - concentric reversed polarity axially magnetised rings

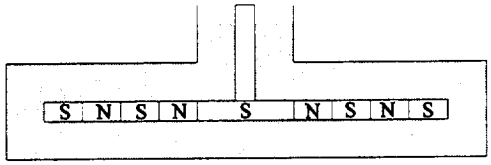

4a - concentric reversed polarity radially magnetised rings

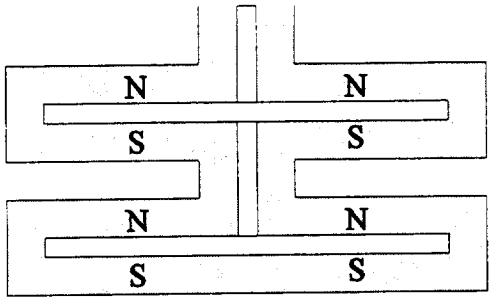

5a - multiple stage axially magnetised disks

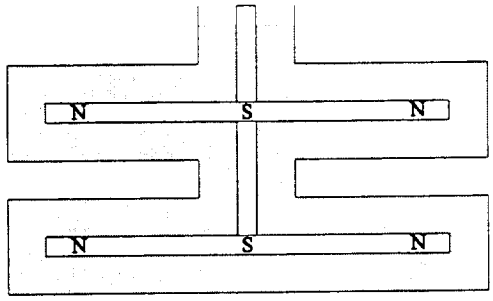

6a - multiple stage radially magnetised disks

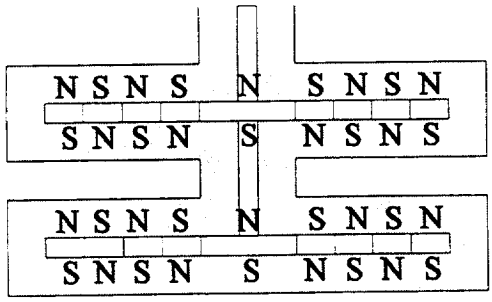

7a - multiple stage concentric reversed polarity axially magnetised rings

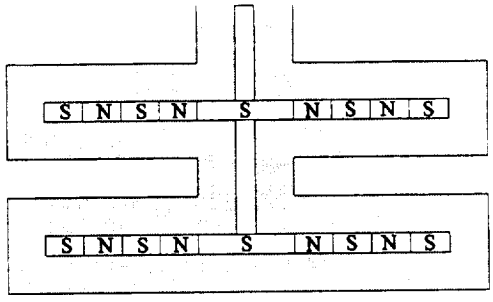

8a - multiple stage concentric reversed polarity radially magnetised rings

Figure 3.2b - Class 2 axially oriented ferrofluid stabilizer

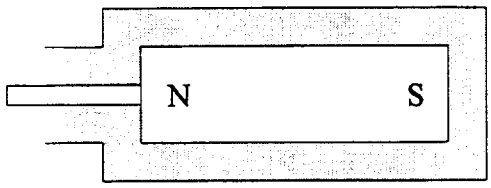

1r - axial magnetic field

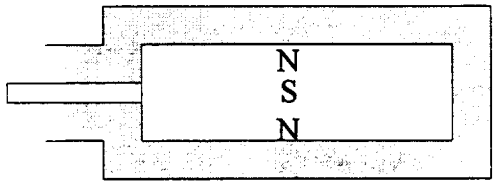

2r - radial magnetic field

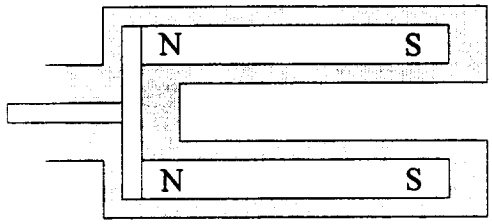

3r - cylinder with axial magnetic field

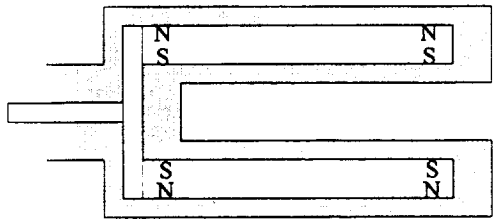

4r - cylinder with radial magnetic field

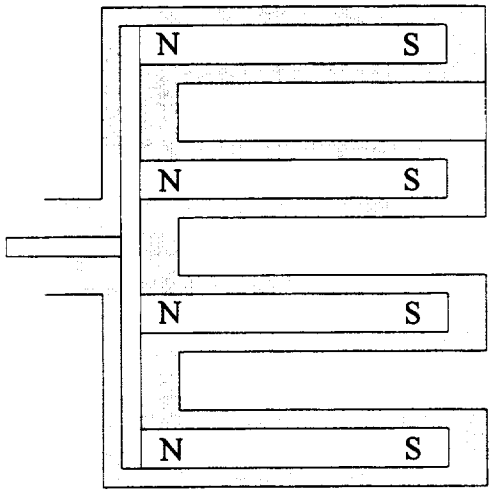

5r - concentric cylinders with axial magnetic field

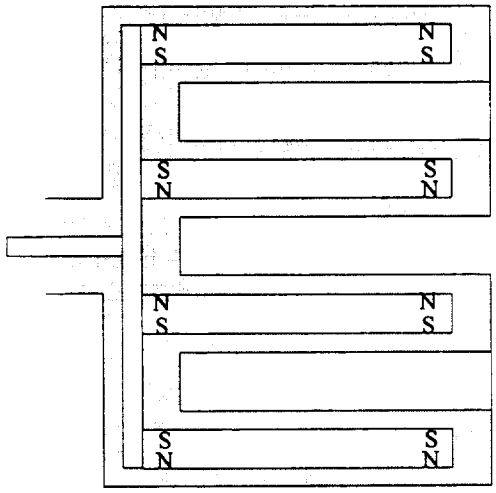

6r - concentric cylinder with radial magnetic field

Figure 3.2c - Class 3 radially oriented ferrofluid stabilizer

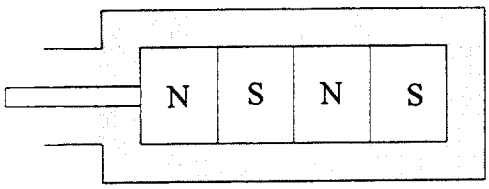

7r - stacked disk with
axial magnetic field

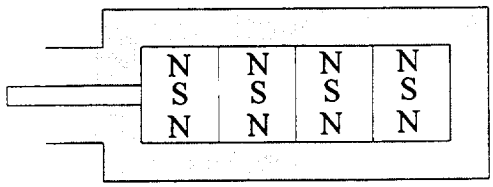

8r - stacked disk with
radial magnetic field

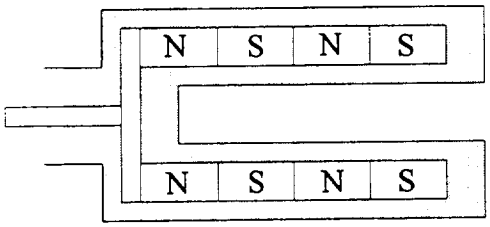

9r - stacked cylinder with
axial magnetic field

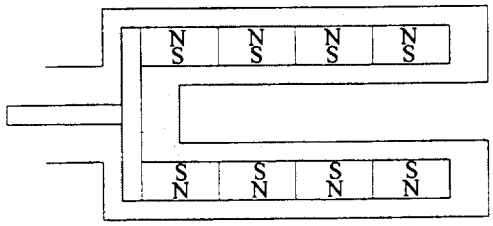

10r - stacked cylinder with
radial magnetic field

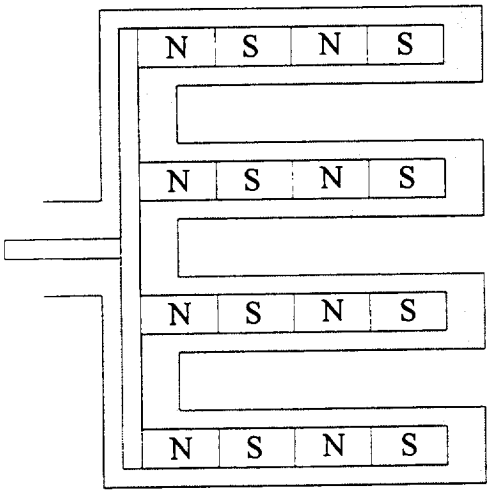

11r - stacked concentric cylinders
with axial magnetic field

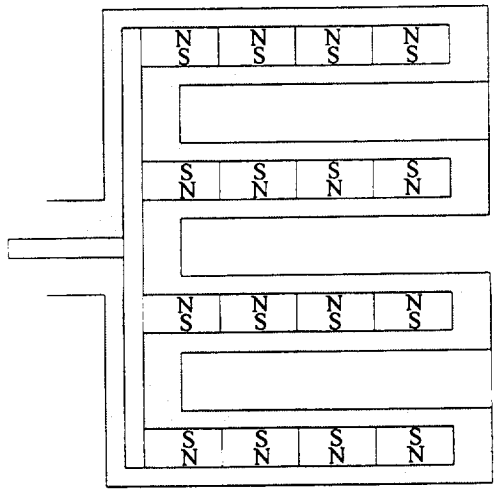

12r - stacked concentric cylinders
with radial magnetic field

Figure 3.2c - Class 3 radially oriented ferrofluid stabilizer

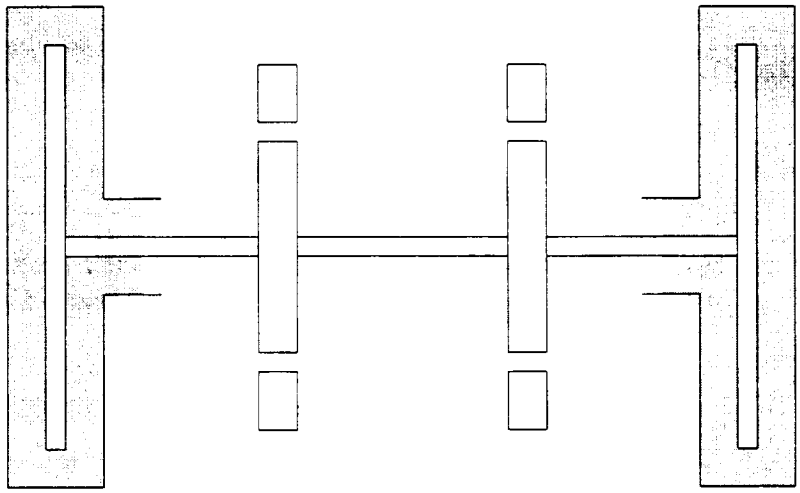

Design #1 - disk / annular disk radial bearing
disk ferrofluid stabilizer

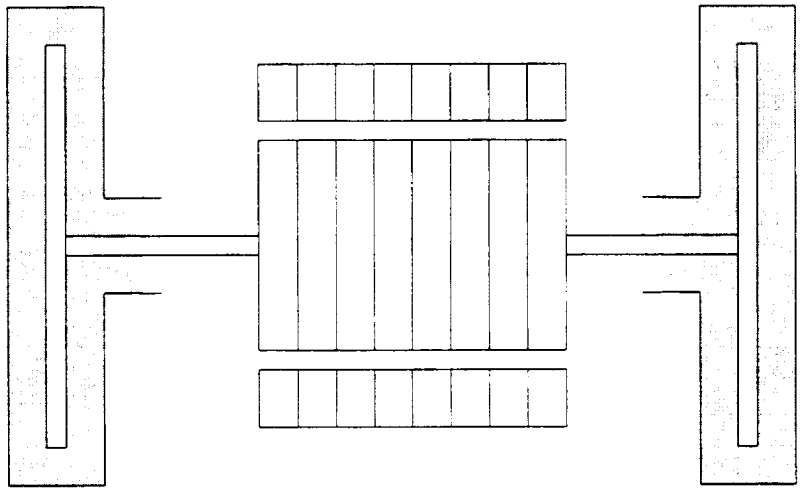

Design #2 - stacked disk / annular disk radial bearing
disk ferrofluid stabilizer

Figure 3.3a - Bearing designs with axial stabilization

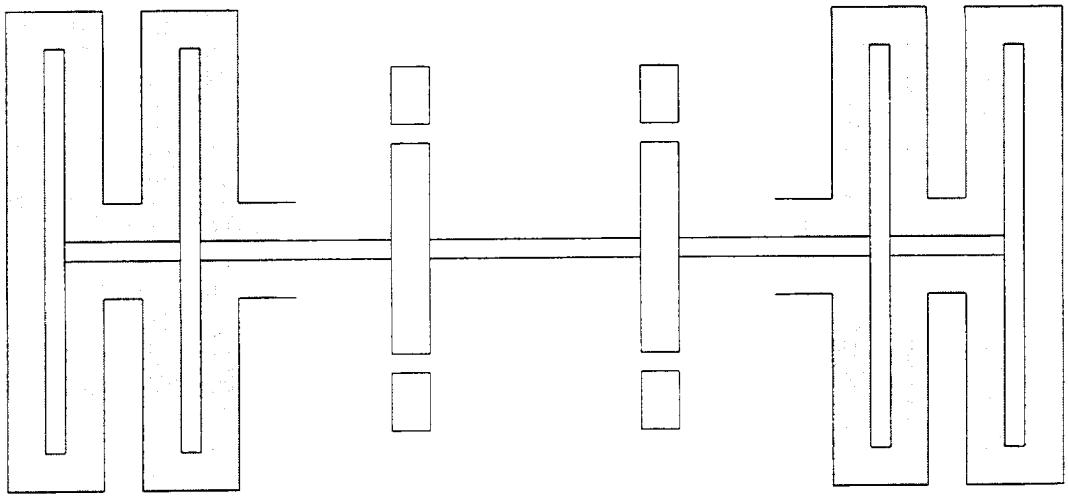

Design #3 - disk / annular disk radial bearing
multiple stage disk ferrofluid stabilizer

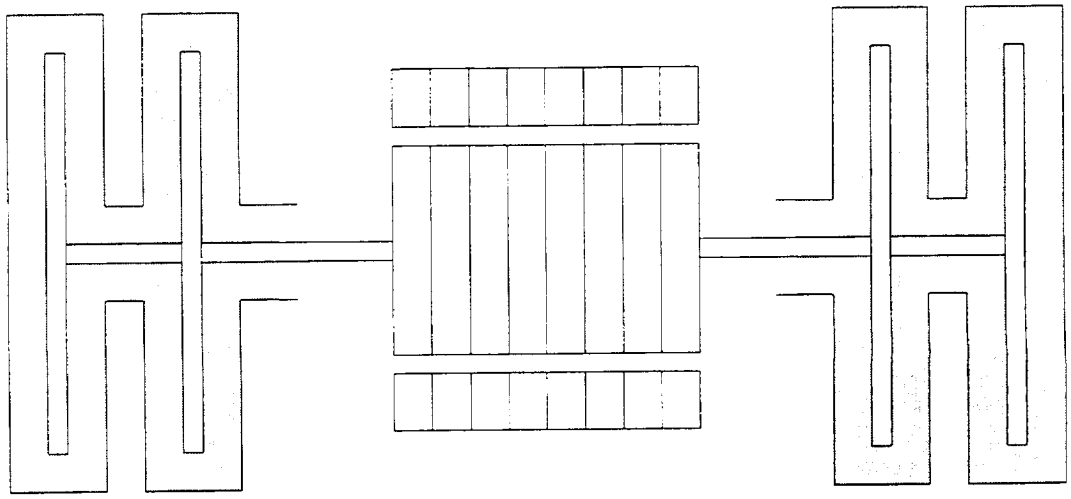

Design #4 - stacked disk / annular disk radial bearing
multiple stage disk ferrofluid stabilizer

Figure 3.3a - Bearing systems with axial stabilization

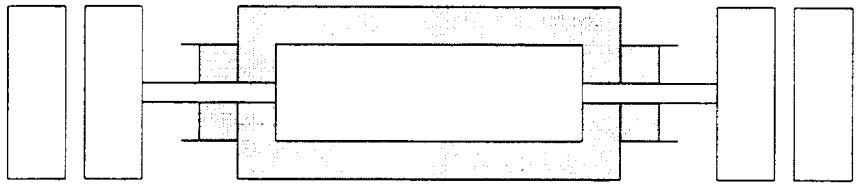

Design #5 - two disk axial bearing
long disk ferrofluid stabilizer

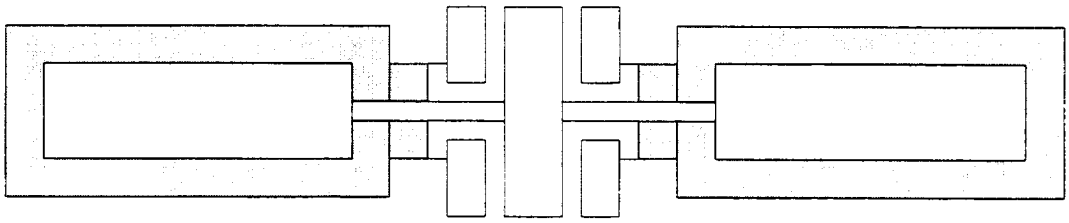

Design #6 - three disk axial bearing
2 long disk ferrofliuid stabilizers

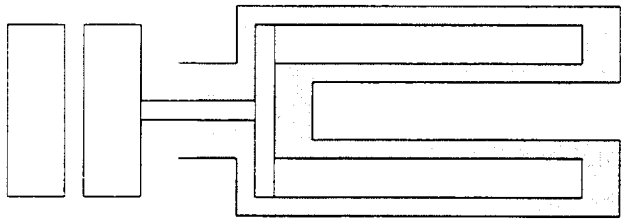

Design #7 - single two disk axial bearing
cylindrical ferrofluid stabilizer

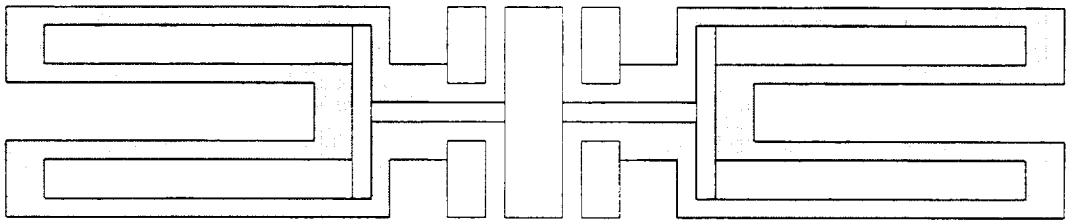

Design #8 - three disk axial bearing
2 cylindrical ferrofluid stabilizers

Figure 3.3b - Bearing systems with radial stabilization

Chapter 4: Radial Bearing Design

4.1 Basic Design

The magnet configuration used for a radial permanent magnet bearing consists of a magnetic rotor disk concentrically located within a magnetic stator ring (Figure 4.1a). The magnetic poles are aligned in order to provide like polarity on the adjacent faces of the two magnets. The resulting force is repulsive in the radial direction and the rotor magnet seeks an equilibrium position concentric to the stator magnet in the absence of external forces. An unstable axial equilibrium position exists at the point where the rotor magnet and the stator magnet are aligned in the z axis. As per Earnshaw's Theorem the sum of the orthogonal stiffness values must be zero. Therefore the axial stiffness is equal to the negative of the sum of the radial stiffness vectors in the x and y direction.

4.2 Experimental

Three parameters of the radial bearing were experimentally measured. The first parameter is the stiffness of the bearing as a function of radial displacement from the concentric equilibrium position. Second is the maximum load carrying capacity. Third is the stroke of the bearing. A large number of possible rotor / stator magnet combinations exist so the maximum load and stroke are used as a screening criterion before the stiffness test is conducted. The load and stroke measurements can be made quickly, thereby lending themselves well to a screening test.

4.2.1 Stiffness measurement

Two methods are used to measure stiffness, the frequency and the displacement technique. One test rig is constructed to make the measurements required for each method.

4.2.1.1 Frequency Techniques for Stiffness Measurement

The frequency method of stiffness testing outlined by Plimmer[7] for radial magnet bearings relies on measurement of the mass and natural frequency of the rotor and pendulum section in order to calculate the stiffness of the rotor / stator magnet combination. An analytical model which relates the natural frequency and stiffness is developed. Experimental measurements of mass and natural frequency are entered into the model and the stiffness is calculated. This technique yields a stiffness value with is the average stiffness over the stroke of the rotor when the measurement is made. It is not possible to find stiffness as a function of displacement using this technique however it can be used to dynamically validate the measurements made using the displacement method.

An analytical rotor model is developed to relate the measured frequency to a linear stiffness coefficient. Figure 4.2.1.1a is a schematic representation of the system. It consists of a pivoted rod with length from pivot point to end of r_r and mass m_r. The stator magnet has a mass of m_m located at r_m from the pivot point. The rod is displaced from equilibrium by an angle of θ and is under a gravitational

acceleration of g. The magnetic restoring force is represented as kx where x is the distance from the $\theta = 0$ position. Three assumptions are made in this model. The magnet height is assumed to be negligible compared to the length of the rod ($r_m = r_r = r$). The actual length ratio, r_m / r_r, is 0.9811. The angle of oscillation is small, therefore $\sin\theta \approx \theta$. The worst case deflection is 1.87 degrees. The pivot is assumed to have a damping coefficient of c. A torsional model is developed about the pivot point. The torque is:

$$T = -m_r g\theta\left(\frac{r}{2}\right) - m_m g\theta r - kr\theta r$$

The moment of inertia of the system about the pivot is

$I = I_r + I_m$ where I_r and I_m are the moments of the rod and the magnet

$$I_r = \tfrac{1}{12} m_r r^2 + m_r\left(\frac{r}{2}\right)^2 = \tfrac{1}{3} m_r r^2$$

$$I_m = m_m r^2$$

$$I = m_m r^2 + \tfrac{1}{3} m_r r^2$$

Setting $T = I\alpha$

$$r\left(-\tfrac{1}{2} m_r g\theta - m_m g\theta - kr\theta\right) = r^2\left(m_m + \tfrac{1}{3} m_r\right)\alpha$$

Transforming this into a standard form second order linear homogeneous differential equation with $\theta = \Theta, \alpha = \Theta''$ yields

$$\Theta'' + c\Theta' - \frac{\left(\frac{1}{2} m_r g + m_m g + kr\right)}{r\left(m_m + \frac{1}{3} m_r\right)}\Theta = 0$$

Reducing the coefficients gives

$$\Theta'' + a\Theta' + b\Theta = 0$$

The characteristic equation is

$$\lambda^2 + a\lambda + b = 0$$

The roots are

$$\lambda = \frac{-a \pm \sqrt{a^2 - 4b}}{2}$$

We have experimentally determined that this is an underdamped system so the solution is

$$u = \mathrm{Re}^{-at/2} \cos(\mu t - \delta) \qquad \text{where } \mu = \sqrt{4b - a^2}/2;\ \delta = \text{phase angle}$$

This equation is shown in Figure 4.2.1.1b. Now we solve for k from the coefficient b:

$$k = \frac{-br(m_m + \frac{1}{3}m_r) - \frac{1}{2}m_r g - m_m g}{r}$$

The damping coefficient is:

$$c = a$$

With this model we can measure natural frequency, mass, and dimensions of the components and solve for the stiffness and damping coefficient of the system.

The following experimental procedure was used for the frequency method. The rotor and stator magnets are installed in the radial bearing test fixture described hereafter. The entire test is conducted with the test fixture in the vertical position. A

displacement probe is used to track the position of the rotor magnet. Signal processing hardware is used to set the centered position output to 0V and the full scale to ± 5V. The signal is recorded on a digital oscilloscope. The rotor magnet is moved to its maximum displacement and released. A time trace of the probe output is recorded. This time trace is converted into the frequency domain and recorded. Typical traces are shown in Figure 4.2.1.1c,d. The digital oscilloscope is used to measure the peak height of the first positive peak in the time trace. A second marker is used at the second positive peak to measure the period and decay of the first complete oscillation. A marker is also used in the frequency trace to measure first mode natural frequency. This measurement is used as a confirmation of the first measurement. Trace lengths were 4 seconds with a sampling rate of 800Hz. Voltage measurements were 5V peak to peak with an resolution of 3.41mv. The experimental data is used to calculate R, a, b, c, and k. Using the first and second positive peaks results in $\delta = 0$ and $R = \Theta(t_0)$ where t_0 is the time of the first peak. The period is $T = t_1 - t_0$ where t_1 is the time of the second peak. The natural frequency is $\omega_n = 1/T = \mu$. Now solving for a and b as a function of the known variables:

$$a = \frac{2}{T}\ln\left(\frac{\Theta(t_1)}{R}\right) \qquad b = \varpi_n^2 + \tfrac{1}{4}a^2$$

These parameters are used in the analytical model to solve for stiffness and damping coefficient.

4.2.1.2 Displacement Technique for Stiffness Measurement

The Displacement Method of stiffness testing consists of statically loading the rotor and making displacement measurements of the rotor position. This method enables stiffness data to be plotted as a function of the displacement. The rotor load is gradually increased from no load until the load exceeds the maximum load capacity, at which the rotor and stator magnets come into physical contact. A minimum of 10 load / displacement measurements were taken for each rotor / stator magnet pair. The experimental points are fittted with a second order polynomial curve fit using a standard software package. The derivative of the load / displacement polynomial curve fit is taken in order to find stiffness as a function of displacement.

The following experimental procedure is used for the displacement method. Measurements are made using the radial bearing test fixture described hereafter. First the rotor and stator magnet are installed in the test fixture. The test fixture is oriented vertically and an initial position probe voltage is measured corresponding to no load. The test fixture is reoriented horizontally for the remainder of the test. A second voltage measurement is made without the weight pan. This corresponds to a load at the pan of 40g, the weight of the rod. A third measurement was made with the 50g weight pan in place resulting in a 90g load. The main section of the test consists of recording position probe voltages as the load on pan is incrementally increased until the rotor and stator magnets comes into contact. Typically a 10g or 20g increment is used resulting in 15 to 20 measurements over the stroke of the bearing.

4.2.1.3 Test Fixture

A single test fixture, capable of stiffness testing using the frequency or displacement method, is assembled in order to conduct stiffness testing on radial magnetic bearings. The system consists of a pendulum arm on which the rotor magnet is fixed and a stator magnet mounted on the base. Frequency method measurements are made with the pendulum arm vertically oriented while displacement method measurements are made horizontally.

The radial stiffness test fixture oriented for measurements using the frequency method is shown schematically in Figure 4.2.1.3a and pictorially in Figure 4.2.1.3b. The stator magnet to be tested is affixed to the base with a pair of screw clamps. The stator magnet is positioned concentrically in relation to the pendulum arm and is vertically aligned with the rotor magnet using spacer blocks. The pendulum arm is pivoted on a hardened 1/16" pin which is fixed in a mounting bracket attached to the base. An eddy-current position probe is mounted near the top of the pendulum enabling measurement of a large stroke at the bottom of the pendulum. The probe output is a nominal 10V output which is recorded on a digital oscilloscope. The recorded trace can be analyzed in the frequency or time domain.

The radial stiffness test fixture oriented for measurements using the displacement method is shown in Figure 4.2.1.3c and Figure 4.2.1.3d. The magnets are mounted using the same technique described previously. The position probe is again used to measure the position of the pendulum arm. A weight pan is hung at a detent position on the pendulum arm to load the rotor magnet. Additional weights are

added to the weight pan to increase the loading. The voltage output of the probe is measured using a digital voltmeter and is recorded manually. Displacement data and load curves are generated after the test.

The position sensor is based on the eddy current effect. Figure 4.2.1.3e shows the basic electronic setup of the probe. A DC power supply is used to provide an 18 V excitation signal. The primary probe coil produces an RF signal at 0.5 to 2.0Mhz. The secondary probe coil measures the amplitude of RF signal. When a metal target is introduced into the field the signal amplitude decreases. A proximeter is used to convert the RF signal amplitude into a DC voltage. The voltage signal produced by the probe is nearly linear in relationship to the distance between the probe and the target. Bently-Nevada probe model 19000-00-15-36-02 was used with a model 20929-2 proximeter box and 15 feet of 2789 miniature BNC cable. This system has a range of 10 to 60 mils. The voltage signal is then measured using a digital voltmeter or an oscilloscope. The Fluke 77 digital voltmeter was used for the displacement method of stiffness testing since measurements are made in a static condition. A HP3566A/67A digital oscilloscope was used to make measurements for the frequency method of stiffness testing. This digital oscilloscope consisted of a PC computer with an analog data acquisition board. A software package was used which enabled the computer to simulate the functions of a standard oscilloscope as well as providing the ability to digitally record the traces. The proximeter signal was conditioned with a

DC bias and an amplification in order to scale to ±5 V full scale with 0V at the concentric rotor magnet position.

The position sensor had to be calibrated using the pendulum rod as the target in order to accurately measure the position of the pendulum in the radial stiffness test fixture. In order to accomplish this the pendulum rod was mounted on a micrometer. The position probe was mounted to a fixed base on which the micrometer was affixed. The calibration fixture is shown in Figure 4.2.1.3f. The calibration procedure entailed measuring the output voltage of the probe as the pendulum rod is moved from a position in contact with the probe to a location out of the probe's range. The voltage / displacement relationship for the probe was measured at 187mV/mil. The probe output was less than the nominal 200mv/mil specified by the manufacture because the target was not the required diameter.

4.2.2 Maximum Load Measurement

The maximum load is a function of stiffness and stroke of the rotor / stator magnet combination. Measurements were made using the same test equipment used for the displacement technique of stiffness measurement. The rotor was loaded in 10g increments until it came into contact with the stator. The load at the rotor is equal to:

$$F_r = F_w\left(\frac{L_w}{L_r}\right)$$

where: F_r is the load at the rotor
F_w is the load at the pan

L_w is the length from the pin to the pan
L_r is the length from the pin to the center line of the rotor

This test can be performed quickly and was used as a screening criterion.

4.2.3 Stroke Measurement

The stroke of the bearing, defined as the displacement of the center magnet from the equilibrium position to the position of contact with the outer ring magnet, is determined by the sizes of the magnets which are being used. The stroke is equal to :

$$stroke = (id_s - od_r)/2$$

where: id_s is the inner diameter of the stator magnet
od_r is the outer diameter of the rotor magnet

The stroke calculation was done using the dimensions specified by the magnet manufacture. This calculation can be performed quickly and was used as a screening criterion.

4.2.4 Results

The load and stroke tests were used to screen the rotor and stator magnets. Candidate rotor and stator magnets are listed in Table 4.2.4a and Table 4.2.4.b. Two suppliers were used, however five different manufactures were represented. Rotor magnets all share a disk geometry with an outside diameter range of 0.478cm to 5.781cm and thickness between 0.160cm and 0.635cm. All stator magnets had an annular disk geometry with an outer diameter of 1.524 to 9.525cm, the inner diameter of 0.788 to 4.445cm, and thickness between 0.318 and 1.664cm. Rotor mass varied

from 0.2 to 75.9g while stator mass varied from 4.0g to 451.5g. Five different materials were used. From strongest to weakest intrinsic magnetic strength these were Neodymium Iron Boron, Ceramic 8, Ceramic 5, Ceramic 1, and Ceramic. The material specifications are included in Appendix A, Table A- 1. Different magnetic field orientations were also used depending on the manufacture.

The results of the screening tests are listed in Table 4.2.4c. Rotor magnets #1-3 were excluded from tests because their diameter was too small for the overall system. Rotor magnet #10 was excluded because its diameter was greater than the inner diameter of any stator magnet. Stator magnets #1-7 and #14 were excluded because their inner diameter was smaller than any of the remaining rotors. If the stroke of a rotor / stator combination was less than 0.100cm no test was conducted. The resultant test matrix consisted of 17 tests in which stroke and load were measured and a nominal stiffness was calculated. Stroke varied from 0.00257m to 0.01595m. Maximum load varied from 0.0572kg to .5976kg. The nominal stiffness ranged from 4.56kg/m to 78.4kg/m. Screening test minimum criteria were set at load > .100 kg, stroke > .00350m, and stiffness < 50kg/m. The load criterion was derived from the expected rotor weight. The stiffness requirement is based on preliminary testing of the ferrofluid stabilizer which indicated a target stiffness of 35kg/m to 45kg/m. Six rotor/stator combinations passed the screening test, 4-11, 4-13, 5-10, 5-13, 5-15, and 6-15. Combinations 4-11 and 5-13 were selected for further testing. Test 4-11 was nearest to the low stiffness target and had the lowest rotor magnet mass and stroke of

the set. Test 5-13 was nearest to the upper target stiffness and had a large stroke. Combination 4-11 will be referred to as radial bearing #1 and combination 5-13 will be referred to as radial bearing #2.

Frequency method stiffness measurements were conducted on radial bearing #1 and #2. Each pair was tested twice with the stator magnet rotated 90° for the second test. This method enabled a measurement of the inhomogeneity of the magnets. The time and frequency response graphs for the four tests are included in Appendix A Figure A-1 to A-8. The calculated stiffness, damping coefficient and natural frequency are shown in Table 4.2.4d along with the measured natural frequency and important parameters of the vibration model.

Six displacement method tests were conducted, four on radial bearing #1 and two on radial bearing #2. The stator magnet was rotated 90° between test #2 and #3 on bearing #1 and between test #1 and #2 on bearing #2. A typical data set is shown in Table 4.2.4e. The complete results are included in Appendix A Table A-2 to A-7. The actual probe voltage is shown in the Disp(V) column. The displacement in inches and meters are calculated using the probe calibration data. The weight of the rod, pan, and gram weights are listed under Wgt(kg). The load on the bearing is calculated from the ratio of the magnet and weight pan torque arm lengths (0.519). Analytical curve fit and stiffness results are listed and will be discussed in the following section.

4.2.5 Analysis

The displacement method stiffness data warranted a numerical model in order to find force and stiffness as a function of rotor magnet displacement. The model that was expected to fit the data the best was a second order polynomial fit. The reason is that the concentric rotor / stator magnet geometry is expected to have a force response which is analogous to two point charges. It is well known that this is an inverse square law. In order to confirm the theory 1st, 2nd, and 3rd order polynomial fits were generated for radial bearing #1, test #1. The results, shown in Table 4.2.5a, indicate that our hypothesis is correct since the correlation coefficient R is 0.9999 for the second order model. Second order models were generated for all six displacement method tests. The first derivative of these fits yields a stiffness model. The coefficients for the force and stiffness models are shown in Table 4.2.5b,c. Graphical representations of the models applied to individual tests are included in Appendix A, Table A-2 to A-7. The force and stiffness models for all tests on radial bearing #1, and #2 are plotted in Figure 4.2.5a,b. The displacement model indicates a center stiffness of 20kg/m for bearing #1 and 18kg/m for #2. The maximum stiffness for bearing #1 is 48kg/m while bearing #2 is 58kg/m. The bearing can be compared to a hardening spring, with an increase of 140% for bearing #1 and 220% for bearing #2 from the center stiffness to the maximum stiffness.

4.3 Discussion

Load, stroke, and stiffness measurements using frequency and displacement technique are made. The most important information ascertained is the stiffness as a function of the radial displacement for bearings #1 and #2. However, the amount of information gathered enables us to make some additional observations.

The first topic is the accuracy of the displacement probe measurements. The displacement data included in Appendix A indicates a measured maximum stroke of 0.00371m for bearing #1 and 0.00565m for bearing #2. Micrometer measurements on bearing #1 and #2 indicate an actual stroke of 0.00389m and 0.00550m. This indicates an inaccuracy of approximately 5%. Note that a comparison of the maximum displacement in bearing #1 test #1 and #2 indicate a repeatability of 99.5% if the rotor magnet is not replaced. This leads to the conclusion that the direction in which the pendulum rod is installed has an effect on the probe output. This is likely because the rod diameter is only 40% of that specified by the manufacturer. If the rod position moves slightly off center during the rotor magnet installation the errors that have been measured will be produced.

The second consideration is the inhomogeneity in the magnets. This is a result of manufacturing defects which lead to higher concentrations of oriented magnetic particles in certain parts of the magnet. The effect of this is a difference in the force and stiffness properties of a rotor / stator magnet combination if they are rotated relative to one another. These tests were conducted using both the frequency

and displacement methods indicating a 6% and 9% difference respectively. This difference must be considered in determining the safety factor of the overall design.

The accuracy of the analytical vibration model is verified by the frequency test results. The natural frequency calculated using the model is compared to the frequency determined by performing a fast fourier transform (FFT) on the displacement trace. The FFT accuracy is 0.125 Hz. The worst case error is 0.63 Hz which is 3.27%.

The correlation coefficient of the second order numerical model for the displacement method force results is greater than 0.9990 for all cases. This indicates a good numerical fit, as well as confirming that this type of magnet geometry will have an inverse square law force. The maximum stiffness model error between tests was 8.2%. This indicates that we can proceed with the overall design.

Rotor Magnetic Disks							
#	OD (cm)	L (cm)	Mass (g)	Material	Orientation	Supplier	Part#
1	0.478	0.160	0.2	NbFeB	LD	Edmond	M38,428
2	0.635	0.318	0.7	NbFeB	LD	Edmond	M38,429
3	0.953	0.254	1.2	NbFeB	LD	Edmond	M35,104
4	1.257	0.635	3.8	Ceramic 8	Length	Dexter	646200
5	1.956	1.016	15.0	Ceramic 8	Length	Dexter	643610
6	2.540	0.635	16.8	Ceramic 1	Isotropic	Dexter	1-25
7	2.921	0.635	31.3	NbFeB27	Length	Dexter	NCA64A415
8	3.175	0.635	23.6	Ceramic 1	Isotropic	Dexter	F50A625
9	3.810	0.825	45.9	Ceramic 8	Length	Dexter	P68C0325B
10	5.781	0.635	75.9	Ceramic 1	Isotropic	Dexter	28156

Table 4.2.4a

Stator Magnetic Annular Disks								
#	OD (cm)	ID (cm)	L (cm)	Mass (g)	Material	Orienta-tion	Supplier	Part#
1	1.524	0.788	0.635	4.0	Ceramic 1	Isotropic	Dexter	398
2	1.905	0.688	0.635	7.3	Ceramic 1	Isotropic	Dexter	120B
3	2.741	1.516	0.635	12.0	Ceramic 1	Isotropic	Dexter	416
4	2.858	0.953	0.635	16.2	Ceramic 1	Isotropic	Dexter	121
5	3.010	1.270	0.635	18.0	Ceramic 5	Length	Dexter	P65A6040B
6	3.175	1.270	0.635	18.8	Ceramic	LD	Edmond	M35,746
7	3.810	1.270	0.475	23.3	Ceramic 8	Length	Dexter	646330
8	4.445	1.905	0.635	35.5	Ceramic	LD	Edmond	M38,670
9	4.445	2.065	0.318	22.2	Ceramic	LD	Edmond	M31,570
10	4.826	3.050	0.348	18.8	Ceramic 8	Length	Dexter	29784
11	5.334	2.032	0.699	65.6	Ceramic 5	Length	Dexter	65A0053B
12	6.045	2.578	0.635	67.7	Ceramic 1	Isotropic	Dexter	191-.250
13	7.112	3.056	0.838	137.5	Ceramic 5	Length	Dexter	17367
14	7.620	0.953	0.762	154.7	Ceramic 1	Isotropic	Dexter	132-.300
15	9.525	4.445	1.664	451.5	Ceramic 8	Length	Dexter	27593

Table 4.2.4b

Screening Test Matrix

Stator	Rotor	4	5	6	7	8	9
8	Stroke(m)	.00325	X	X	X	X	X
	Load(kgf)	0.0675					
	Stiffness(kgf/m)	20.7					
9	Stroke(m)	.00404	.00056	X	X	X	X
	Load(kgf)	0.0935	X				
	Stiffness(kgf/m)	23.1					
10	Stroke(m)	.00897	.00549	.00257	.00066	X	X
	Load(kgf)	0.0987	0.1403	0.0572	X		
	Stiffness(kgf/m)	11.0	25.5	22.3			
11	Stroke(m)	.00389	.00038	X	X	X	X
	Load(kgf)	0.1247	X				
	Stiffness(kgf/m)	32.1					
12	Stroke(m)	.00660	.00312	.00020	X	X	X
	Load(kgf)	0.0831	0.1091	X			
	Stiffness(kgf/m)	12.6	35.0				
13	Stroke(m)	.00899	.00550	.00259	.00069	X	X
	Load(kgf)	0.1559	0.2546	0.0987	X		
	Stiffness(kgf/m)	17.3	46.29	39.1			
15	Stroke(m)	.01595	.01245	.00953	.00762	.00635	.00318
	Load(kgf)	0.0727	0.3898	0.1351	.5976	0.0727	0.2806
	Stiffness(kgf/m)	4.56	31.3	14.2	78.4	11.4	88.2

Table 4.2.4c

Frequency Method Test Results

Bearing	Test	k (kgf/m)	c (rad/s)	ω_n (1/s)	ω_{meas} (1/s)	b ($1/s^2$)	R (V)
1	1	16.13	13.62	19.32	19.5	419.7	1.711
	2	17.83	19.95	20.48	20.25	519.0	1.813
2	1	25.01	9.599	19.88	19.25	418.4	3.949
	2	25.67	13.32	18.78	18.75	441.7	2.749

Table 4.2.4d

Radial Bearing #1

Rotor: 1.257cm O.D. x 0.635cm 3.8g
Stator: 5.335cm O.D. / 2.032cm I.D. x 0.699cm 65.6g
Test : #1 Method: Displacement

Disp(V)	Disp(in)	Disp(m)	Wgt(kg)	Load(kg)	2(O)Fit(kg)	Stiff(kg/m)
9.8	0	0	0	0	0.0002	19.809
			0.04	0.0208		
11.65	0.069799	0.001773	0.09	0.0468	0.046056	31.92136
11.83	0.07659	0.001945	0.1	0.0519	0.051664	33.09985
12	0.083004	0.002108	0.11	0.0572	0.057147	34.21288
12.16	0.08904	0.002262	0.12	0.0623	0.062473	35.26044
12.31	0.0947	0.002405	0.13	0.0675	0.067612	36.24252
12.46	0.100359	0.002549	0.14	0.0727	0.072893	37.2246
12.61	0.106018	0.002693	0.15	0.0779	0.078314	38.20669
12.75	0.111301	0.002827	0.16	0.0831	0.083502	39.1233
12.89	0.116583	0.002961	0.17	0.0883	0.088812	40.03991
13.02	0.121487	0.003086	0.18	0.0935	0.093853	40.89105
13.15	0.126392	0.00321	0.19	0.0987	0.099001	41.74218
13.27	0.13092	0.003325	0.2	0.1039	0.103846	42.52785
13.39	0.135447	0.00344	0.21	0.1091	0.108782	43.31352
13.51	0.139975	0.003555	0.22	0.1143	0.113808	44.09918
13.61	0.143747	0.003651	0.23	0.1195		
13.61	0.143747	0.003651	0.24	0.1247		
13.61	0.143747	0.003651	0.25	0.1299		

Table 4.2.4e

Polynomial Fit Accuracy

Order	x^0	x^1	x^2	x^3	R
1	-.0081	37.769			0.9828
2	0.0002	19.809	3416		0.9999
3	7e-7	23.626	640.81	495300	1.0000

Table 4.2.5a

Coefficients of Force Model					
Bearing	Test	x^0	x^1	x^2	R
1	1	0.0002	19.809	3416	0.9999
	2	0.0001	18.776	3719.4	0.9998
	3	-0.0002	21.588	3676.3	0.9999
	4	0.0002	20.335	3866.1	0.9998
2	1	-0.0009	17.952	3490.1	0.9997
	2	-0.0001	17.126	3727.7	0.9990

Table 4.2.5b

Coefficients of Stiffness Model			
Bearing	Test	x^0	x^1
1	1	19.809	6832
	2	18.776	7438.8
	3	21.588	7352.6
	4	20.335	7732.2
2	1	17.952	6980.2
	2	17.126	7455.4

Table 4.2.5c

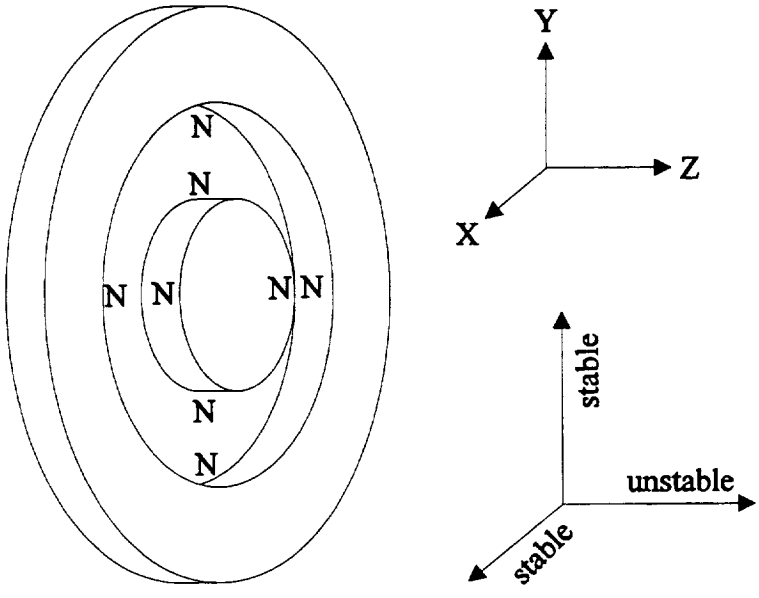

Figure 4.1a - Configuration of radial permanent magnet bearing

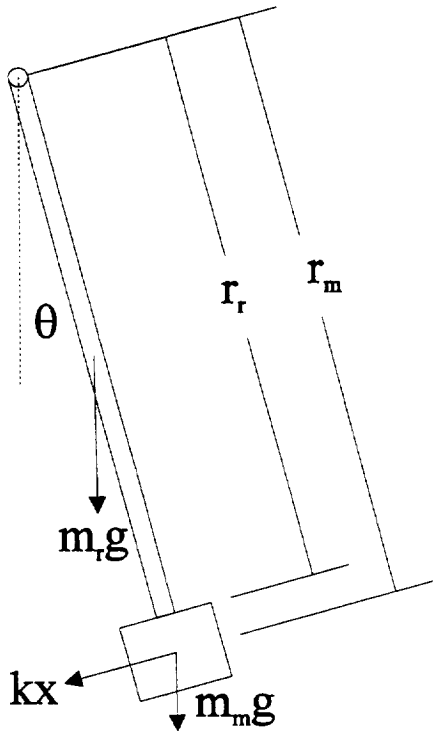

Figure 4.2.1.1a - Schematic representation of frequency test rig

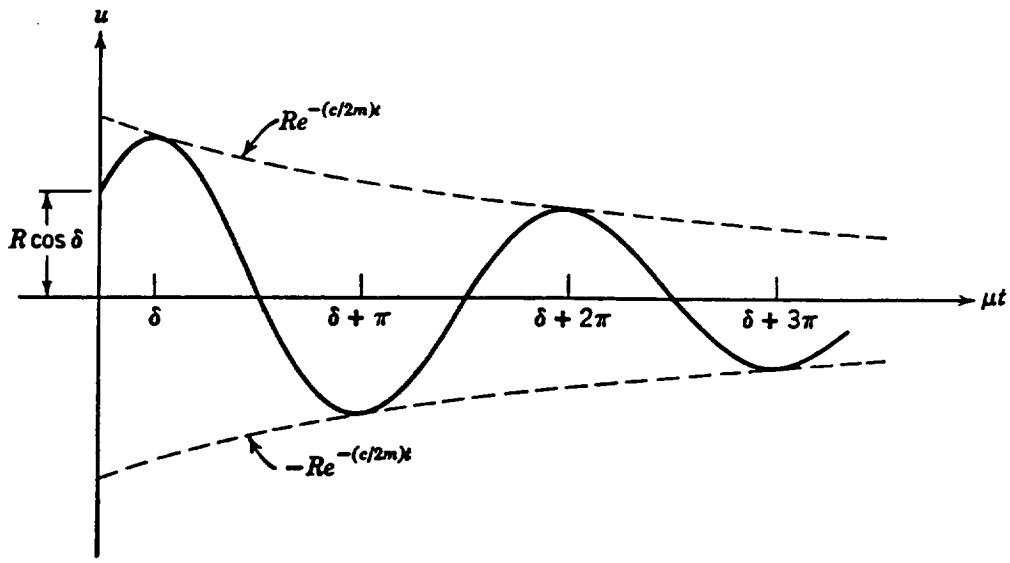

Figure 4.2.1.1b - Solution of characteristic equation for underdamped case

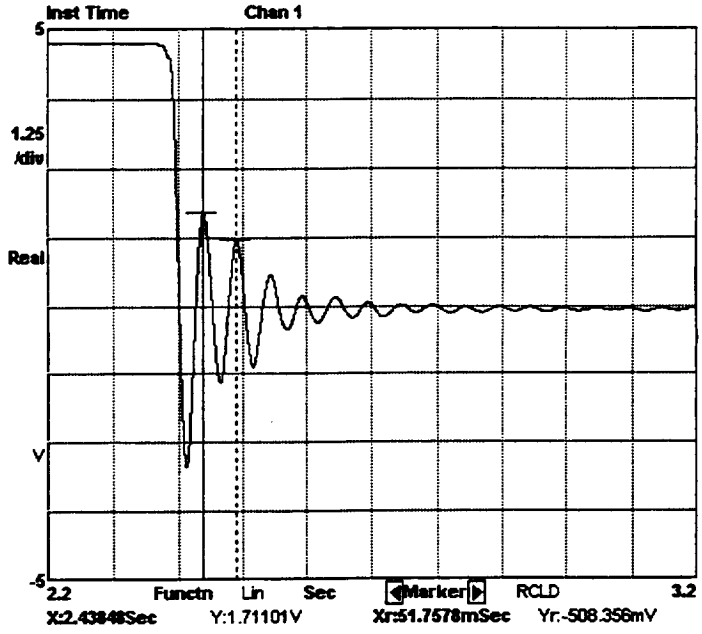

Figure 4.2.1.1c - Typical time trace of position probe voltage

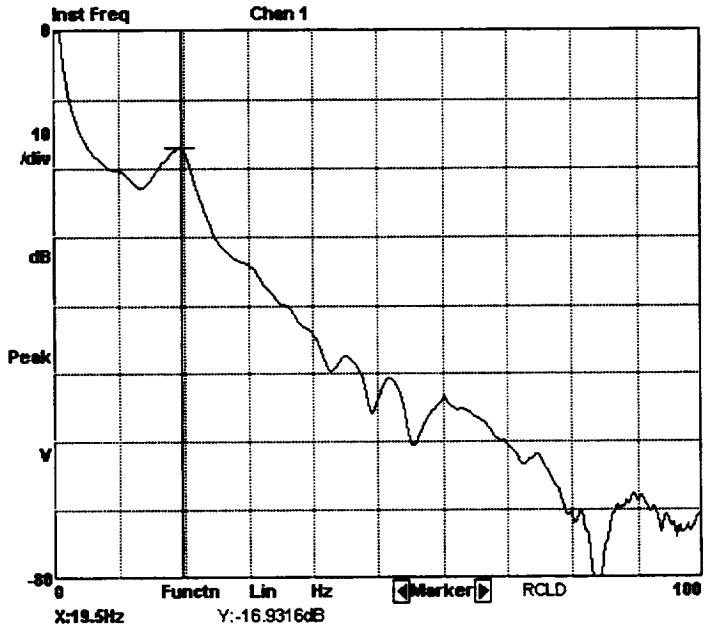

Figure 4.2.1.1d - Typical frequency spectrum of position probe output

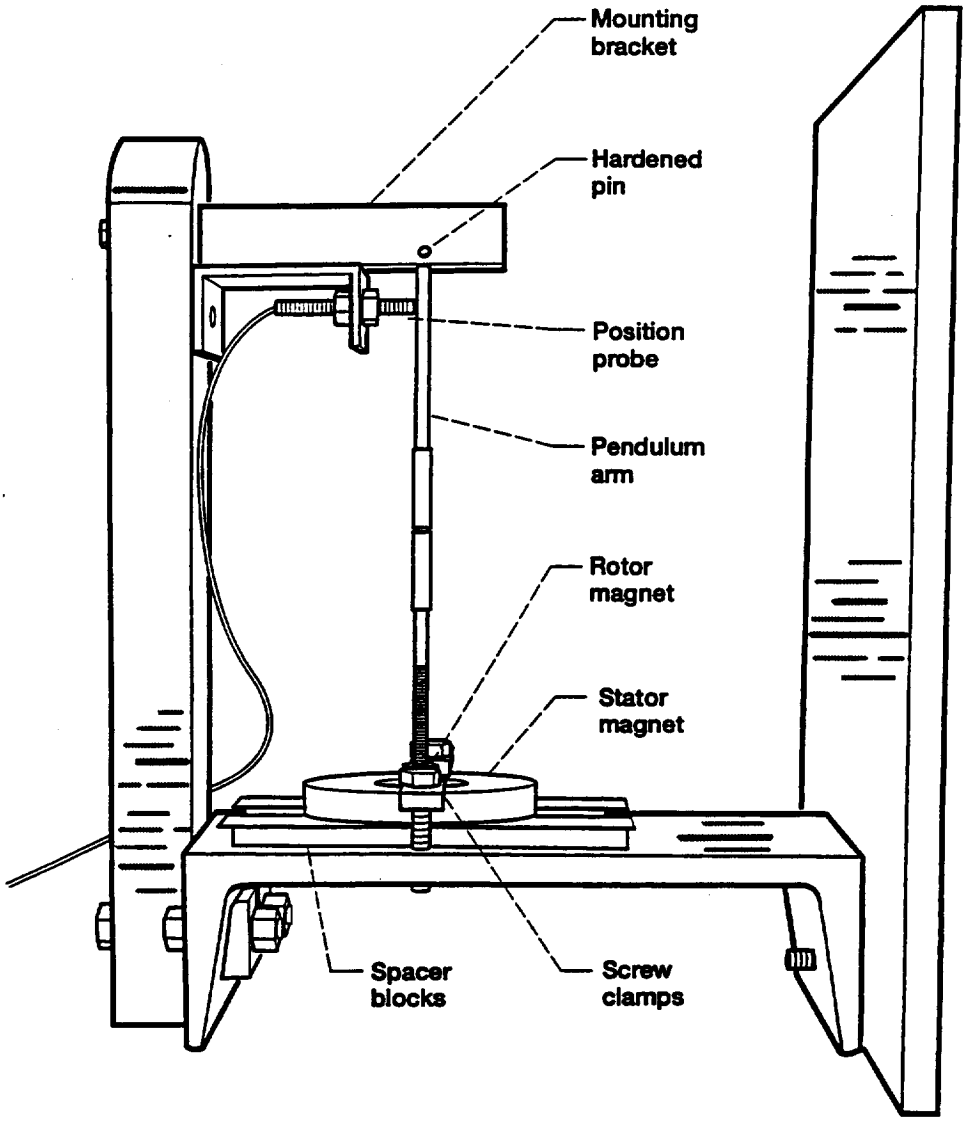

Figure 4.2.1.3a - Radial bearing tester oriented for frequency test method

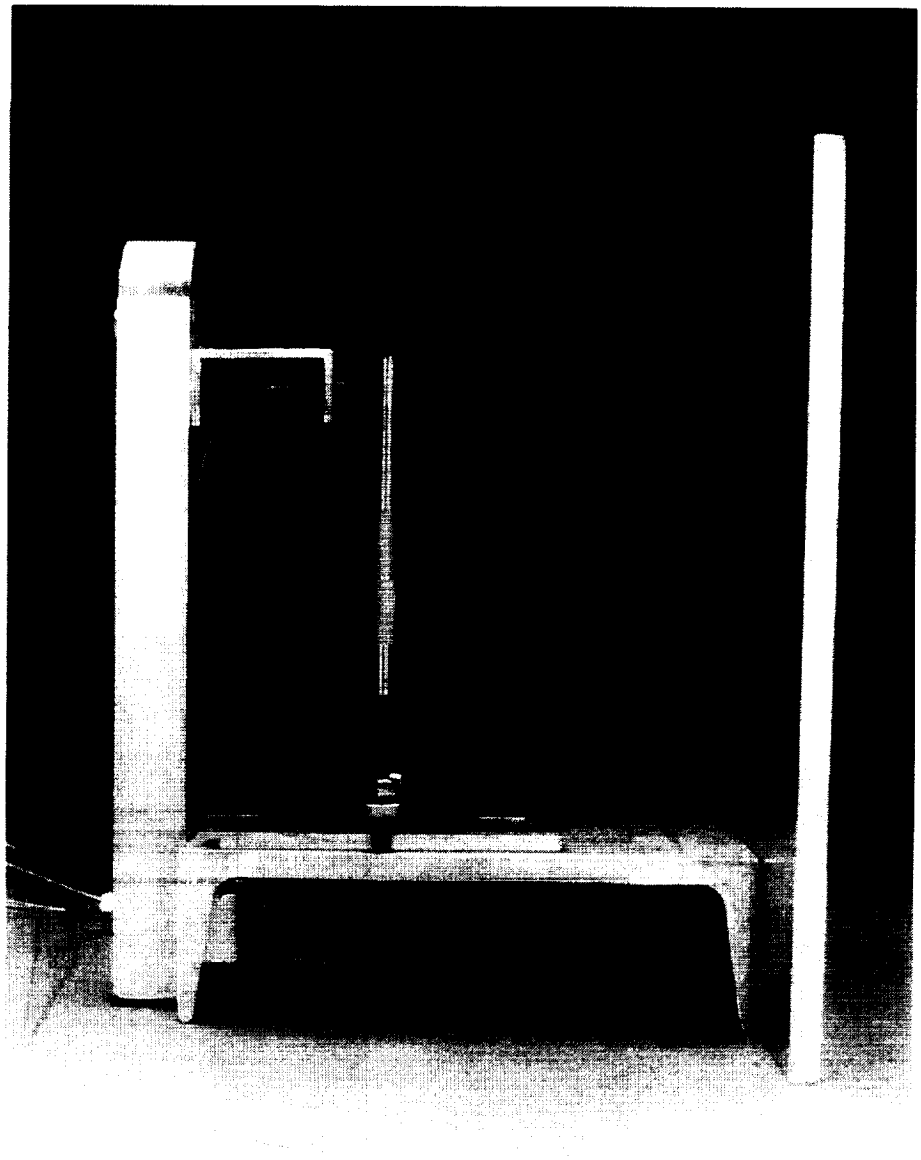

Figure 4.2.1.3b - Picture of radial bearing tester oriented for frequency test method

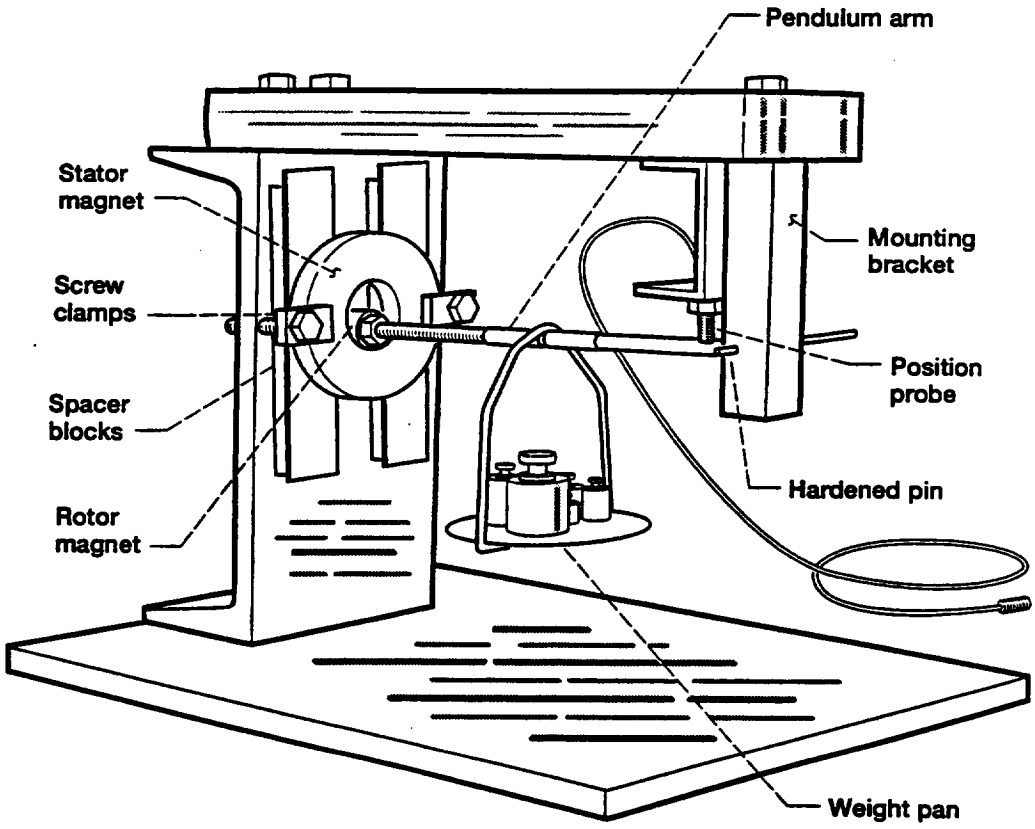

Figure 4.2.1.3c - Radial bearing tester oriented for displacement test method

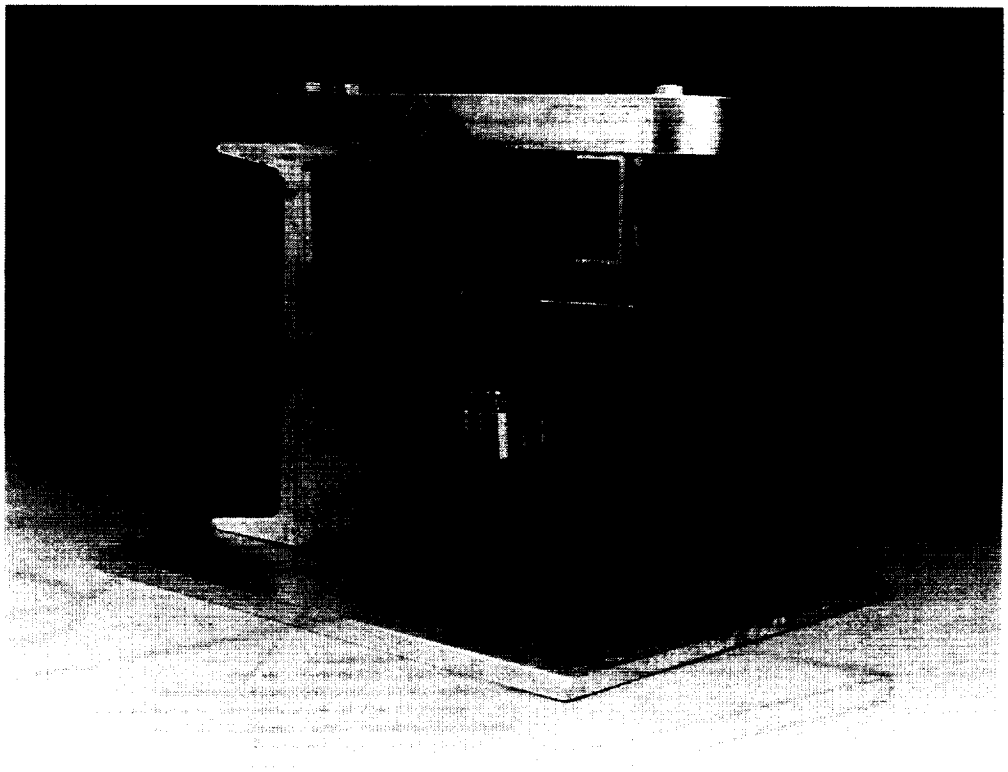

Figure 4.2.1.3d - Picture of radial bearing tester oriented for displacement test method

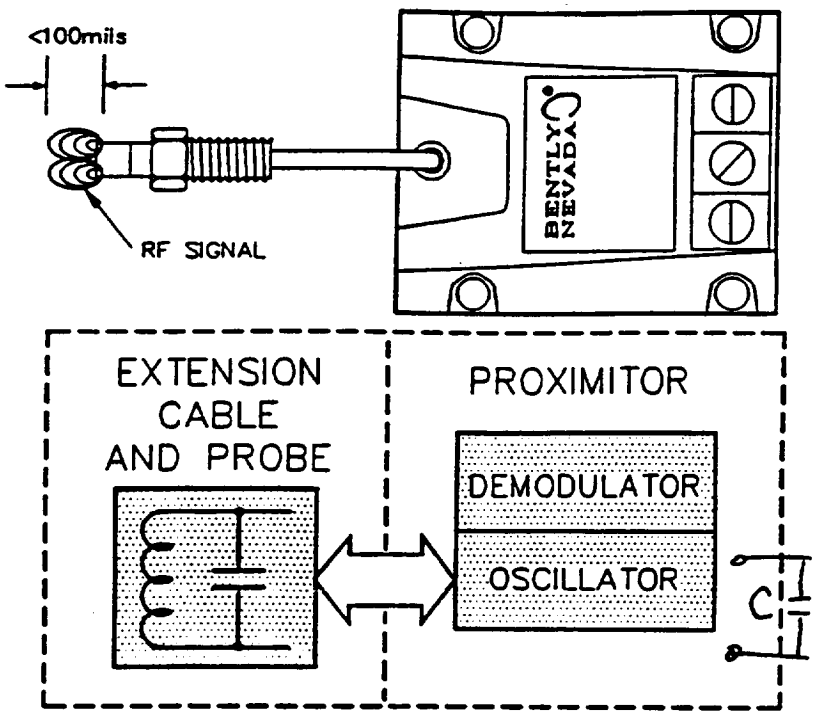

Figure 4.2.1.3e - Electronic configuration of position probe

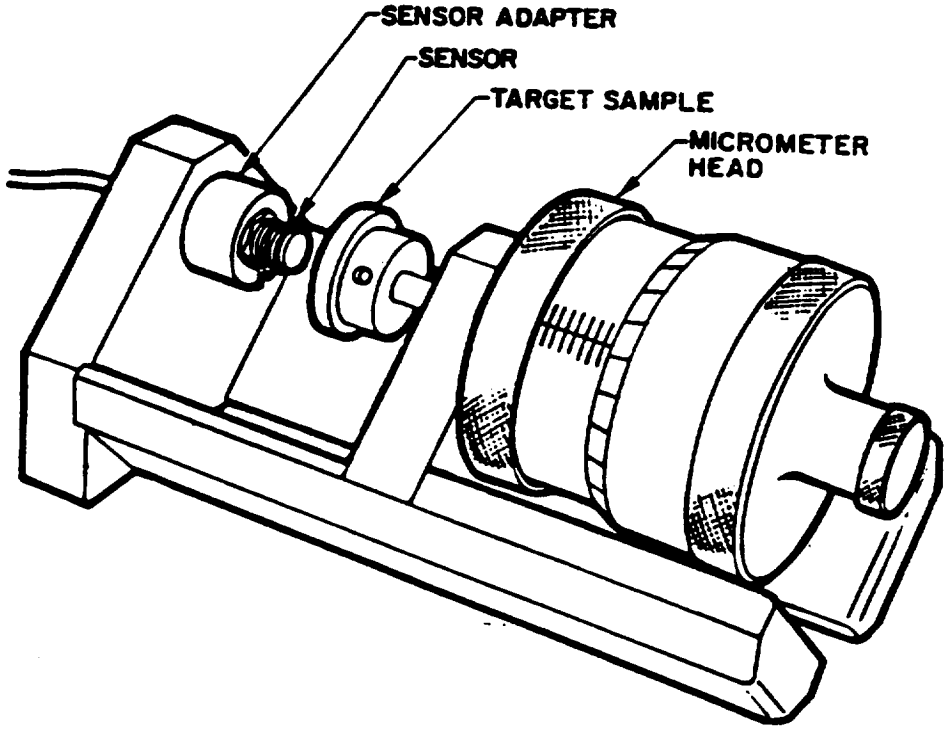

Figure 4.2.1.3f - Position probe calibration fixture

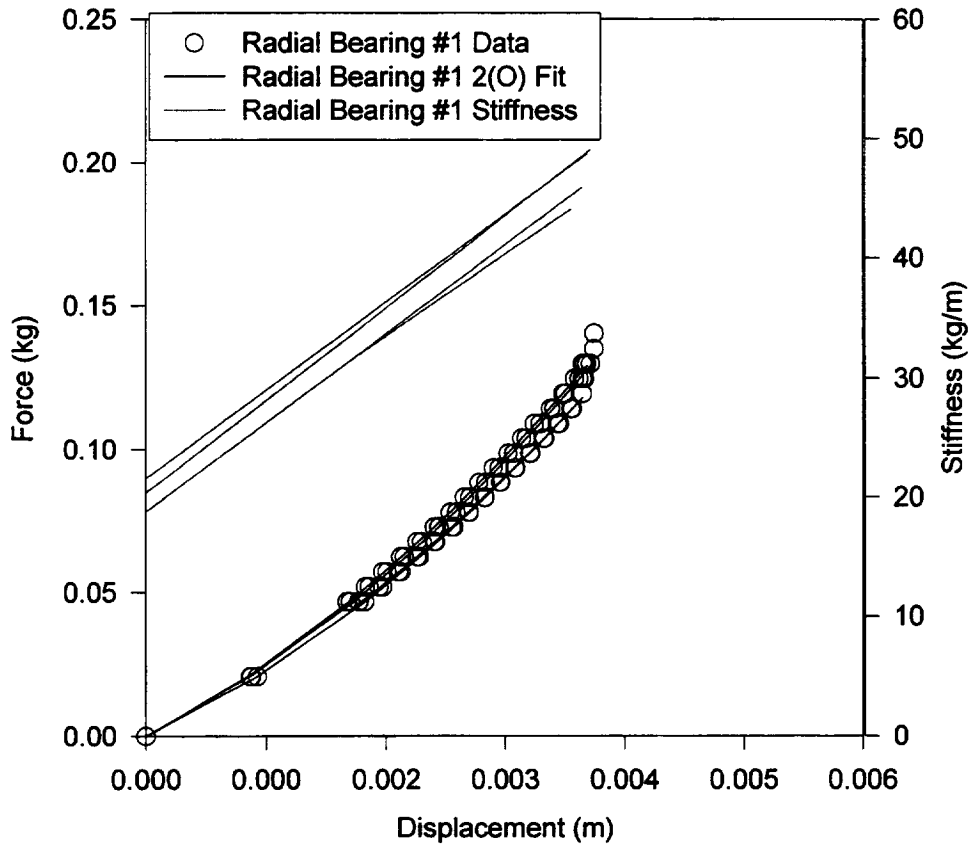

Figure 4.2.5a - Force and stiffness model for radial bearing #1

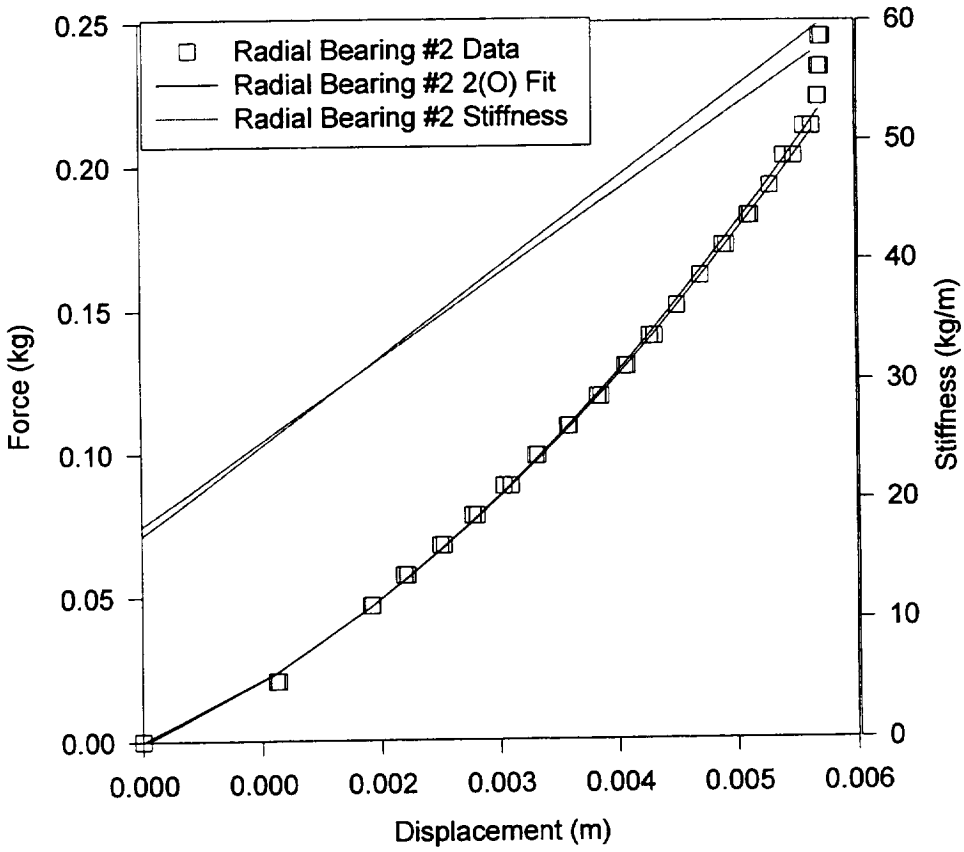

Figure 4.2.5b - Force and stiffness model for radial bearing #2

Chapter 5: Ferrofluid Stabilizer Design

5.1 Basic Design

The configuration used for the ferrofluid stabilizer consists of a magnetic rotor disk immersed within a non magnetic reservoir containing magnetic fluid (Figure 5.1a). The system is stable in all three axes. In the absence of external forces the magnet will seek equilibrium in the center of the reservoir at a depth where the magnetic force equals the sum of the gravitational and buoyant forces. If the free surface is sufficiently distant from the magnet such that the field strength at the free surface is much less than the strength at the magnetic surface, the magnetic force in the z direction can be represented as a function of the gap between the magnet and the reservoir bottom. Restoring forces also exist in the x-y plane, however the goal is to maximize the z interaction.

5.2 Experimental Stiffness Measurement

The experimental objective is to measure the z direction magnetic force as a function of gap between the magnet and the reservoir. Forces in the x-y plane will not be measured, however the experiment will be conducted using a symmetrical system to ensure that the magnet is in stable x-y equilibrium during the z measurement.

5.2.1 Procedure

The stiffness measurement technique used for the ferrofluid stabilizer consists of measuring the force exerted by the permanent magnet interaction with the ferrofluid as a function of the distance between the bottom of the ferrofluid reservoir and the lower surface of the magnet. The ferrofluid reservoir is designed with an inner diameter significantly larger than the outer diameter of the magnet to be tested. This was done in order to minimize the effects of the wall interaction on the measurement, reducing it to a one dimensional problem. The reservoir was also made deep enough that the interaction force between the magnet moves and the free surface of the ferrofluid would be negligible when the magnet is near the bottom of the reservoir.

The experimental procedure consists of incrementally lowering the test magnet through the ferrofluid reservoir and recording force measurements. The test began with the test magnet approximately 1" above the bottom of the reservoir. The magnet was initially lowered in increments of .050" until the force exerted increased at a rate of more than 20g per increment. The magnet continued to be lowered at increments of .025" and then .005" until the magnet came in contact with the bottom of the reservoir. Due to the highly opaque nature of the ferrofluid it was impossible to see the magnet in contact with the bottom of the reservoir however the force measurement increased dramatically indicating a solid-solid interaction. After contact with the bottom of the reservoir the procedure was reversed in order to

confirm the force measurements made on the down stroke. Any hystresis effect could also be detected using this bi-directional measurement technique.

5.2.2 Test Fixture

A test fixture was assembled to measure the stiffness of the ferrofluid stabilizer. The test fixture is based on a concept described by Barkov and Fertman[8]. The fixture is designed to displace a magnet within a ferrofluid reservoir and measure the force required. Figure 5.2.2a and Figure 5.2.2b show the test setup schematically and pictorially. The magnet to be tested is attached to a threaded rod using a nut attached to the magnet with a two part epoxy resin. The rod is mounted in a micrometer which has a 1.25" travel and is graduated in .001" increments. The micrometer is attached to the base plate via a mounting fixture. The base plate and the mounting fixtures are both composed of a nonmagnetic aluminum alloy. An electronic balance is used to measure the force exerted by the magnet in the ferrofluid reservoir. A thick non magnetic spacer was introduced between the ferrofluid reservoir and the balance in order to eliminate electronic problems and stop the force interaction between the magnet and the magnetic components of the balance. The reservoir was filled with 10cm of ferrofluid.

5.2.3 Results

Two types of magnetic disks were tested in a standard magnetic fluid. The magnetic fluid was Ferrofluidics Model # APG-027. This fluid has a synthetic ester base oil with a saturation magnetization of 325 gauss and a viscosity of 130cp at 27°C. Two magnet configurations manufactured by Magnet Sales & Mfg. Co., both utilized Neodymium-Iron-Boron 39H whose properties and demagnetization curve are shown in Appendix B Figure B-1. The first magnet consisted of a disk with an axially oriented magnetic field (Figure 5.2.3a). The second type of magnet was constructed of a series of concentric magnetic rings. Each ring had an axial magnetic orientation, however the polarity was reversed between each ring (Figure 5.2.3b). Both disks had a diameter of 3.00" and a thickness of 0.100".

Two tests were conducted on stabilizer #1 and three tests were conducted on stabilizer #2. Typical data is shown in Table 5.2.3a. Position is the direct measurement made using the micrometer. Corrected position is the gap between the magnet and the reservoir which is calculated after the test. Force is the recorded measurement from the electronic balance. The force and stiffness curve fit data shown will be discussed in the next section. The data collected is shown in Appendix B Table B-1 to B-5.

5.2.4 Analysis

A numerical model was generated to fit the force displacement curves for the ferrofluid stabilizer tests. A polynomial model was chosen, however it was not clear which order should be expected. Rosensweig[9] indicates that an inverse fourth power

relationship exists as the gap becomes large, however a more complex function governs close interactions. Polynomial models of order one to six were generated for stabilizer #1 test #1. Using the correlation coefficient R as an indication of accuracy shows that there is a diminishing return when the model order exceeds five. A concern exists that the model will overfit the data, however the number of data points exceeds the order of the polynomial by a factor of three, thereby minimizing this problem.

The results of the fifth order polynomial fit are shown Table 5.2.4b. The stiffness model is the first derivative of the force relationship. The coefficients of the fourth order stiffness model are shown in Table 5.2.4c. Graphical representations of the models applied to each data set are included in Appendix B Table B-2 to B-6. The combined force and stiffness results for stabilizer #1 and #2 are shown in Figure 5.2.4a,b. Maximum force output for each stabilizer was 1.2kg at zero gap. Stiffness results were similar for both stabilizers throughout the displacement curve. Stiffness at 0.015m gap was 40kg/m and increased non-linearly to 260kg/m at zero gap. Tests were repeatable within 2% for stabilizer #1, and within 10% for stabilizer #2.

5.3 Discussion

The force and stiffness measurements for the two stabilizer units were completed successfully. It is interesting to note that the plain disk (stabilizer #1) and concentric ring geometry (stabilizer #2) exhibited similar performance. The goal of

the concentric ring design is to have a high magnetic flux concentration near the surface of the magnet and a lower flux at a large gap. This would result in a system which has more stiffness increase as the gap approaches zero in comparison with the plain disk geometry. The measurements do not clearly show whether this happens. Scattter in the multiring data, especially close to the zero gap position, is to severe. Visual observations of the free surface shape of ferrofluid around stabilizer #1 and #2 indicated that the actual magnetic fields are similar. Further consideration of the design of stabilizer #2 indicates that the concentric rings should not increase linearly in diameter. Each ring should contain an equal amount of magnetic material. Stabilizer #2 should be redesigned with concentric rings which have an inverse square diameter profile.

Repeatability of measurements for stabilizer #1 was high however a greater margin of error existed in stabilizer #2 measurements. Detailed examination of the data in Appendix B for stabilizer #2 indicates that the force profile did not continue to increase when the gap went to zero. As the test magnet continued to be lowered the force would increase and decrease. After a number of oscillations the force would continue to increase. Since force was used as the indicator of zero gap, it was difficult to determine when the magnet came in contact with the reservoir. The data was processed with the first contact being considered zero gap, however this resulted in high error. It must be noted that the test magnet rotated with the micrometer as it lowered through the reservoir. The force profile seems to indicate the bottom of the

reservoir and the face of the magnet were not parallel. As the magnet neared the bottom of the reservoir only certain portions made contact, and that contact point moved as the magnet continued to be lowered. These tests were not repeated since the measurement accuracy attained was sufficient.

Ferrofluid Stabilizer #1

Rotor: 3.0"x0.10 Disk
Stator: 0.050" Clearance
Test : #1 Method: Displacement

Position(in)	CorrPos(in)	Position(m)	Force(kg)	5(O)Fit(kg)	Stiff(kg/m)
1	0.625	0.015875	0	-0.00303	-42.5239
0.95	0.575	0.014605	0.033	0.037723	-27.683
0.9	0.525	0.013335	0.068	0.068972	-25.6921
0.85	0.475	0.012065	0.106	0.102958	-30.5178
0.8	0.425	0.010795	0.149	0.145337	-37.8195
0.75	0.375	0.009525	0.198	0.19733	-44.9488
0.7	0.325	0.008255	0.255	0.25788	-50.9502
0.65	0.275	0.006985	0.32	0.325795	-56.5608
0.6	0.225	0.005715	0.399	0.4019	-64.2102
0.55	0.175	0.004445	0.497	0.49119	-78.0206
0.525	0.15	0.00381	0.539	0.544006	-88.9872
0.5	0.125	0.003175	0.62	0.604971	-103.807
0.475	0.1	0.00254	0.672	0.676836	-123.471
0.45	0.075	0.001905	0.769	0.763018	-149.076
0.425	0.05	0.00127	0.856	0.867666	-181.826
0.4	0.025	0.000635	0.991	0.995723	-223.029
0.375	0	0	1.16	1.153	-274.1
0.374			1.14		
0.373			1.174		
0.372			1.213		
0.371			1.286		
0.37			1.52		
0.367			1.719		

Table 5.2.3a

Polynomial Fit Accuracy								
Order	x^0	x^1	x^2	x^3	x^4	x^5	x^6	R
1	0.8896	-65.18						0.9008
2	1.0503	-139.6	4843.6					0.9846
3	1.1169	-200.3	14975	-4.32e5				0.9971
4	1.1416	-241.3	27968	-1.76e6	4.265e7			0.9991
5	1.153	-274.1	4.44e4	-4.70e6	2.561e8	-5.42e9		0.9997
6	1.158	-296.2	6.071e4	-9.12e6	7.997e8	-3.6e10	6.54e11	0.9998

Table 5.2.4a

Coefficients of Force Model								
Stabilizer	Test	x^0	x^1	x^2	x^3	x^4	x^5	R
1	1	1.153	-274.1	4.44e4	-4.70e6	2.56e8	-5.42e9	0.9997
	2	1.159	-279.5	4.57e4	-4.82e6	2.60e8	-5.46e9	0.9998
2	1	.8234	-230.3	4.69e4	-6.25e6	4.22e8	-1.10e10	0.9998
	2	.6770	-214.4	5.31e4	-8.76e6	7.25e8	-2.29e10	0.9996
	3	1.193	-600.9	1.83e5	-2.91e7	2.18e9	-6.17e10	0.9987

Table 5.2.4b

Coefficients of Stiffness Model							
Stabilizer	Test	x^0	x^1	x^2	x^3	x^4	R
1	1	-274.1	8.898e4	-1.411e7	1.024e9	-2.711e10	0.9997
	2	-279.5	9.154e4	-1.446e7	1.042e9	-2.731e10	0.9998
2	1	-230.3	9.376e4	-1.874e7	1.688e9	-5.505e10	0.9998
	2	-214.4	1.062e5	-2.629e7	2.898e9	-1.143e11	0.9996
	3	-600.9	3.658e5	-8.721e7	8.736e9	-3.085e11	0.9987

Table 5.2.4c

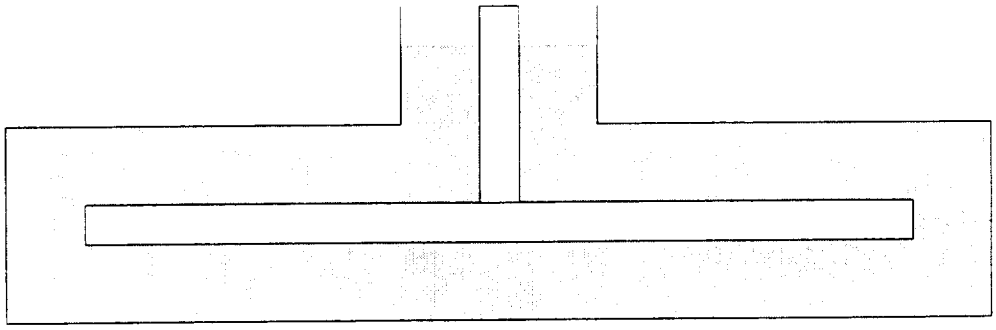

Figure 5.1a - Magnet in ferrofluid

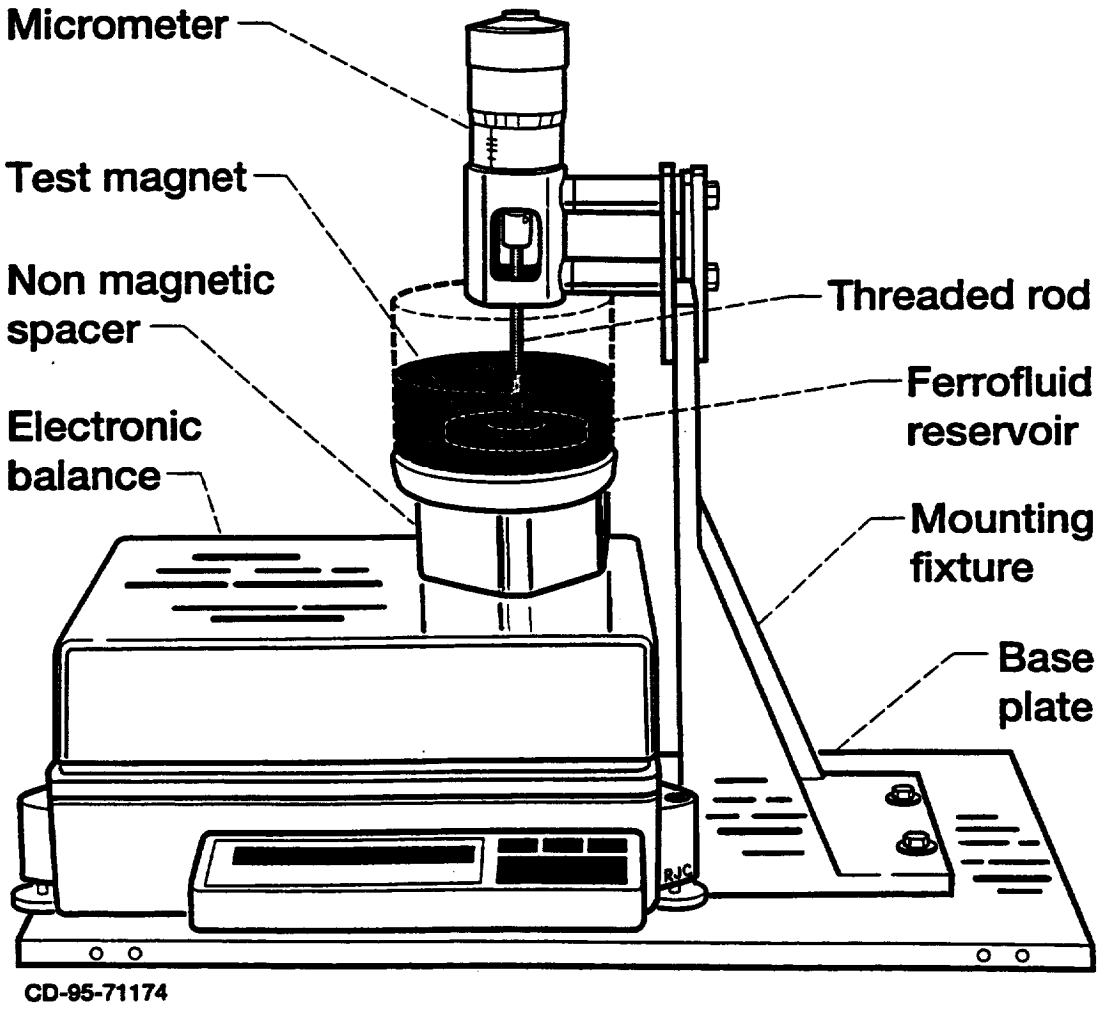

Figure 5.2.2a - Ferrofluid stabilizer test fixture

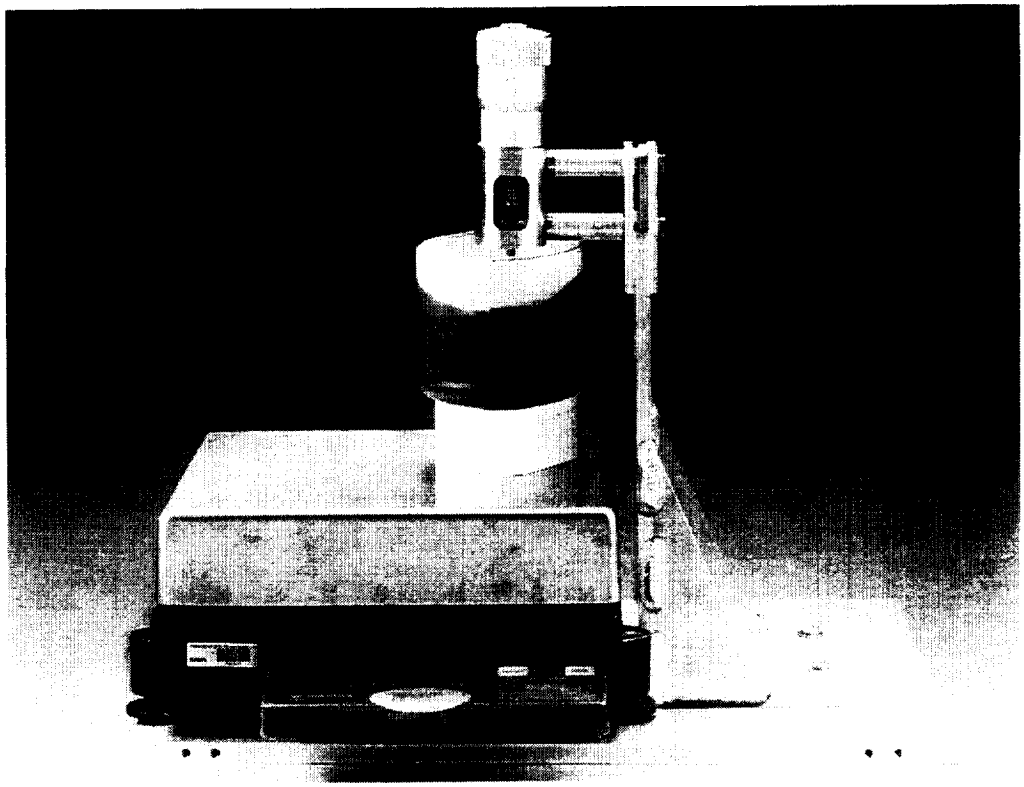

Figure 5.2.2b - Picture of ferrofluid stabilizer test fixture

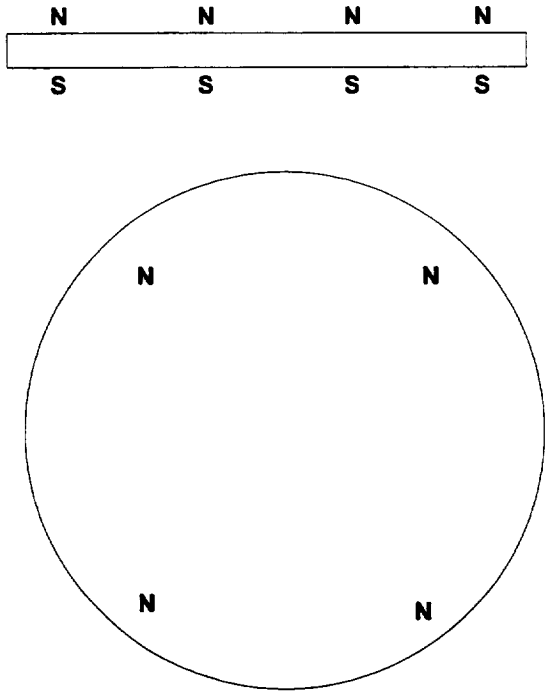

Figure 5.2.3a - Magnetic disk with axial field orientation

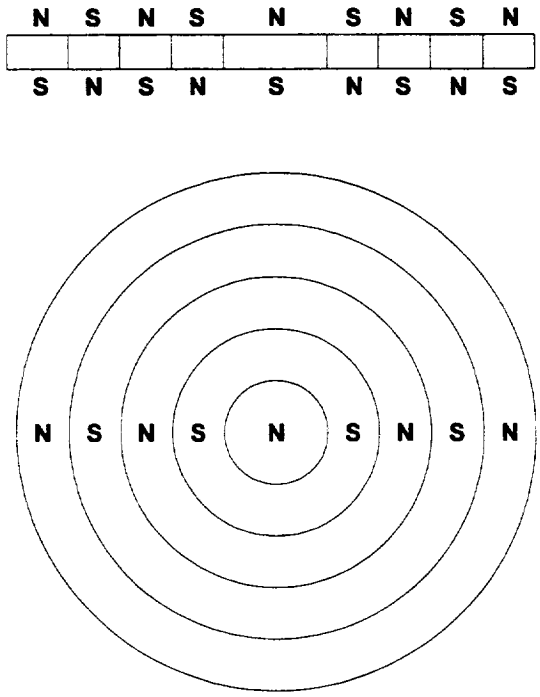

Figure 5.2.3b - Concentric ring magnets with reverse polarity axial field

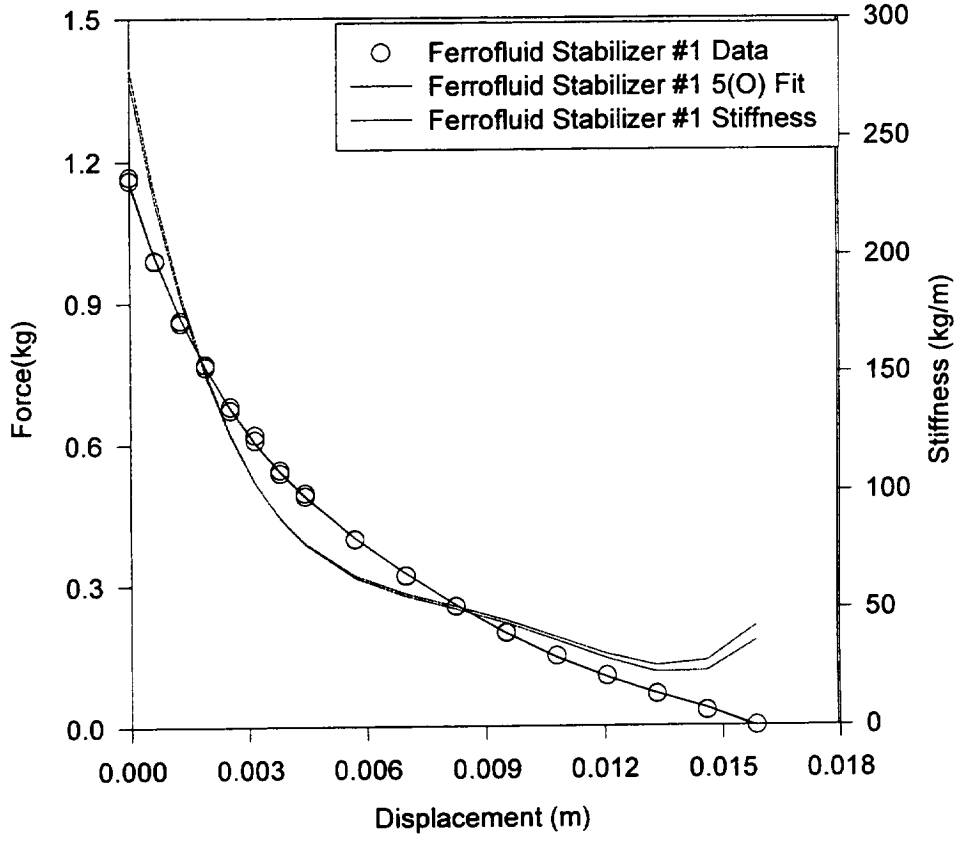

Figure 5.2.4a - Force and stiffness model for ferrofluid stabilizer #1

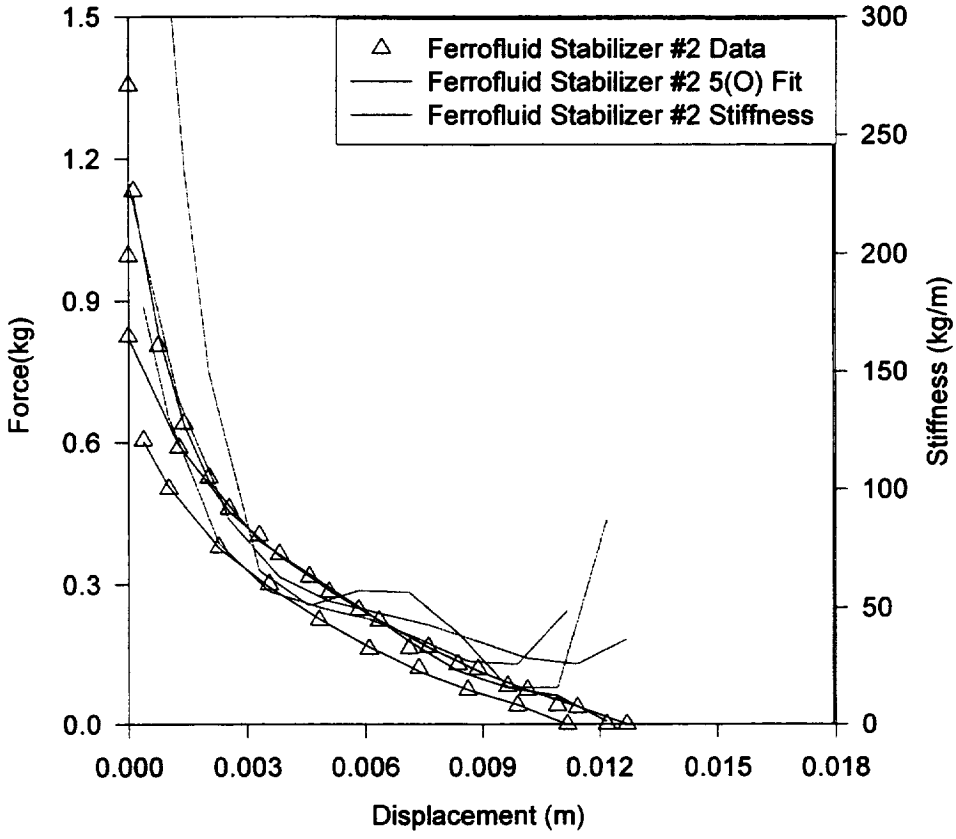

Figure 5.2.4b - Force and stiffness model for ferrofluid stabilizer #2

Chapter 6: Prototype design

6.1 Analytical Design

The prototype design was determined analytically based on the governing equations and magnet test results. The purpose of the analysis is to calculate the maximum allowable gap in the ferrofluid stabilizer based on the governing equations and experimental measurements made in the previous two sections. The driving factor in the design is the mass of the rotor:

$$m_r = m_{rm} + m_{fs} + m_{rod}$$

Where m_r is the total rotor mass
m_{rm} is the mass of the radial bearing magnet
m_{fs} is the mass of the ferrofluid stabilizer magnet
m_{rod} is the mass of the shaft connecting the radial and ferrofluid magnets

The loading on an individual radial magnet bearing is:

$$l_{rm} = m_r / n_{rm}$$

Where l_{rm} is the load on a single radial magnet bearing
n_{rm} is the number of radial magnet bearings

Recalling the load equation of the radial magnet bearing and setting it equal to the actual load:

$$l_{rm} = a_2 x_r^2 + a_1 x_r + a_0$$

Where a_n is the experimentally determined force model coefficient
x_r is the radial displacement

Solving for the radial displacement:

$$x_r = \frac{-a_1 \pm \sqrt{a_1^2 - 4a_2(a_0 - l_{rm})}}{2a_2}$$

Plugging the radial displacement into the radial magnet bearing stiffness model

$$k_r = b_1 x_r + b_0$$

Where k_r is the radial bearing stiffness
b_n is the coefficient of the radial bearing stiffness model

The total axial stiffness is:

$$k_a = 2n_{rm}k_r$$

Where k_a is the total axial stiffness

The required stiffness of each ferrofluid stabilizer is:

$$k_{fs} = k_a / n_{fs}$$

Where k_{fs} is the ferrofluid stabilizer stiffness
n_{fs} is the number of ferrofluid stabilizers

Recalling the stiffness equation for the ferrofluid stabilizer:

$$k_{fs} = a_4 x^4 + a_3 x^3 + a_2 x^2 + a_1 x + a_0$$

Where x is the distance between the ferrofluid stabilizer magnet and the reservoir

Rewriting in the form:

$$x = f(k_{fs})$$

We can solve numerically for x which corresponds to the maximum gap size in the ferrofluid stabilizer at which the system is stable. Using the previous information the system can be designed.

6.2 Results

Four possible designs were considered utilizing all possible combinations of the two radial bearings and two ferrofluid stabilizers which were characterized. The mean force and stiffness coefficients were used for the modeling (Table 6.2a). The combinations were denoted as follows:

Design #1: Radial bearing #1 / Ferrofluid stabilizer #1
Design #2: Radial bearing #1 / Ferrofluid stabilizer #2
Design #3: Radial bearing #2 / Ferrofluid stabilizer #1
Design #4: Radial bearing #2 / Ferrofluid stabilizer #2

Several parameters are common among the designs. Two radial magnetic bearings and two ferrofluid stabilizers are used in all designs. The rotor magnet mass was 3.8g for radial bearing #1 and 15.0g for radial bearing #2. The rotor magnet mass for all the ferrofluid stabilizers was 88.0g. A minimum connecting rod mass of 20g was used for radial bearing #1. Minimum rod mass for radial bearing #2 was 40g. Three performance curves were generated for each design based on the previous analytical work (Figure 6.2a-d). Radial bearing displacement, required ferrofluid stabilizer stiffness, and maximum stabilizer reservoir gap size were plotted against rotor mass. Maximum rotor mass is 220g for radial bearing #1 and 420g for radial bearing #2. The design point based on the minimum rotor mass, 205g and 250g respectively, is shown in each figure.

Design #3 was selected for implementation. Design #1 and #2 require operation too close to the maximum load condition. Design #4 offered no advantage

over #3 and is more difficult to manufacture. The estimated radial displacement under the rotor load is 0.00395m. The minimum ferrofluid stabilizer stiffness is 92.1kg/m resulting in a maximum gap of 0.00369m.

6.3 Hardware Design

The prototype was designed utilizing radial bearing #2 and ferrofluid stabilizer #1. The prototype is shown pictorially in Fig 6.3a, 6.3b, and isometrically in Fig 6.3c. The design drawings for the parts are included in Appendix C. The prototype consists of an aluminum base plate 0.254m (10") x 0.115m (4.5") x 0.0127m (1/2") (part #6) on which 4 acrylic mounting fixtures are bolted. The outer pair of acrylic mounting fixtures (2xPart #1,#2) are used as the magnetic fluid reservoirs. The acrylic plates are 0.00635m (1/4") thick with a 0.0889m (3.5")O.D. bore, 0.000254m (0.100") deep in each plate forming the reservoir. The bore is surrounded with a 0.1016m (4") O-ring to contain the magnetic fluid. A circular bolt pattern is used the clamp the O-ring. The inner acrylic plate in each fixture has a 0.02032m (0.8") I.D. hole for the rotor spindle. A 0.02032m (0.8")I.D. ring extends 0.0127m (1/2") from the face of the inner plate around the point where the spindle enters the chamber. This ring stops the magnetic fluid from leaving the reservoir as the rotor turns because the potential energy . A fluid injection hole is located at the top of each reservoir to insert magnetic fluid. The injection hole can be sealed with a screw and O-ring seal. The inner pair of acrylic mounting fixtures (4x Part#3) are used to hold the radial

bearing stator magnets. A 0.03175m (1.25") I.D. hole is drilled through each 0.00635m (1/4") plate for rotor clearance. A circular bolt pattern is used to clamp the magnet. The rotor consist of three separated spindle parts and four magnets. All of the rotor components were joined using a liquid epoxy glue. The ferrofluid stabilizer magnets are 0.0762m (3") in diameter and 0.00254m (.100") thick and are composed of Neodymium-iron-boron. The radial bearing rotor magnets are 0.01956m O.D. x 0.01016m long and are composed of a Ceramic 8 material.

Mean Force and Stiffness Coefficients						
	x^0	x^1	x^2	x^3	x^4	x^5
Radial Bearing #1						
Force	0.0001	20.127	3669.5			
Stiffness	20.127	7338.9				
Radial Bearing #2						
Force	-0.0005	17.539	3608.9			
Stiffness	17.539	7217.8				
Ferrofluid Stabilizer #1						
Force	1.156	-276.8	4.51e4	-4.76e6	2.58e8	-5.44e9
Stiffness	-276.8	9.026e4	-1.428e7	1.033e9	-2.721e10	
Ferrofluid Stabilizer #2						
Force	0.8978	-348.5	9.43e4	-1.47e7	11.1e9	-3.18e10
Stiffness	-348.5	1.885e5	-4.408e7	4.44e9	-1.592e11	

Table 6.2a

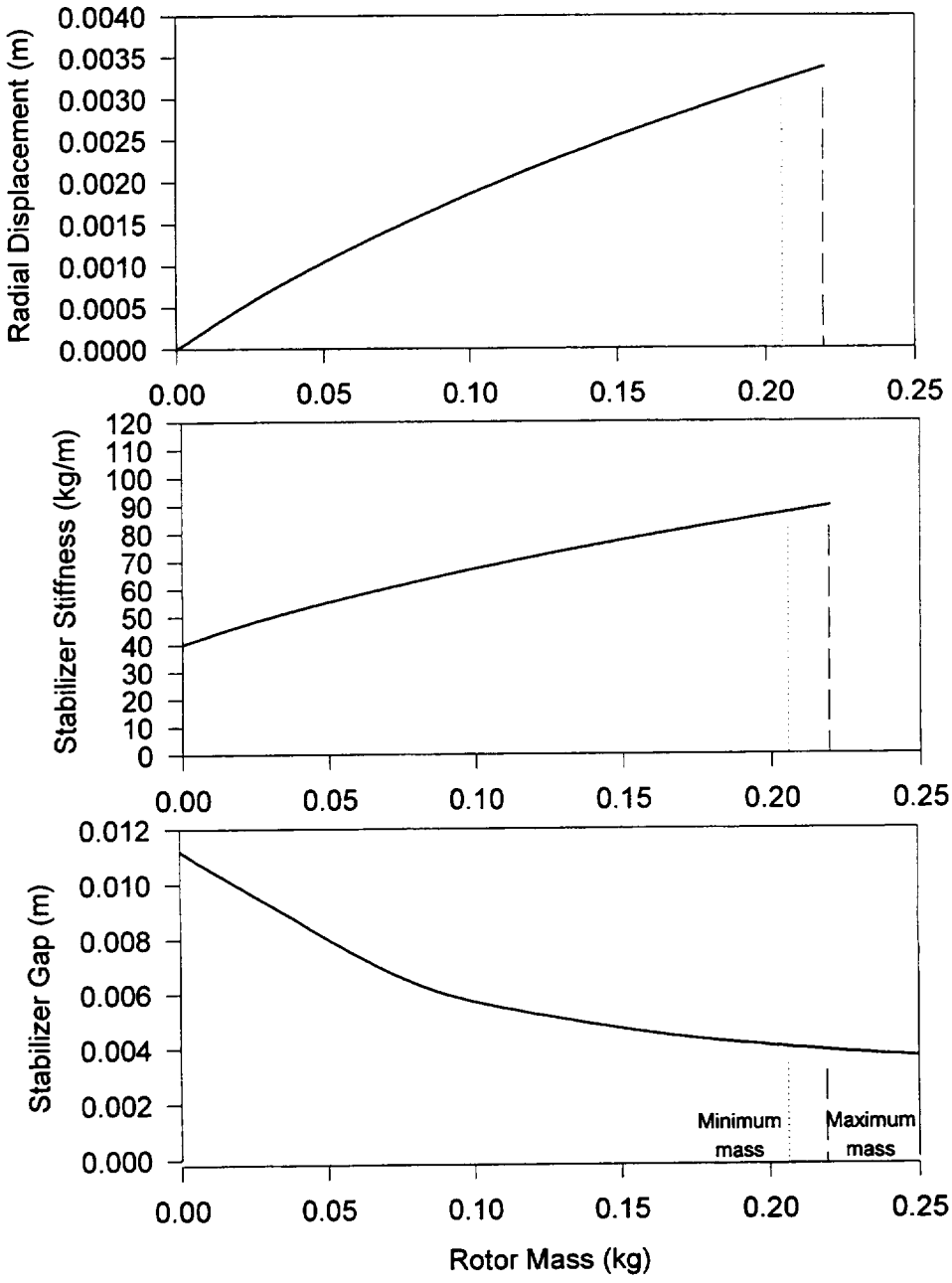

Figure 6.2a - Design #1 - Radial bearing #1 / Ferrofluid stabilizer #1

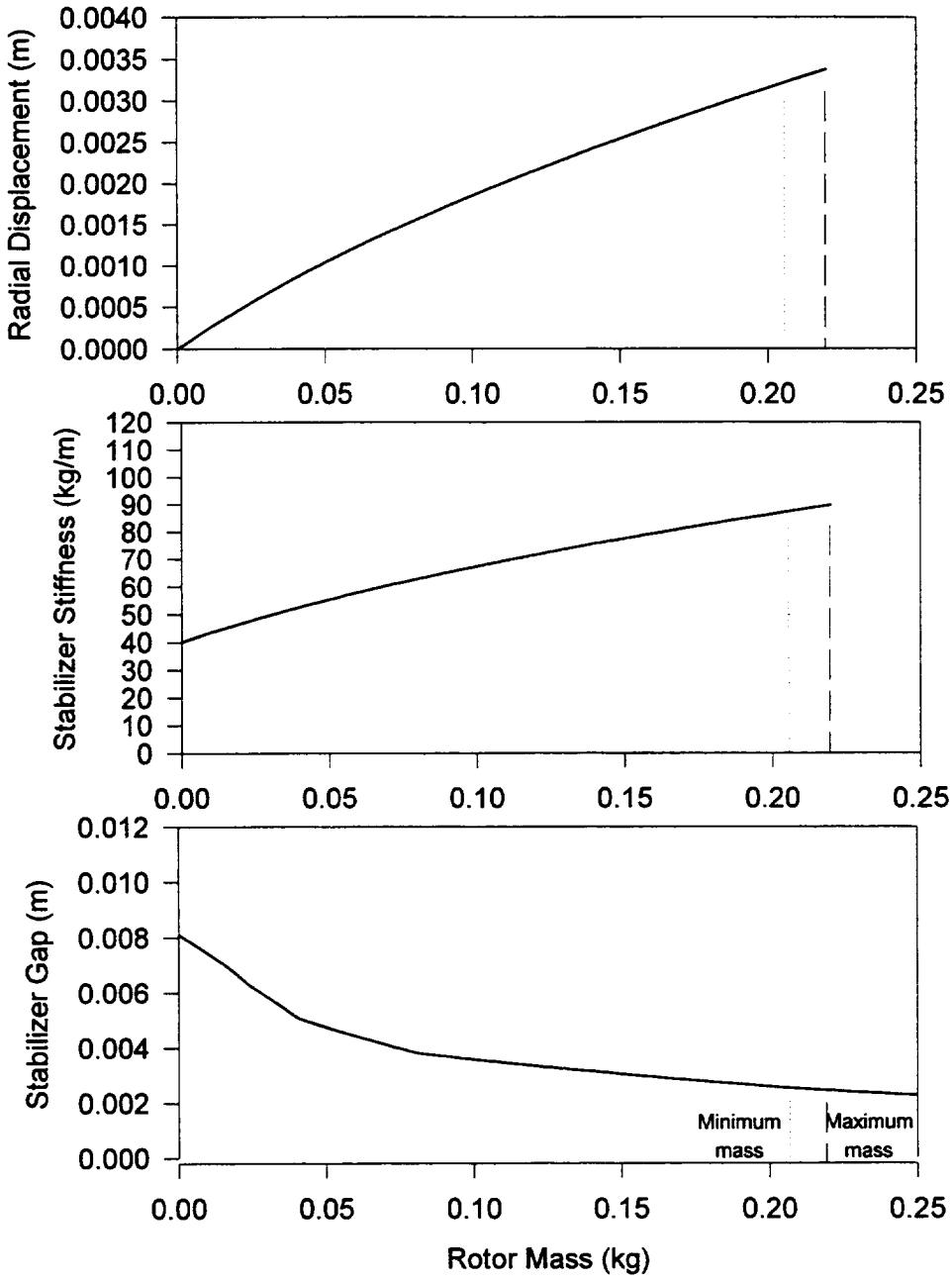

Figure 6.2b - Design #2 - Radial bearing #1 / Ferrofluid stabilizer #2

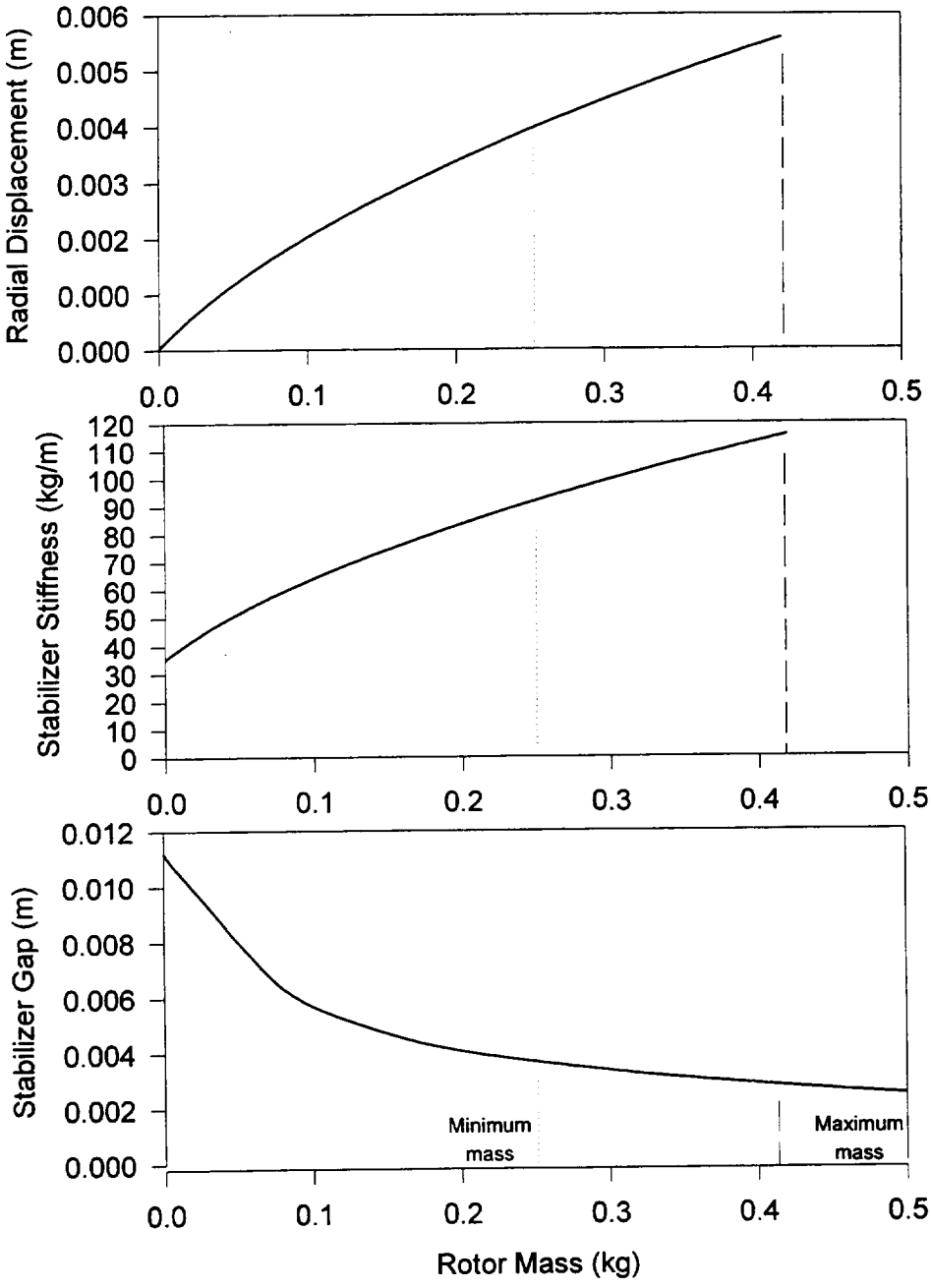

Figure 6.2c - Design #3 - Radial bearing #2 / Ferrofluid stabilizer #1

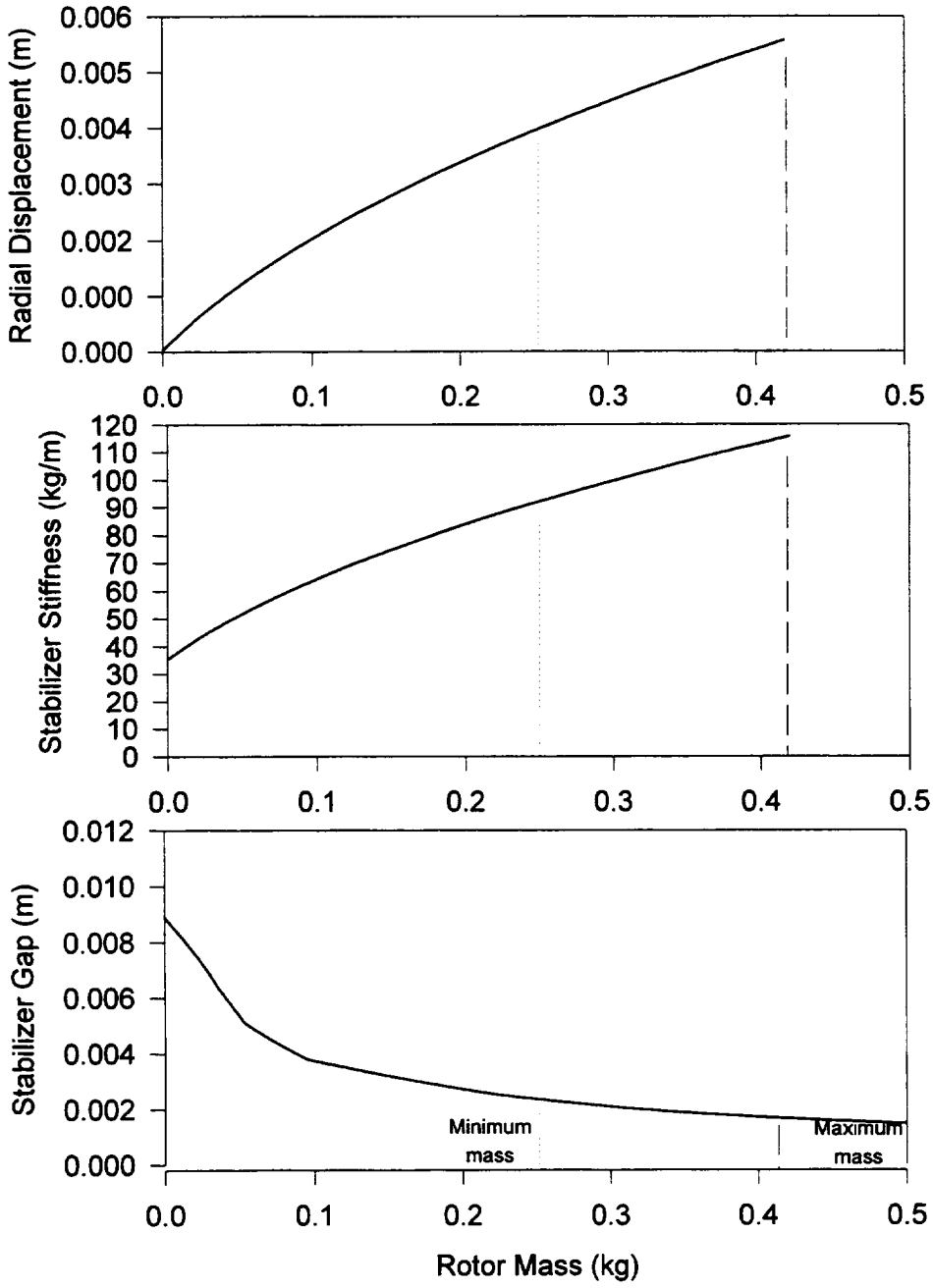

Figure 6.2d - Design #4 - Radial bearing #2 / Ferrofluid stabilizer #2

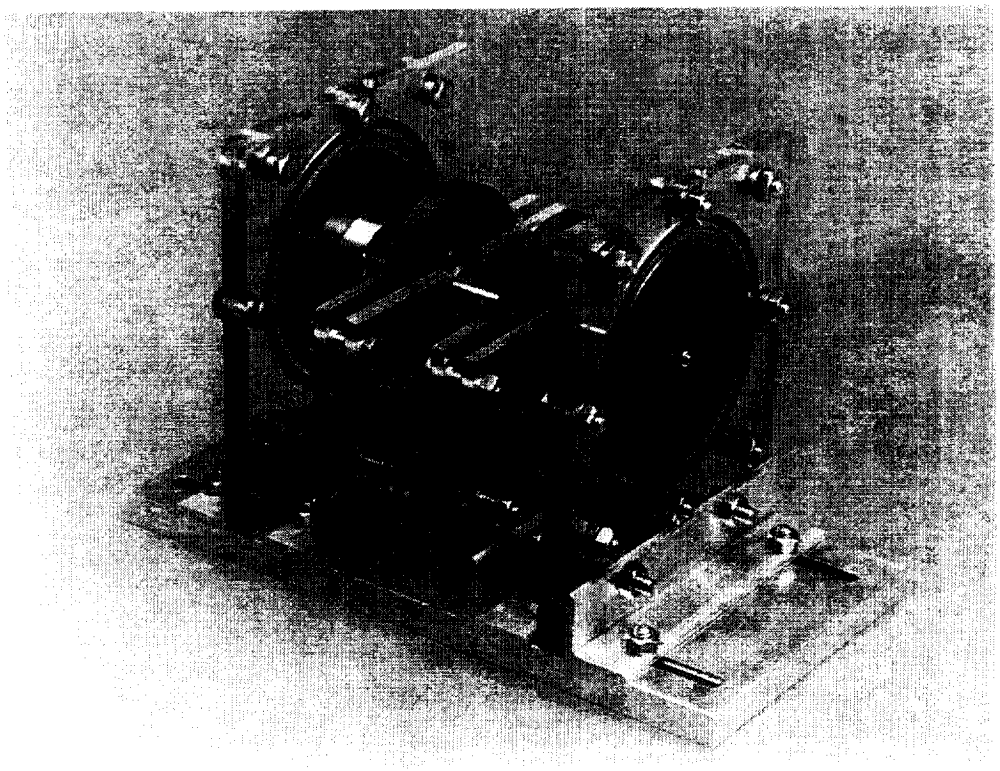

Figure 6.3a - 3/4 view picture of passive magnetic bearing prototype

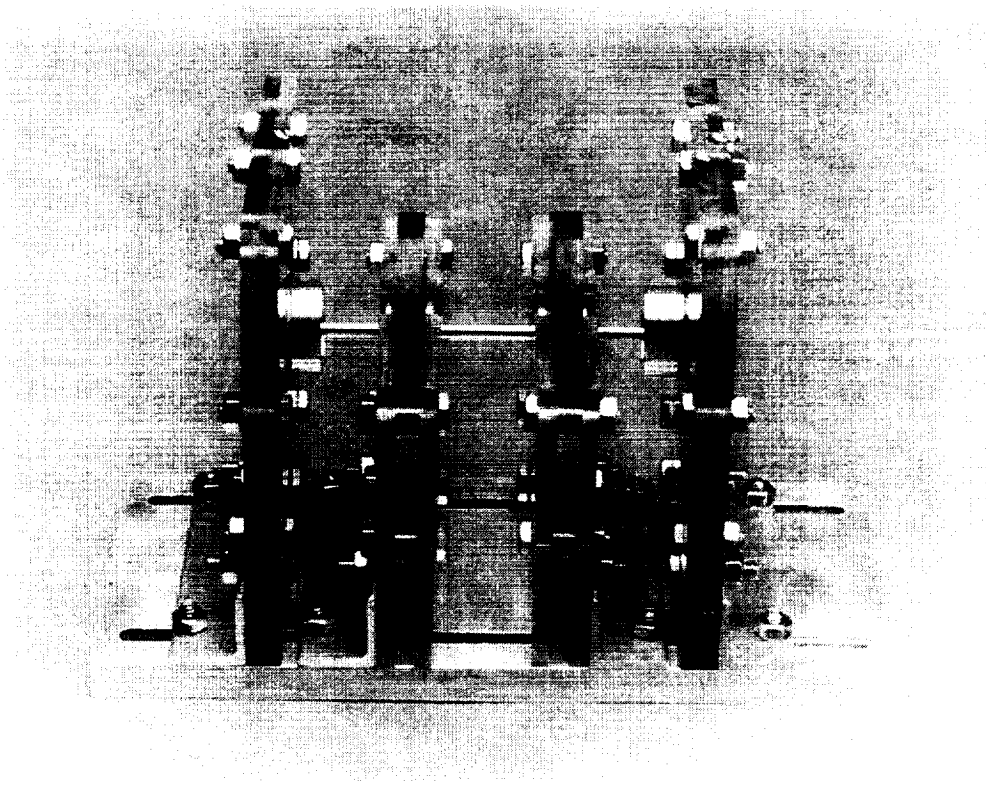

Figure 6.3b - Side view picture of passive magnetic bearing prototype

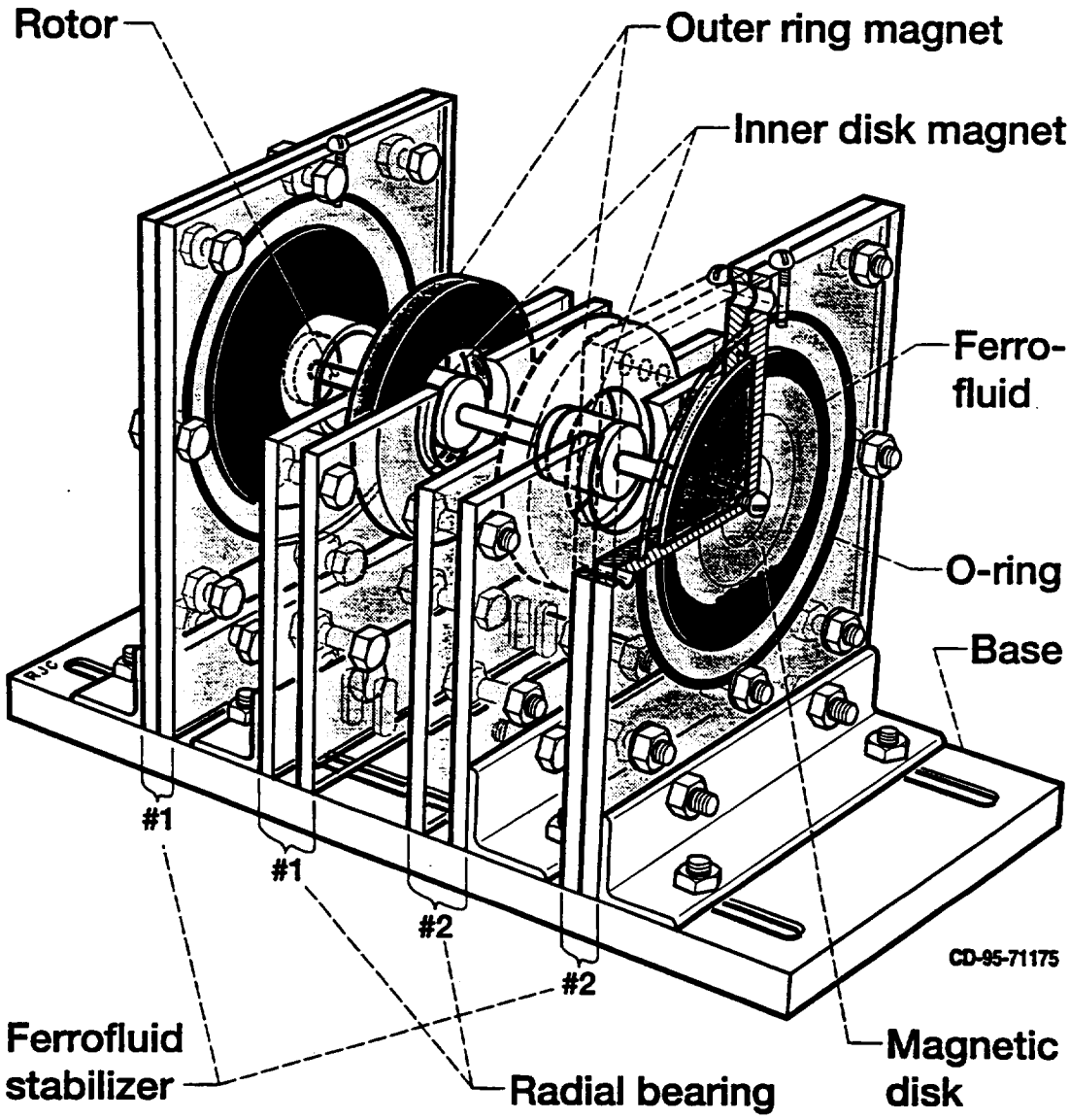

Figure 6.3c - Schematic of passive magnetic bearing prototype

Chapter 7 : Results

7.1 Stability

The magnetic bearing prototype is shown to be stable. Observations of static rotor response show a stable equilibrium point in both the radial and axial directions. Slow speed rotating tests also indicte stable equilibrium in both radial and axial directions. High speed tests were not conducted, however it is clear from the previous modeling that the system will be stable at high speeds if it is stable in the static and slow speed modes.

7.2 Load

A radial load test was conducted to quantify the system performance. The rotor was loaded at center span using gram weights and a loading pan. A blade micrometer was used to measure the displacement of the rotor. One measurement was made with the system vertically oriented in order to find the no load rotor position. The system was measured horizontally with only the rotor load. A weight pan was added and rotor displacement measurements were made as the load was increased in 20g increments. Table 7.2a and Figure 7.2a show a comparison of the measured and predicted prototype performance. The actual load performance is approximately 30% greater than the prediction. The reason for the discrepancy is that the ferrofluid stabilizer have radial load carrying capacity which was completely disregarded in the analysis.

7.3 Vibration

The magnetic bearing system showed potential for vibration isolation. An initial assessment of the vibration characteristics of the prototype was conducted at NASA Lewis by the Structural Systems Division.

Testing was conducted by vibrating the base of the bearing prototype and measuring the frequency response of the rotor. The mounting arrangement is shown in Figure 7.3a. The base of the magnetic bearing was mounting on a MB Dynamics Model C-60 shaker table using a universal adapter fixture. A single excitation axis was used which was perpendicular to the rotor and the gravity vector. The gravity load of the shaft was removed by a supporting string which was affix to the center of the shaft and had a pendulum length of 4 feet. The accelerometer used to control the input vibration was mounted at the base of the magnetic bearing. The response accelerometer was mounted at the center of the rotor shaft.

The test system consists of a shaker table, controls, and data acquisition equipment. The system block diagram is shown in Figure 7.3b. The manufactures of the components of the system are listed in Table 7.3a. Response data from the accelerometers is recorded in both an analog and digital format.

The system response to a 0.1g swept-sinusoidal excitation was measured. The frequency sweep was from 5 Hz to 2000 Hz at a rate of 2.0 Octaves per minute. Figure 7.3c shows the output of the control accelerometer at the base of the magnetic

bearing. The 0.1g response shows that the correct acceleration level was present at the base. Figure 7.3d shows the output of the response accelerometer. The first peak at 11 Hz is the rigid-body bending mode of the rotor shaft. The peaks located above 200 Hz are combined higher order modes in which the base structure and the magnet fixtures began to resonate. In the region between 20 Hz and 200 Hz, the rotor response is less than the base input. In this region the magnetic bearing acts as a vibration isolation system.

Initial tests indicate that it is possible to build a vibration isolation system using this magnetic bearing technology. Whether it is possible to build a vibration isolation system using this technology which is superior to existing passive vibration isolation systems is yet to be determined. In order to make this determination analytical models will need to be developed, and a prototype designed around this goal will need to be constructed and tested.

Prototype Performance			
Predicted		Measured	
mr(kg)	xr(m)	mr(kg)	xr(m)
0	2.83E-05	0	0
0.02	0.000539	0.245	0.003048
0.04	0.000974	0.295	0.003505
0.06	0.001359	0.315	0.003658
0.08	0.001709	0.335	0.003785
0.1	0.002031	0.355	0.003937
0.12	0.002331	0.375	0.004166
0.14	0.002614	0.395	0.004293
0.16	0.002881	0.415	0.00447
0.18	0.003136	0.435	0.004572
0.2	0.00338	0.455	0.00475
0.22	0.003614	0.475	0.004851
0.24	0.003839	0.495	0.005004
0.26	0.004056	0.515	0.005055
0.28	0.004266	0.535	0.005182
0.3	0.00447	0.555	0.005258
0.32	0.004668	0.575	0.005283
0.34	0.00486	0.595	0.00541
0.36	0.005048	0.645	0.005512
0.38	0.005231	0.695	0.005512
0.4	0.00541		
0.42	0.005585		

Table 7.2a

Vibration Test Equipment		
Equipment	Manufacturer	Model
Vibration Shaker	MB Dynamics	C-60
Power Amplifier	Ling Electronics	DMA-48
Control System	Spectral Dynamics	1201
Charge Amplifiers	Unholtz-Dickie	D-22
Tape Recorder	Ampex	RD-200T

Table 7.3a

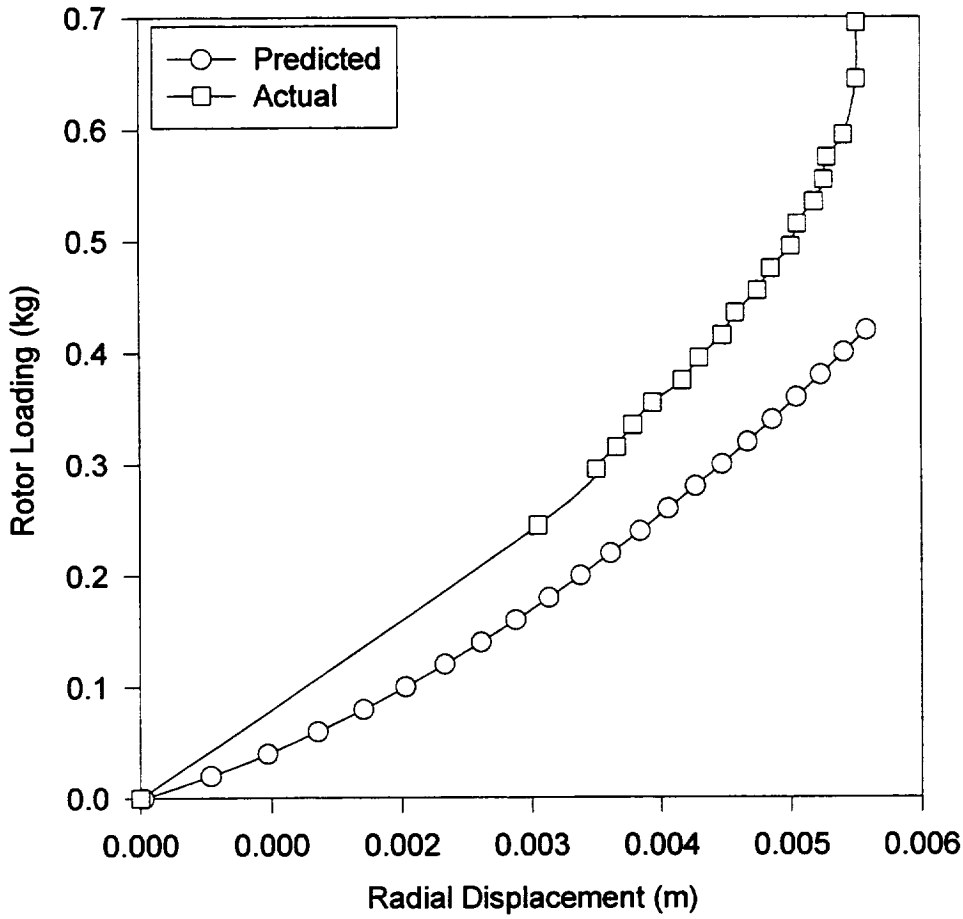

Figure 7.2a - Load response of magnetic bearing prototype

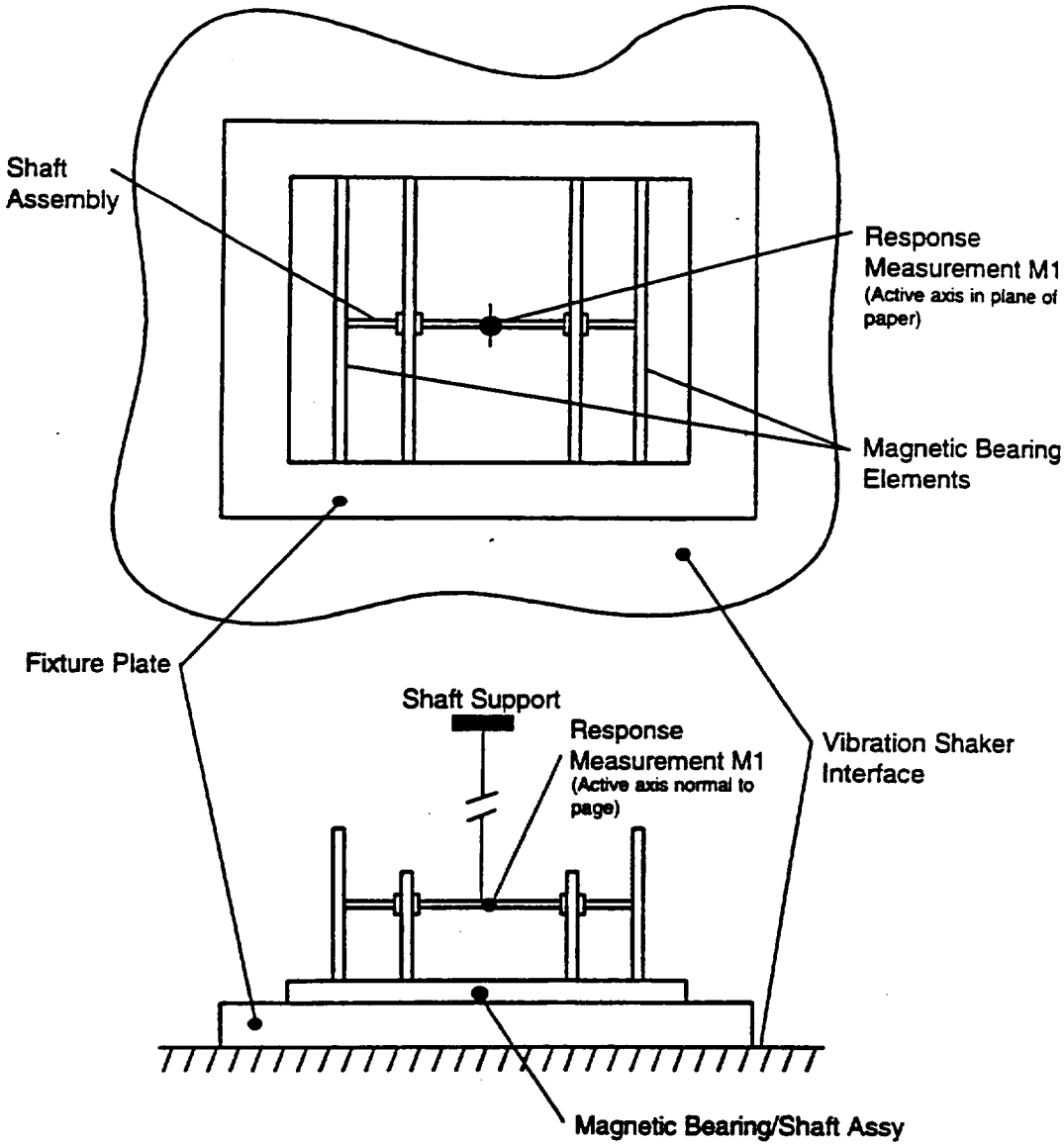

Figure 7.3a - Vibration test setup

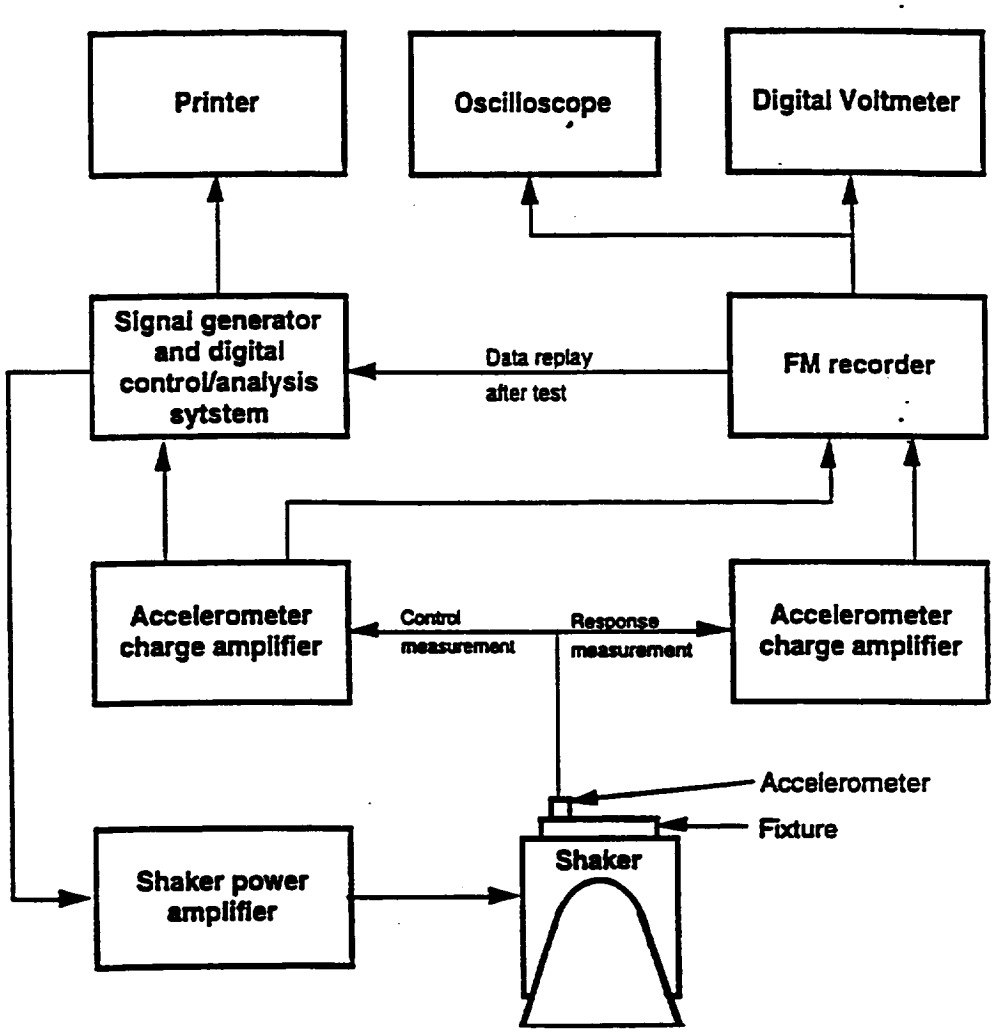

Figure 7.3b - Vibration test system block diagram

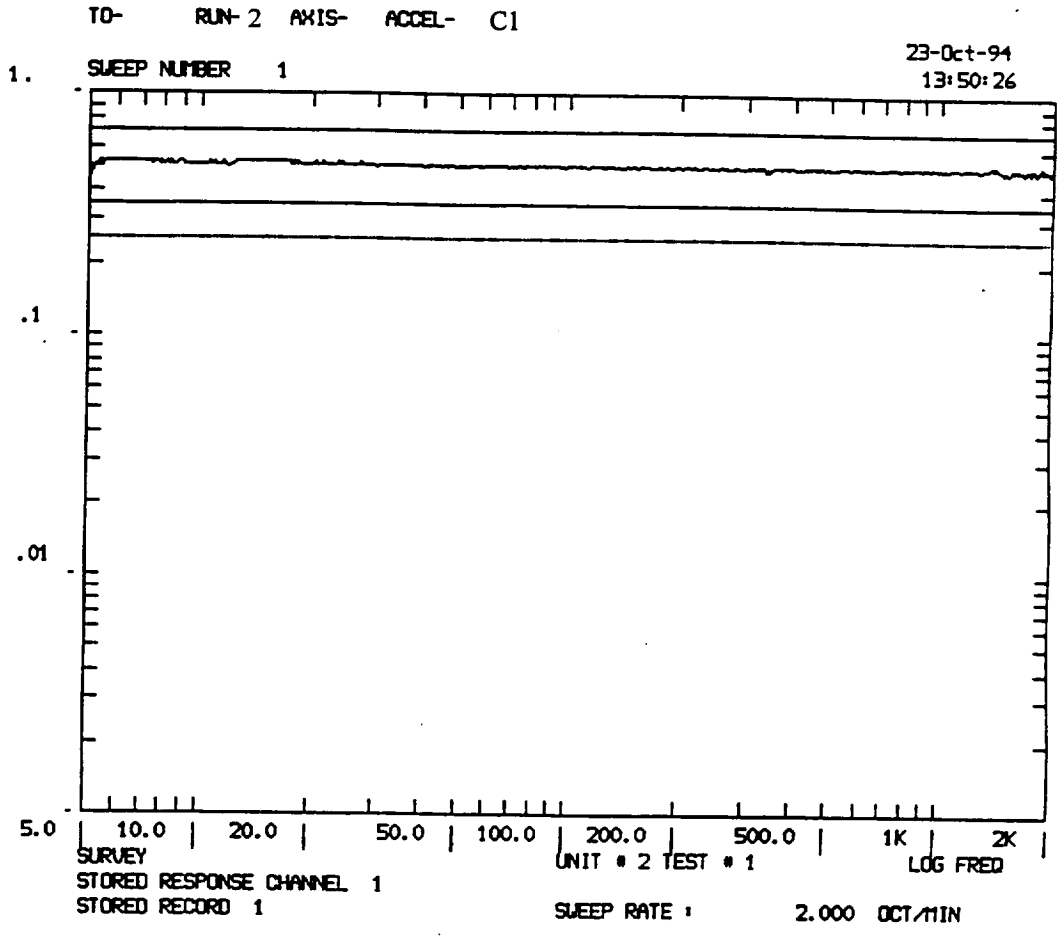

Figure 7.3c - Base mounted control accelerometer output

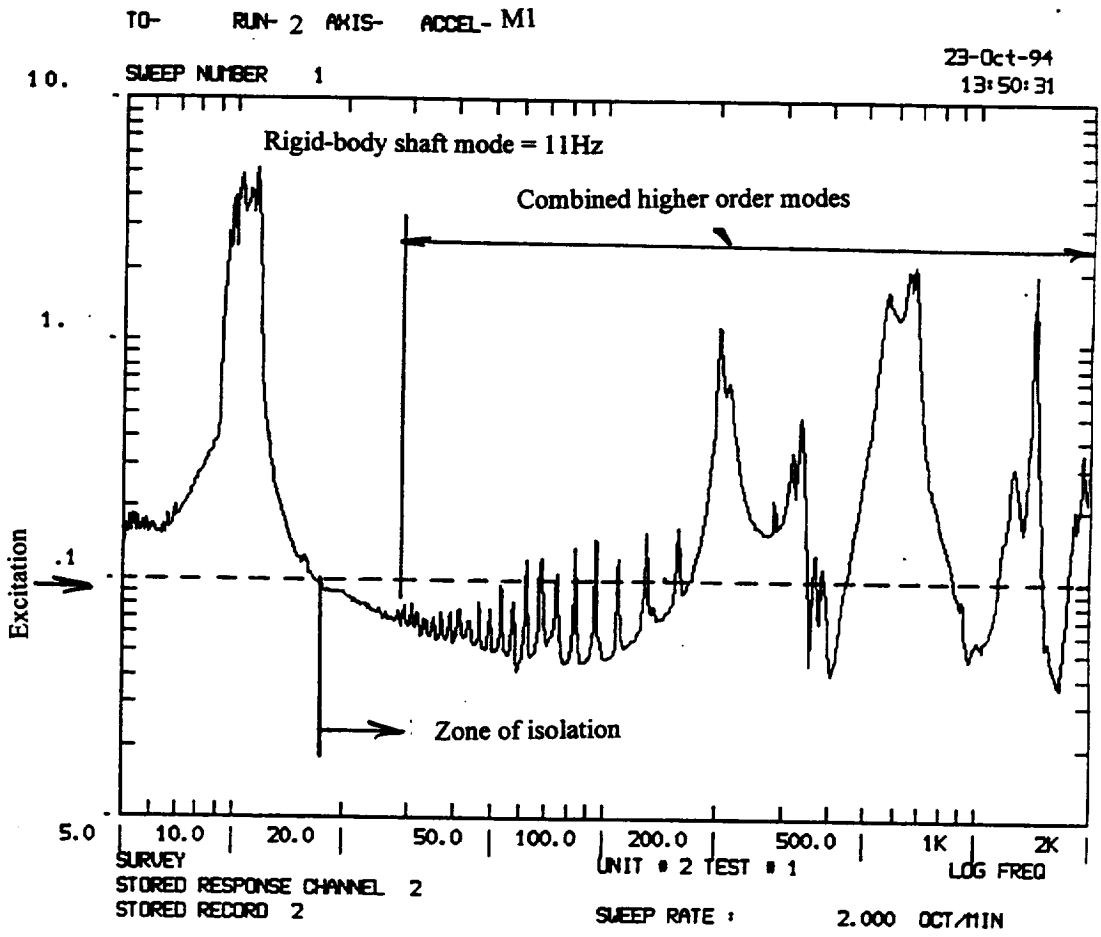

Figure 7.3d - Rotor mounted response accelerometer output

Chapter 8 : Conclusion

A new class of magnetic bearings is shown to exist analytically and demonstrated experimentally. The class of magnetic bearings utilizes a ferrofluid / solid magnet interaction to stabilize the third axis of a permanent magnet radial bearing. The scientific significance of this concept is that a completely passive magnetic system can be achieved without the use of a superconductor. The engineering accomplishment is that a bearing has been constructed which has no wear surfaces and can operate at room temperature without any power or control systems.

Applications of this technology can occur in the areas of slow speed bearings and vibration isolation systems. Bearing areas to be considered include scanning mechanisms and instrumentation bearings. This may be the ideal type of vibration isolation system for microgravity applications. Vibration isolation of common systems which currently use air tables may be replaced with this type of mechanism.

Two major thrusts must occur in future work. An analytical model of the ferrofluid stabilizer must be developed. The important input parameters of this model are magnet geometry and material, ferrofluid viscosity and magnetic properties, reservoir geometry, and rotational speed. The output will be force, stiffness and drag data. The experimental thrust include two areas. The first area is testing of simple ferrofluid stabilizer geometries to verify the analytical work. The second area is development of components, including instrumentation bearings and a vibration isolation system to prove the viability of the technology.

References

1. G. Schweitzer, H. Bleuler, A. Traxler, Active Magnetic Bearings, 1994, Zurich, Germany

2. Bleuler, H., "A Survey of Magnetic Levitation and Magnetic Bearing Types.", ISME International Journal Series III, Vol. 35 No. 3, Sept 1992

3. Soshin Chikazumi, Physics of Magnetism, John Wiley&Sons Inc., 1964

4. V.E. Fertman, Magnetic Fluids Guidebook:Properties and Applications, Hemispher Publishing Corp., 1990

5. B.M. Berkovsky, V.F. Medvedev, M.S. Krakov, Magnetic Fluids Engineering Applications, Oxford University Press, 1993

6. P.J. Geary, Magnetic and Electric Suspensions, 1964, British Scientific Instrument Research Association, Kent, England

7. R. Plimmer, Royal Aircraft Establishment, "A Dynamic Method of Determining the Stiffness and Cross Axis Stability of a Repulsion Magnetic Bearing", Technical Report 77122, Aug 1977

8. Yu. D. Barkov and V.E. Fertman, "Experimental Study of Floating of Magnetic Bodies in a Magnetizable Fluid", Magnitnaya Gidrodinamika, No. 1, pp. 23-26, Jan-Mar, 1978.

9. Ronald E. Rosensweig, "Fluidmagnetic Buoyancy", AIAA Journal October 1966, Vol 4, No 10.

Appendix A : Radial Bearing Data

Magnetic Material Properties				
Material	NdFeB	Ceramic1	Ceramic5	Ceramic8
Max. Energy Product -BdHd	27	1.05	3.4	3.5
Br Residual Induction (gauss)	10700	2300	3800	3850
Hc Coercive Force (Oe)	10100	1860	2400	2950
Hci Intrinsic Coercive Force (Oe)	>18000	3250	2500	3050
Curie Temperature (C)	310	450	450	450
Maximum Operating Temp (C)	150	300	300	300
Temperature Coefficient (%/C)	.110	.129	.190	.190
Density (lb/in3)	.270	.167	.175	.175

Table A-1

NEODYMIUM-IRON-BORON
PREMIUM GRADES

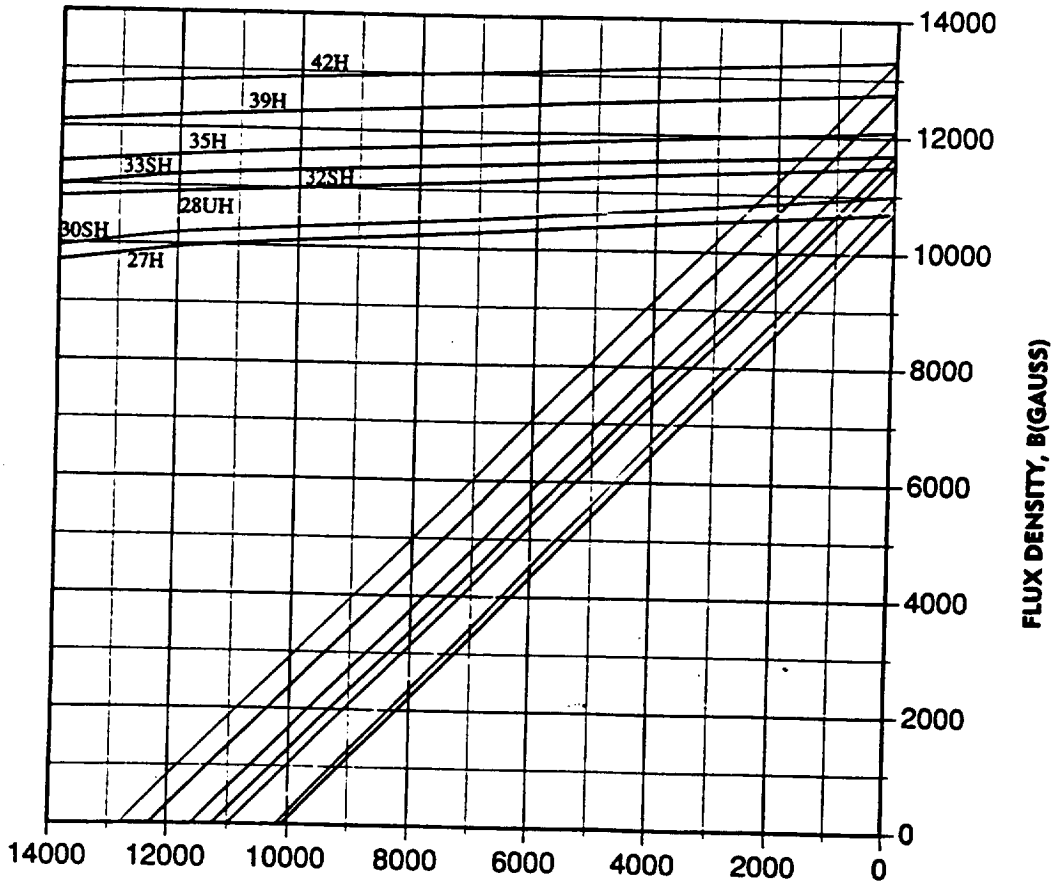

Radial Bearing #1

Rotor: 1.257cm O.D. x 0.635cm 3.8g
Stator: 5.335cm O.D. / 2.032cm I.D. x 0.699cm 65.6g
Test : #1 Method: Frequency
Figure A-1 / A-2

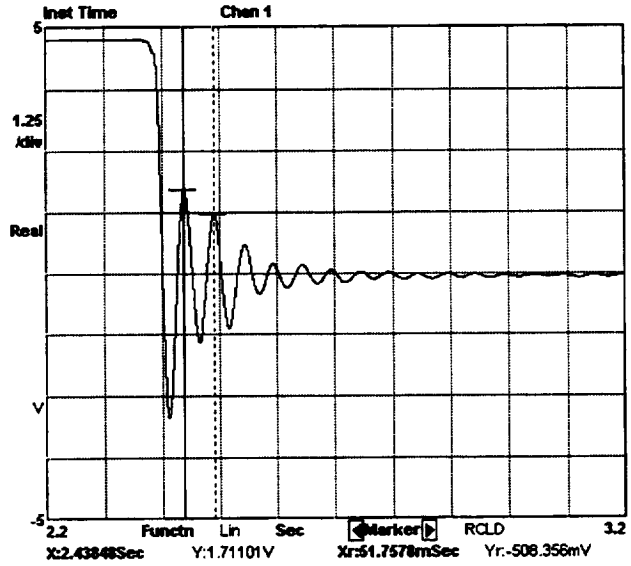

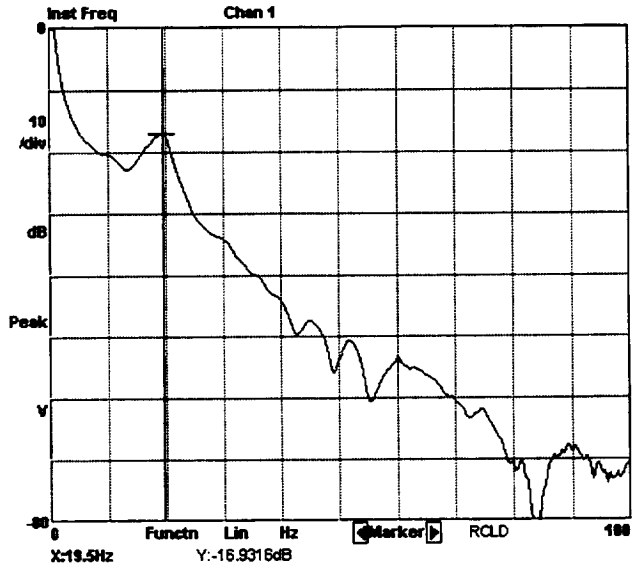

Radial Bearing #1

Rotor: 1.257cm O.D. x 0.635cm 3.8g
Stator: 5.335cm O.D. / 2.032cm I.D. x 0.699cm 65.6g
Test : #2 Method: Frequency
Figure A-3/A-4

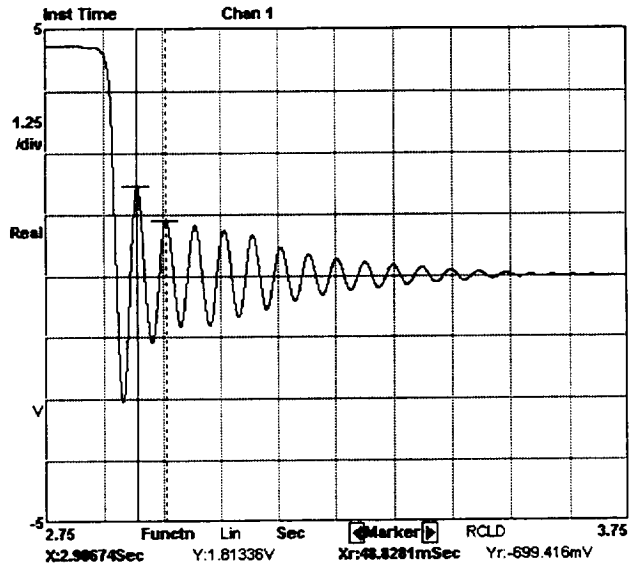

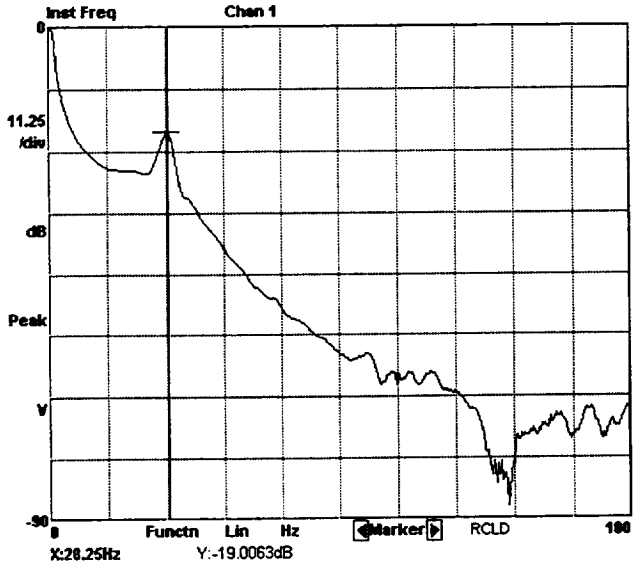

Radial Bearing #2

Rotor: 1.956cm O.D. x 1.016cm 15.0g
Stator: 7.112cm O.D. / 3.056cm I.D. x 0.838cm 137.5g
Test : #1 Method: Frequency
Figure A-5/A-6

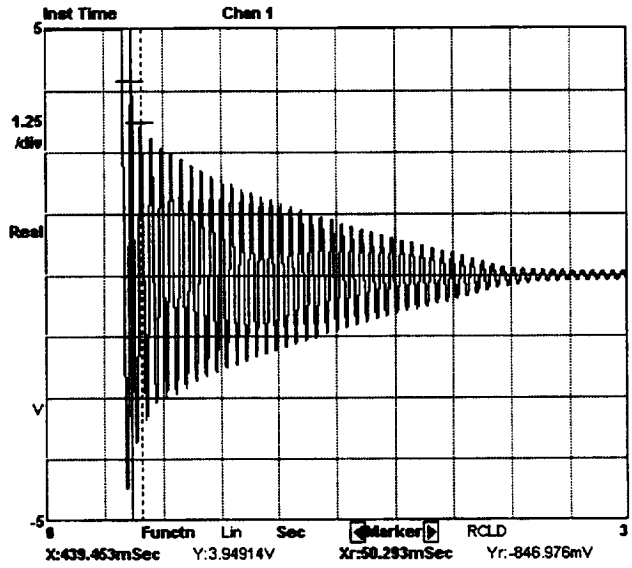

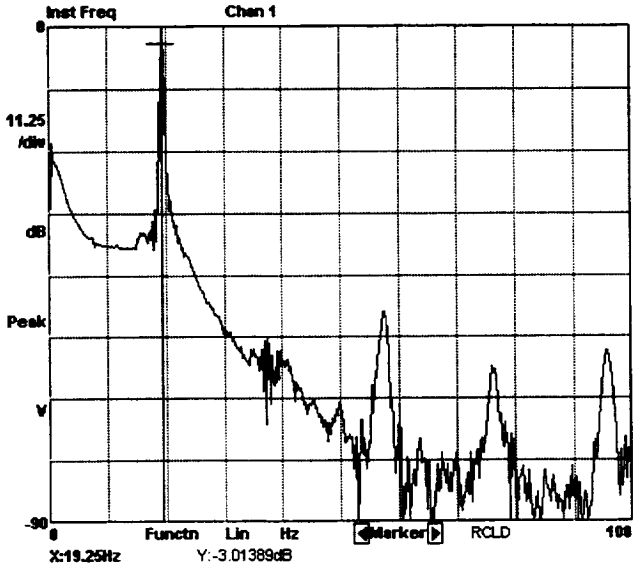

Radial Bearing #2

Rotor: 1.956cm O.D. x 1.016cm 15.0g
Stator: 7.112cm O.D. / 3.056cm I.D. x 0.838cm 137.5g
Test : #2 Method: Frequency
Figure A-7/A-8

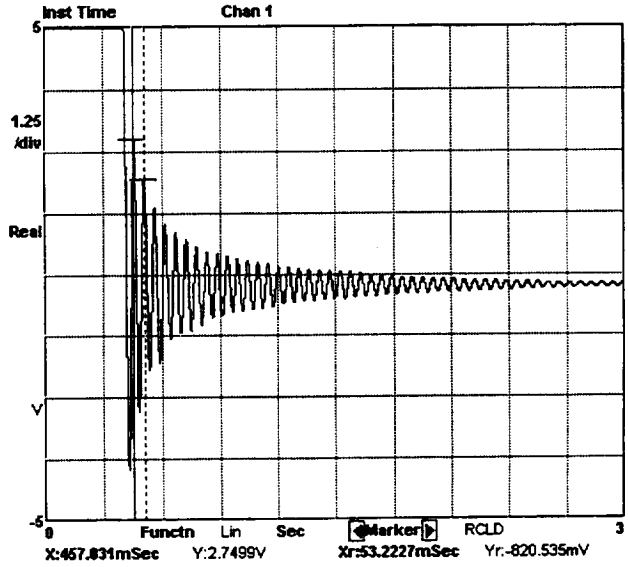

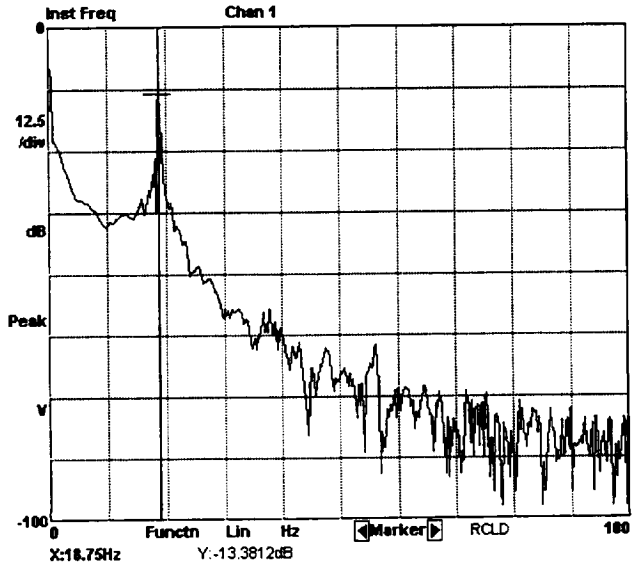

Radial Bearing #1

Rotor: 1.257cm O.D. x 0.635cm 3.8g
Stator: 5.335cm O.D. / 2.032cm I.D. x 0.699cm 65.6g
Test : #1 Method: Displacement

Disp(V)	Disp(in)	Disp(m)	Wgt(kg)	Load(kg)	2(O)Fit(kg)	Stiff(kg/m)
9.8	0	0	0	0	0.0002	19.809
			0.04	0.0208		
11.65	0.069799	0.001773	0.09	0.0468	0.046056	31.92136
11.83	0.07659	0.001945	0.1	0.0519	0.051664	33.09985
12	0.083004	0.002108	0.11	0.0572	0.057147	34.21288
12.16	0.08904	0.002262	0.12	0.0623	0.062473	35.26044
12.31	0.0947	0.002405	0.13	0.0675	0.067612	36.24252
12.46	0.100359	0.002549	0.14	0.0727	0.072893	37.2246
12.61	0.106018	0.002693	0.15	0.0779	0.078314	38.20669
12.75	0.111301	0.002827	0.16	0.0831	0.083502	39.1233
12.89	0.116583	0.002961	0.17	0.0883	0.088812	40.03991
13.02	0.121487	0.003086	0.18	0.0935	0.093853	40.89105
13.15	0.126392	0.00321	0.19	0.0987	0.099001	41.74218
13.27	0.13092	0.003325	0.2	0.1039	0.103846	42.52785
13.39	0.135447	0.00344	0.21	0.1091	0.108782	43.31352
13.51	0.139975	0.003555	0.22	0.1143	0.113808	44.09918
13.61	0.143747	0.003651	0.23	0.1195		
13.61	0.143747	0.003651	0.24	0.1247		
13.61	0.143747	0.003651	0.25	0.1299		

Table A-2

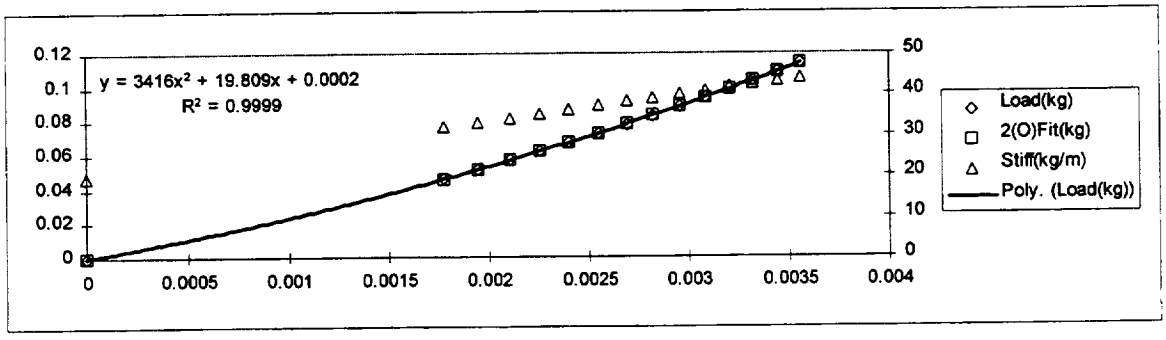

Radial Bearing #1

Rotor: 1.257cm O.D. x 0.635cm 3.8g
Stator: 5.335cm O.D. / 2.032cm I.D. x 0.699cm 65.6g
Test : #2 Method: Displacement

Disp(V)	Disp(in)	Disp(m)	Wgt(kg)	Load(kg)	2(O)Fit(kg)	Stiff(kg/m)
9.8	0	0	0	0	0.0001	18.776
10.77	0.036597	0.00093	0.04	0.0208	0.020767	25.69086
11.7	0.071685	0.001821	0.09	0.0468	0.046618	32.32058
11.86	0.077722	0.001974	0.1	0.0519	0.051662	33.46117
12.02	0.083758	0.002127	0.11	0.0572	0.05688	34.60177
12.18	0.089795	0.002281	0.12	0.0623	0.062273	35.74237
12.32	0.095077	0.002415	0.13	0.0675	0.067135	36.74039
12.48	0.101114	0.002568	0.14	0.0727	0.072856	37.88098
12.62	0.106396	0.002702	0.15	0.0779	0.078005	38.87901
12.76	0.111678	0.002837	0.16	0.0831	0.083288	39.87703
12.9	0.11696	0.002971	0.17	0.0883	0.088705	40.87505
13.03	0.121865	0.003095	0.18	0.0935	0.093855	41.80178
13.16	0.126769	0.00322	0.19	0.0987	0.099121	42.72852
13.28	0.131297	0.003335	0.2	0.1039	0.104083	43.58396
13.41	0.136202	0.00346	0.21	0.1091	0.109571	44.5107
13.52	0.140352	0.003565	0.22	0.1143	0.114304	45.29486
13.61	0.143747	0.003651	0.23	0.1195	0.118239	45.93644
13.63	0.144502	0.00367	0.24	0.1247		
13.63	0.144502	0.00367	0.25	0.1299		

Table A-3

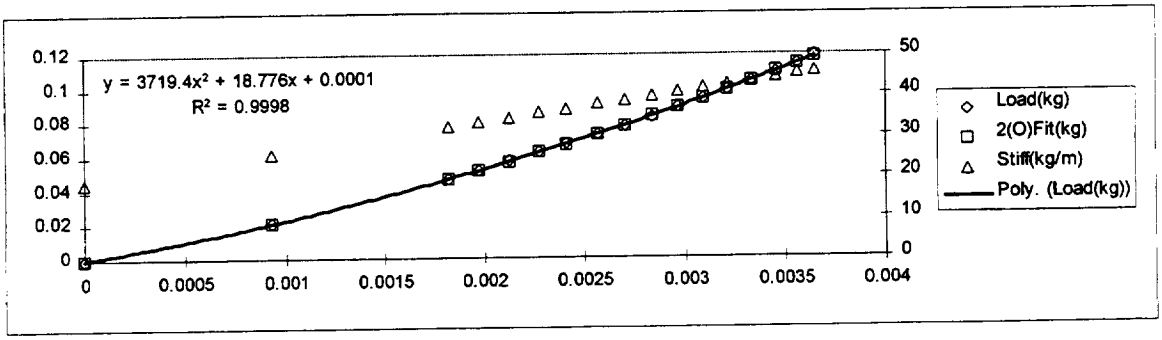

Radial Bearing #1

Rotor: 1.257cm O.D. x 0.635cm 3.8g
Stator: 5.335cm O.D. / 2.032cm I.D. x 0.699cm 65.6g
Test : #3 Method: Displacement

Disp(V)	Disp(in)	Disp(m)	Wgt(kg)	Load(kg)	2(O)Fit(kg)	Stiff(kg/m)
9.89	0	0	0	0	-0.0002	21.588
10.8	0.034333	0.000872	0.04	0.0208	0.021422	27.99997
11.64	0.066026	0.001677	0.09	0.0468	0.046344	33.91871
11.8	0.072062	0.00183	0.1	0.0519	0.051631	35.04609
11.95	0.077722	0.001974	0.11	0.0572	0.056745	36.103
12.11	0.083758	0.002127	0.12	0.0623	0.062367	37.23038
12.25	0.08904	0.002262	0.13	0.0675	0.067428	38.21684
12.4	0.0947	0.002405	0.14	0.0727	0.072998	39.27376
12.54	0.099982	0.00254	0.15	0.0779	0.078333	40.26021
12.66	0.104509	0.002655	0.16	0.0831	0.083011	41.10575
12.79	0.109414	0.002779	0.17	0.0883	0.088189	42.02174
12.92	0.114319	0.002904	0.18	0.0935	0.093482	42.93774
13.05	0.119224	0.003028	0.19	0.0987	0.098888	43.85373
13.17	0.123751	0.003143	0.2	0.1039	0.10398	44.69927
13.28	0.127901	0.003249	0.21	0.1091	0.108732	45.47434
13.42	0.133183	0.003383	0.22	0.1143	0.1149	46.4608
13.53	0.137334	0.003488	0.23	0.1195	0.119838	47.23587
13.63	0.141106	0.003584	0.24	0.1247	0.124399	47.94048
13.74	0.145257	0.00369	0.25	0.1299	0.129493	48.71556
13.8	0.14752	0.003747	0.26	0.1351		
13.8	0.14752	0.003747	0.27	0.1403		

Table A-4

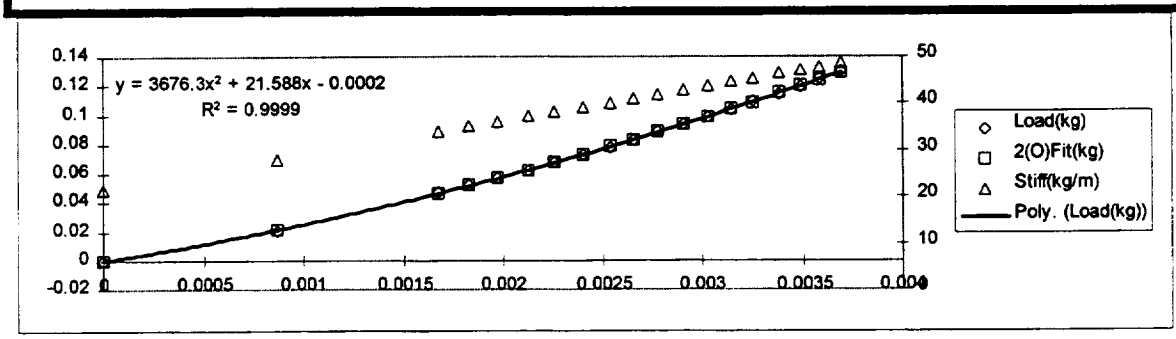

Radial Bearing #1

Rotor: 1.257cm O.D. x 0.635cm 3.8g
Stator: 5.335cm O.D. / 2.032cm I.D. x 0.699cm 65.6g
Test : #4 Method: Displacement

Disp(V)	Disp(in)	Disp(m)	Wgt(kg)	Load(kg)	2(O)Fit(kg)	Stiff(kg/m)
9.93	0	0	0	0	0.0002	20.335
10.85	0.034711	0.000882	0.04	0.0208	0.021134	27.1521
11.71	0.067158	0.001706	0.09	0.0468	0.046137	33.52461
11.87	0.073194	0.001859	0.1	0.0519	0.051368	34.7102
12.03	0.079231	0.002012	0.11	0.0572	0.056781	35.89578
12.18	0.08489	0.002156	0.12	0.0623	0.062021	37.00727
12.33	0.09055	0.0023	0.13	0.0675	0.067421	38.11875
12.48	0.096209	0.002444	0.14	0.0727	0.07298	39.23023
12.63	0.101868	0.002587	0.15	0.0779	0.078699	40.34172
12.75	0.106396	0.002702	0.16	0.0831	0.083389	41.23091
12.89	0.111678	0.002837	0.17	0.0883	0.088991	42.26829
13.01	0.116205	0.002952	0.18	0.0935	0.093903	43.15748
13.14	0.12111	0.003076	0.19	0.0987	0.099339	44.12076
13.25	0.12526	0.003182	0.2	0.1039	0.104033	44.93585
13.37	0.129788	0.003297	0.21	0.1091	0.109252	45.82504
13.49	0.134315	0.003412	0.22	0.1143	0.114573	46.71423
13.59	0.138088	0.003507	0.23	0.1195	0.119085	47.45522
13.71	0.142616	0.003622	0.24	0.1247	0.124593	48.34441
13.81	0.146389	0.003718	0.25	0.1299	0.129262	49.08539
13.84	0.14752	0.003747	0.26	0.1351		
13.84	0.14752	0.003747	0.27	0.1403		

Table A-5

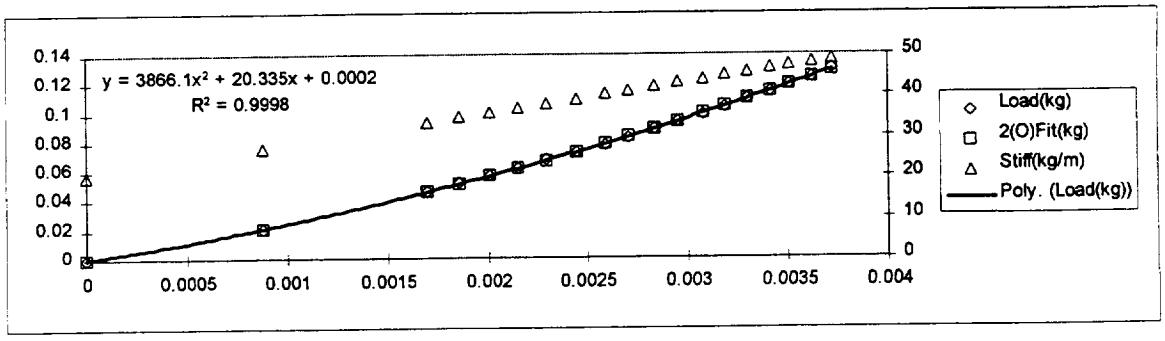

Radial Bearing #2

Rotor: 1.956cm O.D. x 1.016cm 15.0g
Stator: 7.112cm O.D. / 3.056cm I.D. x 0.838cm 137.5g
Test : #1 Method: Displacement

Disp(V)	Disp(in)	Disp(m)	Wgt(kg)	Load(kg)	2(O)Fit(kg)	Stiff(kg/m)
6.74	0	0	0	0	-0.0009	17.952
7.91	0.044143	0.001121	0.04	0.0207	0.023616	25.7785
8.75	0.075836	0.001926	0.09	0.0468	0.046629	31.39752
9.06	0.087532	0.002223	0.11	0.0571	0.056265	33.4712
9.38	0.099606	0.00253	0.13	0.0676	0.066858	35.61178
9.67	0.110547	0.002808	0.15	0.0779	0.077024	37.55169
9.97	0.121866	0.003095	0.17	0.0883	0.088109	39.55848
10.21	0.130921	0.003325	0.19	0.0987	0.097392	41.16391
10.49	0.141485	0.003594	0.21	0.1091	0.108689	43.03692
10.77	0.152049	0.003862	0.23	0.1195	0.120488	44.90993
11	0.160727	0.004082	0.25	0.1299	0.130557	46.44847
11.24	0.169782	0.004312	0.27	0.1403	0.141424	48.05391
11.44	0.177328	0.004504	0.29	0.1507	0.150763	49.39177
11.65	0.185251	0.004705	0.31	0.1611	0.160844	50.79652
11.88	0.193929	0.004926	0.33	0.1715	0.17221	52.33507
12.09	0.201852	0.005127	0.35	0.1819	0.182884	53.73982
12.26	0.208266	0.00529	0.37	0.1923	0.191731	54.877
12.47	0.216189	0.005491	0.39	0.2027	0.202917	56.28176
12.63	0.222226	0.005645	0.41	0.2131	0.211629	57.35205
12.68	0.224113	0.005692	0.43	0.2234		
12.69	0.22449	0.005702	0.45	0.2338		
12.7	0.224867	0.005712	0.47	0.2442		
12.71	0.225245	0.005721	0.49	0.2546		

Table A-6

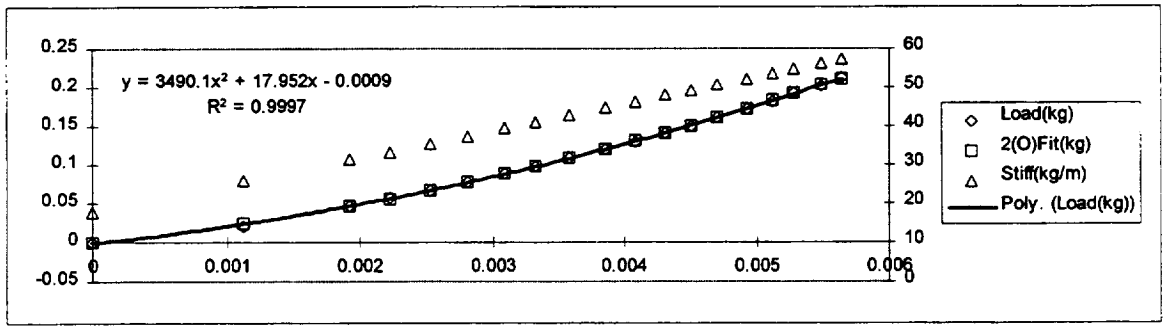

Radial Bearing #2

Rotor: 1.956cm O.D. x 1.016cm 15.0g
Stator: 7.112cm O.D. / 3.056cm I.D. x 0.838cm 137.5g
Test : #2 Method: Displacement

Disp(V)	Disp(in)	Disp(m)	Wgt(kg)	Load(kg)	2(O)Fit(kg)	Stiff(kg/m)
6.72	0	0	0	0	-0.0001	17.126
7.91	0.044898	0.00114	0.04	0.0207	0.024279	25.6282
8.72	0.075459	0.001917	0.09	0.0468	0.046419	31.41542
9.01	0.0864	0.002195	0.11	0.0571	0.055437	33.48738
9.33	0.098474	0.002501	0.13	0.0676	0.066057	35.77369
9.61	0.109038	0.00277	0.15	0.0779	0.075925	37.77421
9.89	0.119602	0.003038	0.17	0.0883	0.086329	39.77473
10.17	0.130166	0.003306	0.19	0.0987	0.09727	41.77525
10.46	0.141108	0.003584	0.21	0.1091	0.109168	43.84721
10.72	0.150918	0.003833	0.23	0.1195	0.120325	45.70484
10.96	0.159973	0.004063	0.25	0.1299	0.131034	47.41957
11.18	0.168273	0.004274	0.27	0.1403	0.141197	48.9914
11.42	0.177328	0.004504	0.29	0.1507	0.152663	50.70613
11.63	0.185251	0.004705	0.31	0.1611	0.163018	52.20652
11.83	0.192797	0.004897	0.33	0.1715	0.173161	53.63546
12.05	0.201098	0.005108	0.35	0.1819	0.184635	55.2073
12.24	0.208266	0.00529	0.37	0.1923	0.194811	56.5648
12.36	0.212794	0.005405	0.39	0.2027	0.201365	57.42216
12.54	0.219585	0.005577	0.41	0.2131	0.211381	58.70821
12.67	0.22449	0.005702	0.43	0.2234	0.218753	59.63702
12.69	0.225245	0.005721	0.45	0.2338		
12.7	0.225622	0.005731	0.47	0.2442		
12.72	0.226376	0.00575	0.49	0.2546		

Table A-7

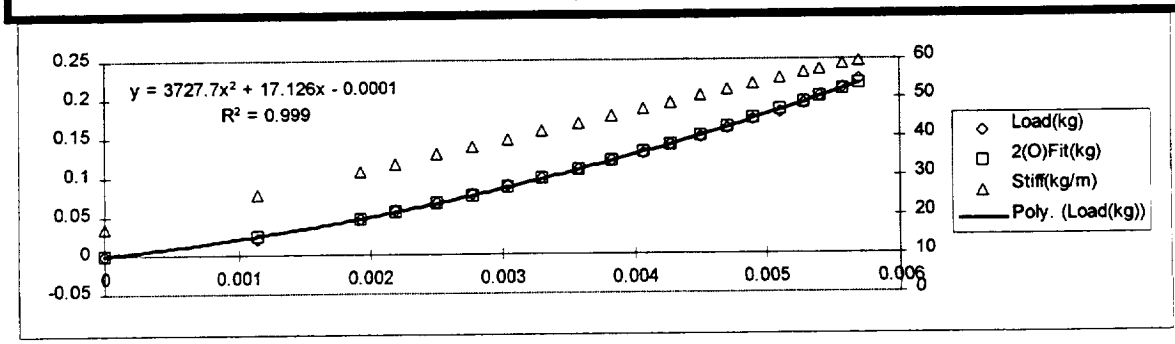

Appendix B : Ferrofluid Stabilizer Data

Properties of Neodymium-Iron-Boron Magnets				
Type	Br(G)	Hc(Oe)	Hci(Oe)	BHmax(MGOe)
27H	10600	10100	17000	27
28UH	10900	10400	25000	28
30H	11200	10700	17000	30
30SH	11200	10700	21000	30
32SH	11500	11000	26000	32
33SH	11700	11100	21000	33
35H	12100	11600	17000	35
39H	12700	12200	19000	39
42H	13300	12800	16000	42

Table B-1

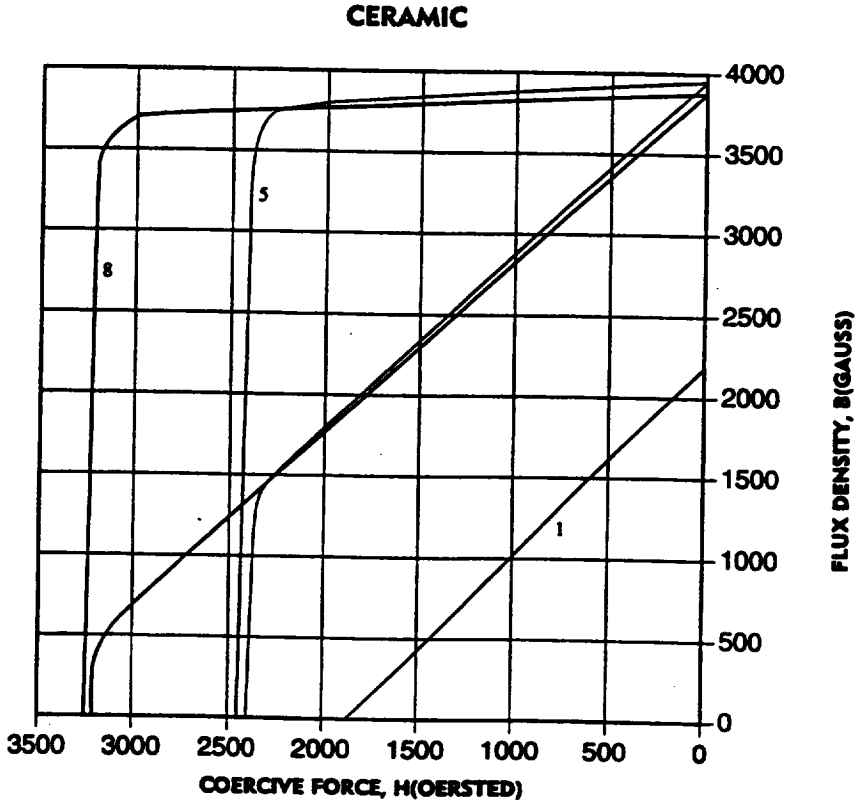

Ferrofluid Stabilizer #1

Rotor: 3.0"x0.10 Disk
Stator: 0.050" Clearance
Test : #1 Method: Displacement

Position(in)	CorrPos(in)	Position(m)	Force(kg)	5(O)Fit(kg)	Stiff(kg/m)
1	0.625	0.015875	0	-0.00303	-42.5239
0.95	0.575	0.014605	0.033	0.037723	-27.683
0.9	0.525	0.013335	0.068	0.068972	-25.6921
0.85	0.475	0.012065	0.106	0.102958	-30.5178
0.8	0.425	0.010795	0.149	0.145337	-37.8195
0.75	0.375	0.009525	0.198	0.19733	-44.9488
0.7	0.325	0.008255	0.255	0.25788	-50.9502
0.65	0.275	0.006985	0.32	0.325795	-56.5608
0.6	0.225	0.005715	0.399	0.4019	-64.2102
0.55	0.175	0.004445	0.497	0.49119	-78.0206
0.525	0.15	0.00381	0.539	0.544006	-88.9872
0.5	0.125	0.003175	0.62	0.604971	-103.807
0.475	0.1	0.00254	0.672	0.676836	-123.471
0.45	0.075	0.001905	0.769	0.763018	-149.076
0.425	0.05	0.00127	0.856	0.867666	-181.826
0.4	0.025	0.000635	0.991	0.995723	-223.029
0.375	0	0	1.16	1.153	-274.1
0.374			1.14		
0.373			1.174		
0.372			1.213		
0.371			1.286		
0.37			1.52		
0.367			1.719		

Table B-2

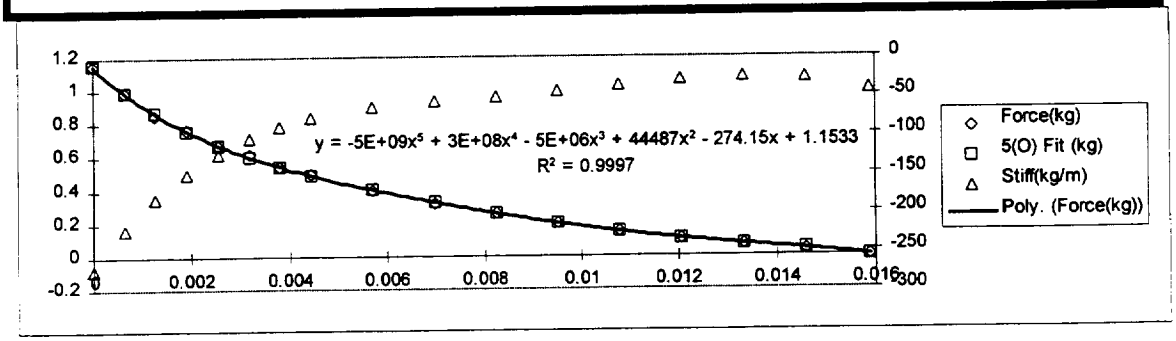

Ferrofluid Stabilizer #1

Rotor: 3.0"x0.10" Disk
Stator: 0.050 Clearance
Test : #2 Method: Displacement

Position(in)	CorrPos(in)	Position(m)	Force(kg)	5(O)Fit(kg)	Stiff(kg/m)
1	0.625	0.015875	0	-0.0005	-36.1783
0.95	0.575	0.014605	0.032	0.03868	-23.3751
0.9	0.525	0.013335	0.067	0.069448	-22.8337
0.85	0.475	0.012065	0.106	0.103525	-28.6045
0.8	0.425	0.010795	0.149	0.146147	-36.4431
0.75	0.375	0.009525	0.199	0.198232	-43.8101
0.7	0.325	0.008255	0.255	0.258545	-49.8713
0.65	0.275	0.006985	0.321	0.325867	-55.4975
0.6	0.225	0.005715	0.398	0.401157	-63.2647
0.55	0.175	0.004445	0.491	0.489721	-77.454
0.525	0.15	0.00381	0.546	0.54236	-88.7609
0.5	0.125	0.003175	0.609	0.603376	-104.051
0.475	0.1	0.00254	0.68	0.675619	-124.34
0.45	0.075	0.001905	0.763	0.762616	-150.748
0.425	0.05	0.00127	0.862	0.868642	-184.503
0.4	0.025	0.000635	0.989	0.99878	-226.94
0.375	0	0	1.168	1.159	-279.5
0.374			1.186		
0.373			1.214		
0.372			1.253		
0.371			1.419		
0.37			1.587		

Table B-3

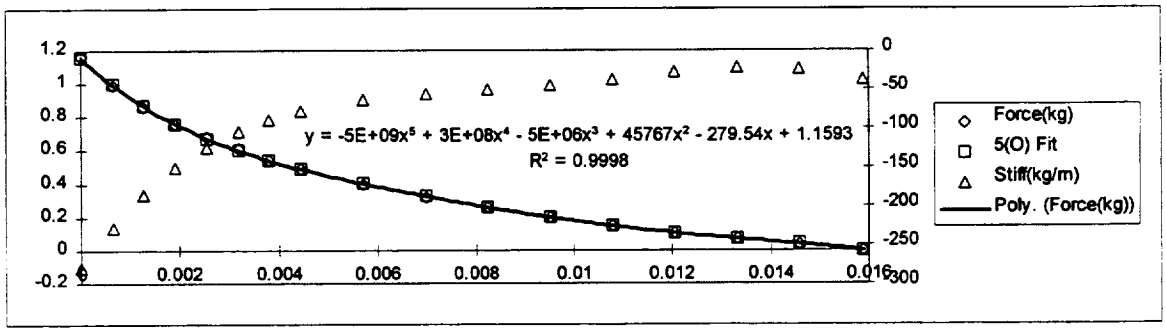

Ferrofluid Stabilizer #2

Rotor: 3.0"x0.10" Concentric Ring
Stator: 0.050 Clearance
Test : #1 Method: Displacement

Position(in)	CorPos(in)	Position(m)	Force(kg)	5(O)Fit(kg)	Stiff(kg/m)
1	0.5	0.0127	0	9.92E-05	-36.5483
0.95	0.45	0.01143	0.036	0.039064	-25.8652
0.9	0.4	0.01016	0.074	0.073679	-28.4055
0.85	0.35	0.00889	0.118	0.115023	-35.7005
0.8	0.3	0.00762	0.166	0.165607	-42.7185
0.75	0.25	0.00635	0.222	0.223729	-47.8649
0.7	0.2	0.00508	0.284	0.287849	-52.9819
0.65	0.15	0.00381	0.364	0.360946	-63.349
0.6	0.1	0.00254	0.46	0.454887	-87.6826
0.55	0.05	0.00127	0.589	0.594793	-138.136
0.5	0	0	0.825	0.8234	-230.3
0.48			2.1		

Table B-4

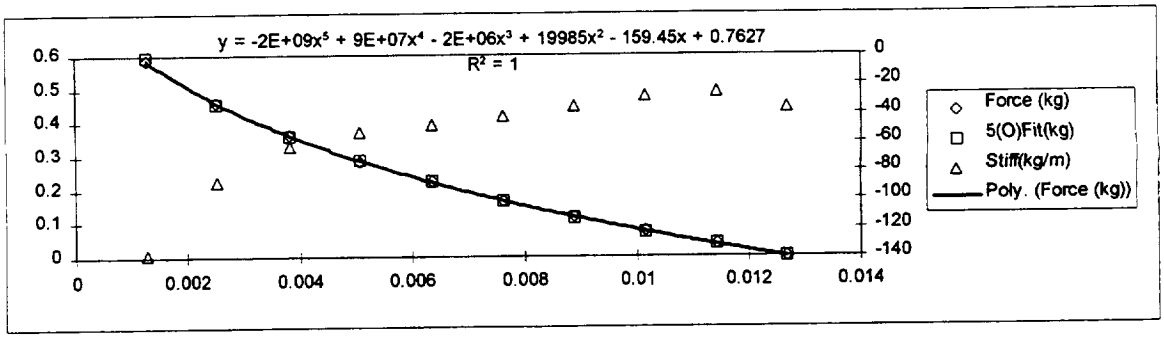

Ferrofluid Stabilizer #2

Rotor: 3.0"x0.10" Concentric Ring
Stator: 0.050 Clearance
Test : #2 Method: Displacement

Position(in)	CorPos(in)	Position(m)	Force(kg)	5(O)Fit(kg)	Stiff(kg/m)
1	0.44	0.011176	0	-0.00062	-49.0106
0.95	0.39	0.009906	0.04	0.042405	-25.7731
0.9	0.34	0.008636	0.074	0.073931	-27.2076
0.85	0.29	0.007366	0.12	0.114021	-36.8366
0.8	0.24	0.006096	0.161	0.166352	-45.3187
0.75	0.19	0.004826	0.224	0.227275	-50.4488
0.7	0.14	0.003556	0.3	0.294877	-57.1582
0.65	0.09	0.002286	0.379	0.378048	-77.5144
0.6	0.04	0.001016	0.501	0.505539	-130.721
0.575	0.015	0.000381	0.605	0.602552	-177.596
0.56	0	0	0.996		
0.55			0.748		
0.541			0.988		
0.525			1.176		
0.5			1.072		
0.475			1.124		
0.462			1.752		

Table B-5

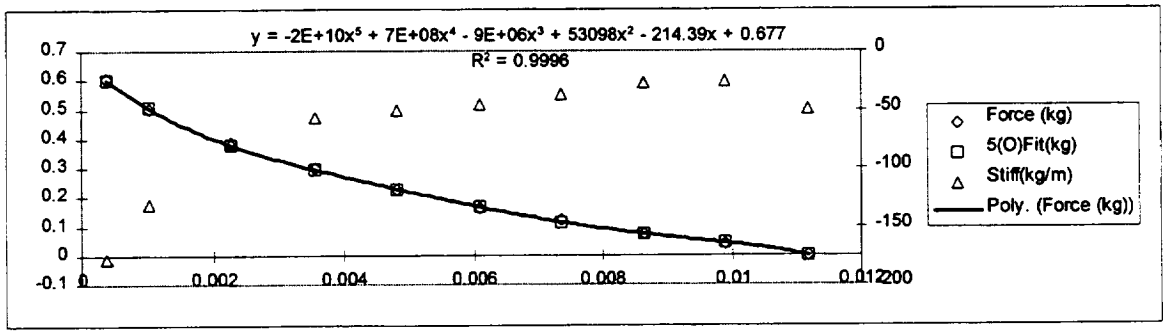

Ferrofluid Stabilizer #2

Rotor: 3.0"x0.10" Concentric Ring
Stator: 0.050 Clearance
Test : #3 Method: Displacement

Position(in)	CorPos(in)	Position(m)	Force(kg)	5(O)Fit(kg)	Stiff(kg/m)
1	0.48	0.012192	0	0.006065	-87.235
0.95	0.43	0.010922	0.04	0.062312	-15.7063
0.9	0.38	0.009652	0.082	0.079129	-15.9831
0.85	0.33	0.008382	0.128	0.114821	-39.4185
0.8	0.28	0.007112	0.162	0.178142	-56.6265
0.75	0.23	0.005842	0.246	0.252756	-57.4826
0.7	0.18	0.004572	0.316	0.321702	-51.1231
0.65	0.13	0.003302	0.404	0.391849	-65.9454
0.6	0.08	0.002032	0.525	0.518364	-149.608
0.575	0.055	0.001397	0.64	0.639226	-237.415
0.55	0.03	0.000762	0.805	0.829172	-369.031
0.525	0.005	0.000127	1.132	1.119577	-555.832
0.52	0	0	1.355		
0.515			1.233		
0.51			1.255		
0.505			1.323		
0.5			1.219		
0.485			1.332		
0.475			1.32		
0.47			1.53		
0.465			1.672		
0.46			1.579		
0.45			1.349		

Table B-5

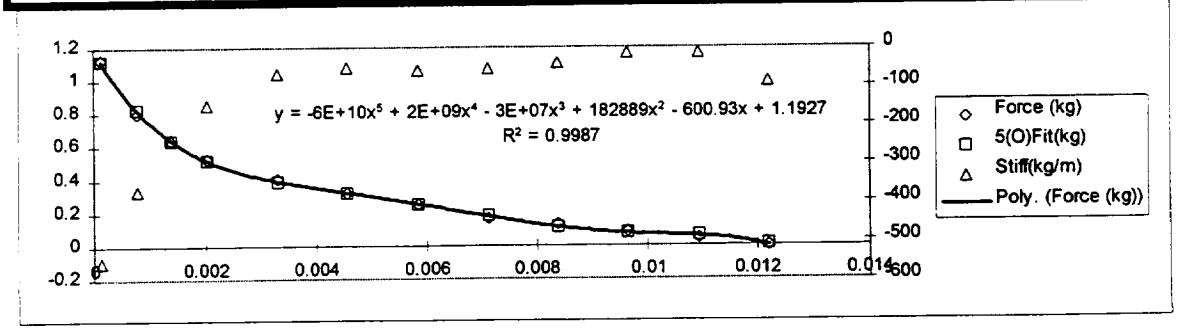

Appendix C: Hardware Drawings

List of Drawings					
Name	Figure	Part#	File	Scale	Date
Assembly drawing	C-1		mag18.dwg	2/1	7/18/94
Ferrofluid Reservoir A	C-2	1	mag12.dwg	1/1	7/15/94
Ferrofluid Reservoir B	C-3	2	mag13.dwg	1/1	7/15/94
Magnet Fixture	C-4	3	mag14.dwg	1/1	7/15/94
Mounting Bracket	C-5	4	mag15.dwg	1/1	7/16/94
Connecting Rod	C-6	5	mag16.dwg	1/1	7/16/94
Base Plate	C-7	6	mag17.dwg	1/1	7/16/94

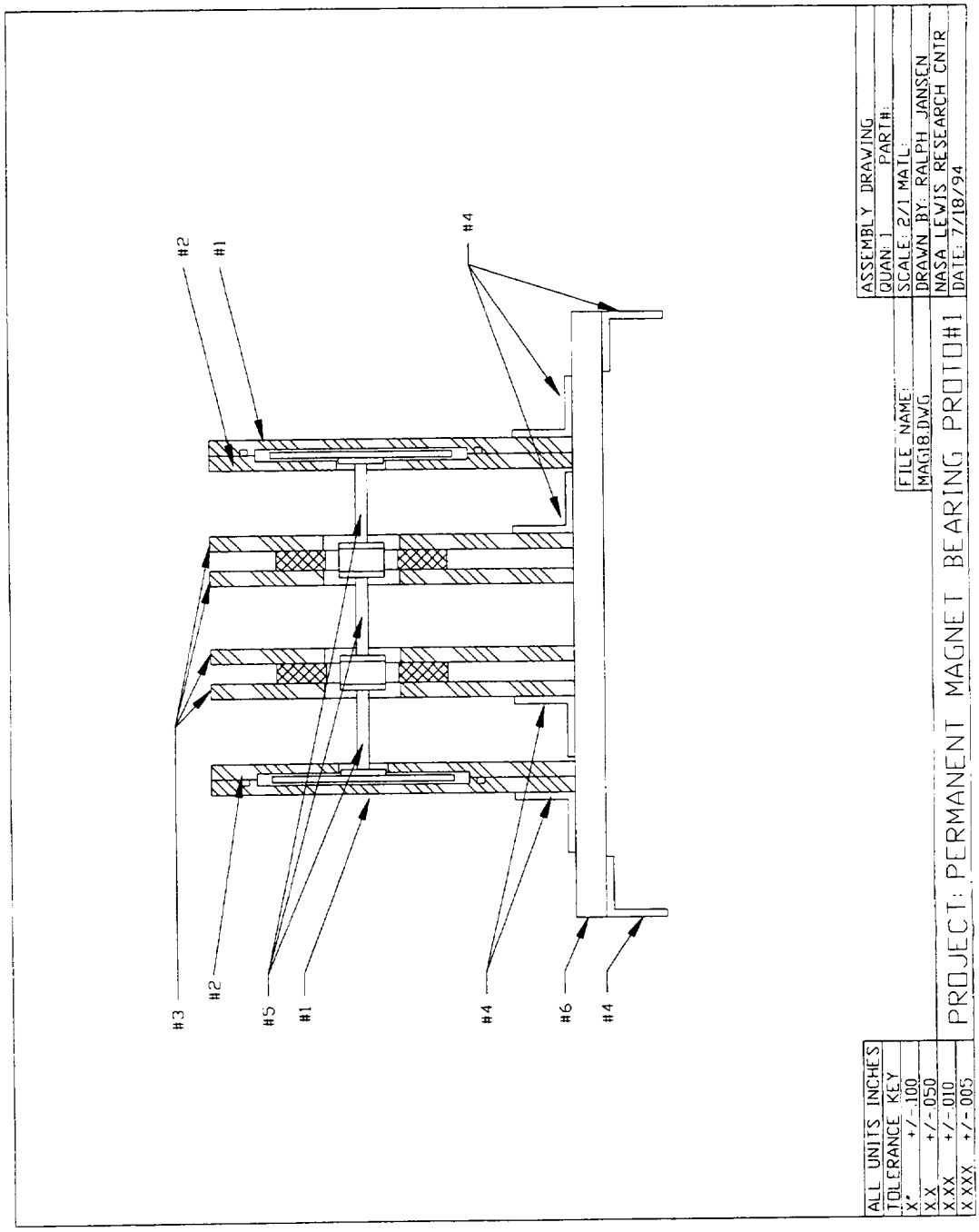

Figure C-1 - Assembly drawing

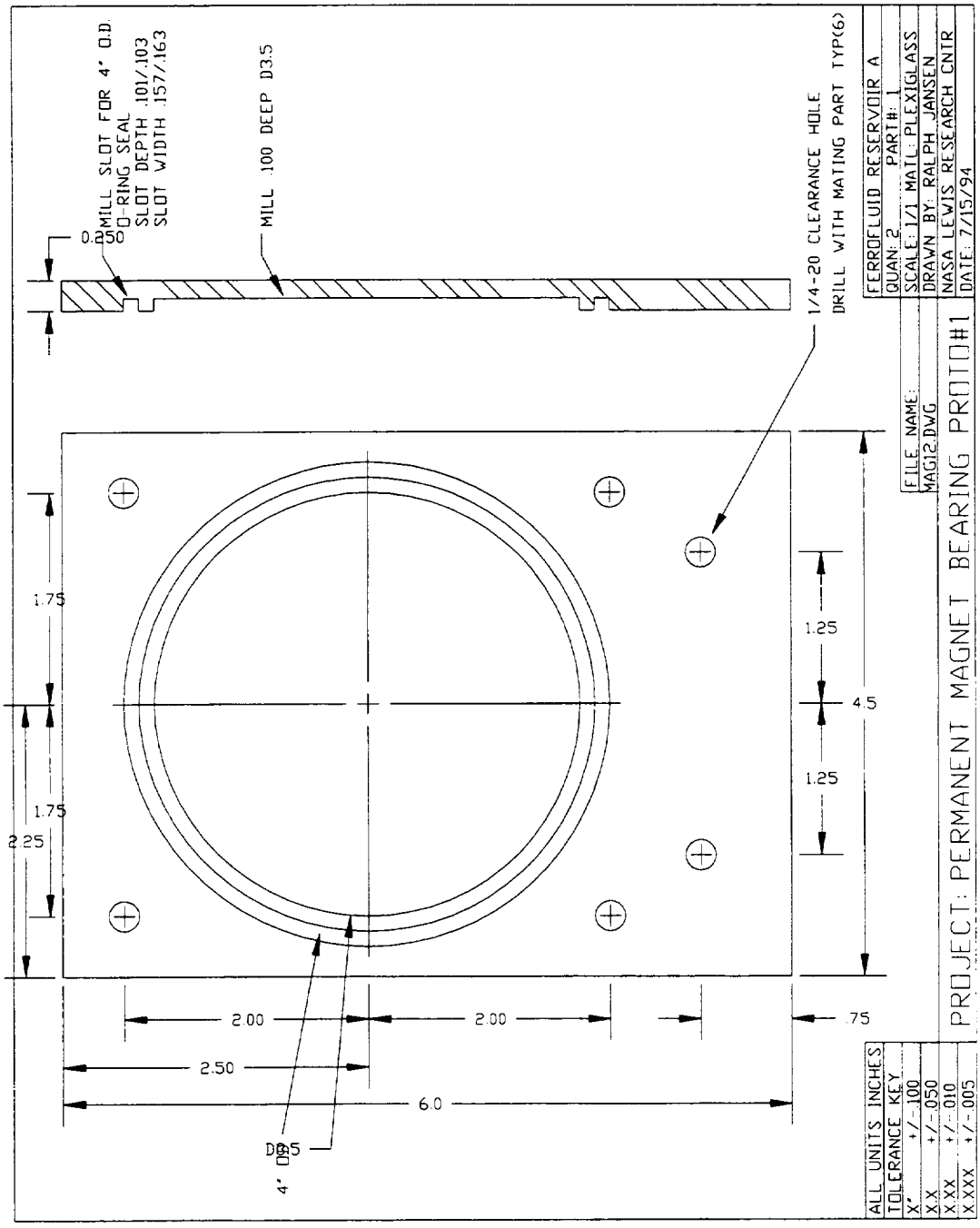

Figure C-2 - ferrofluid reservoir A

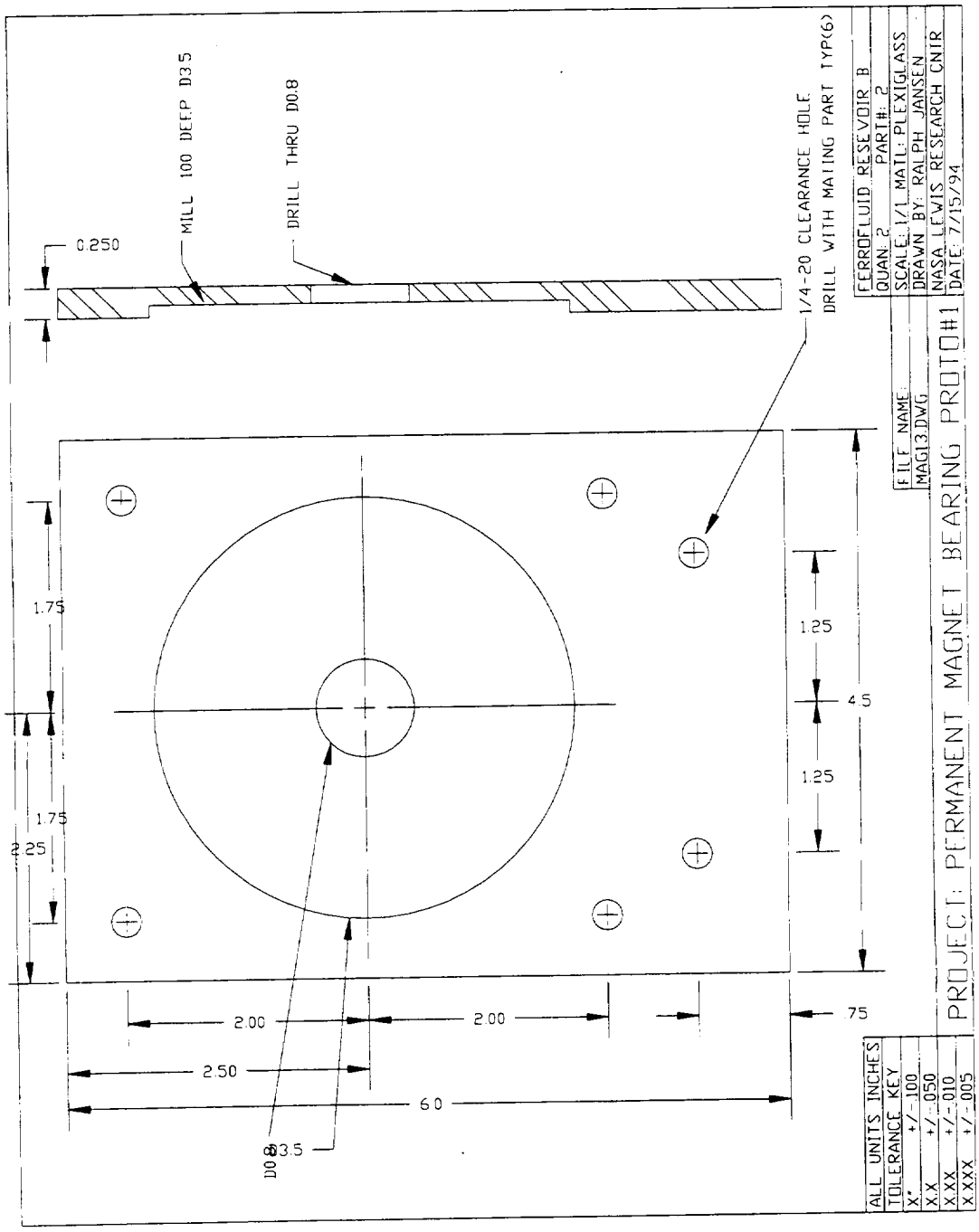

Figure C-3 - ferrofluid reservoir B

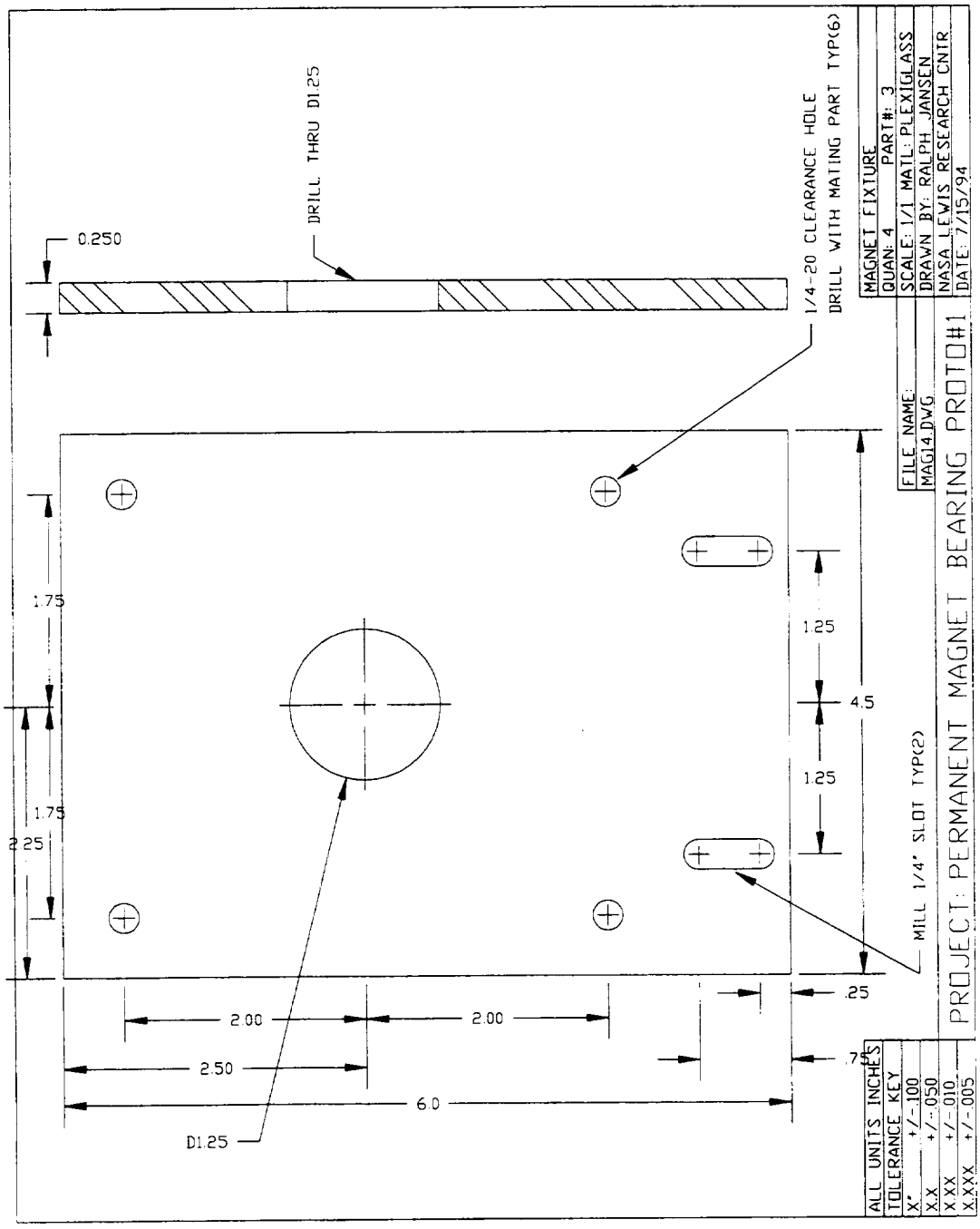

Figure C-4 - magnet fixture

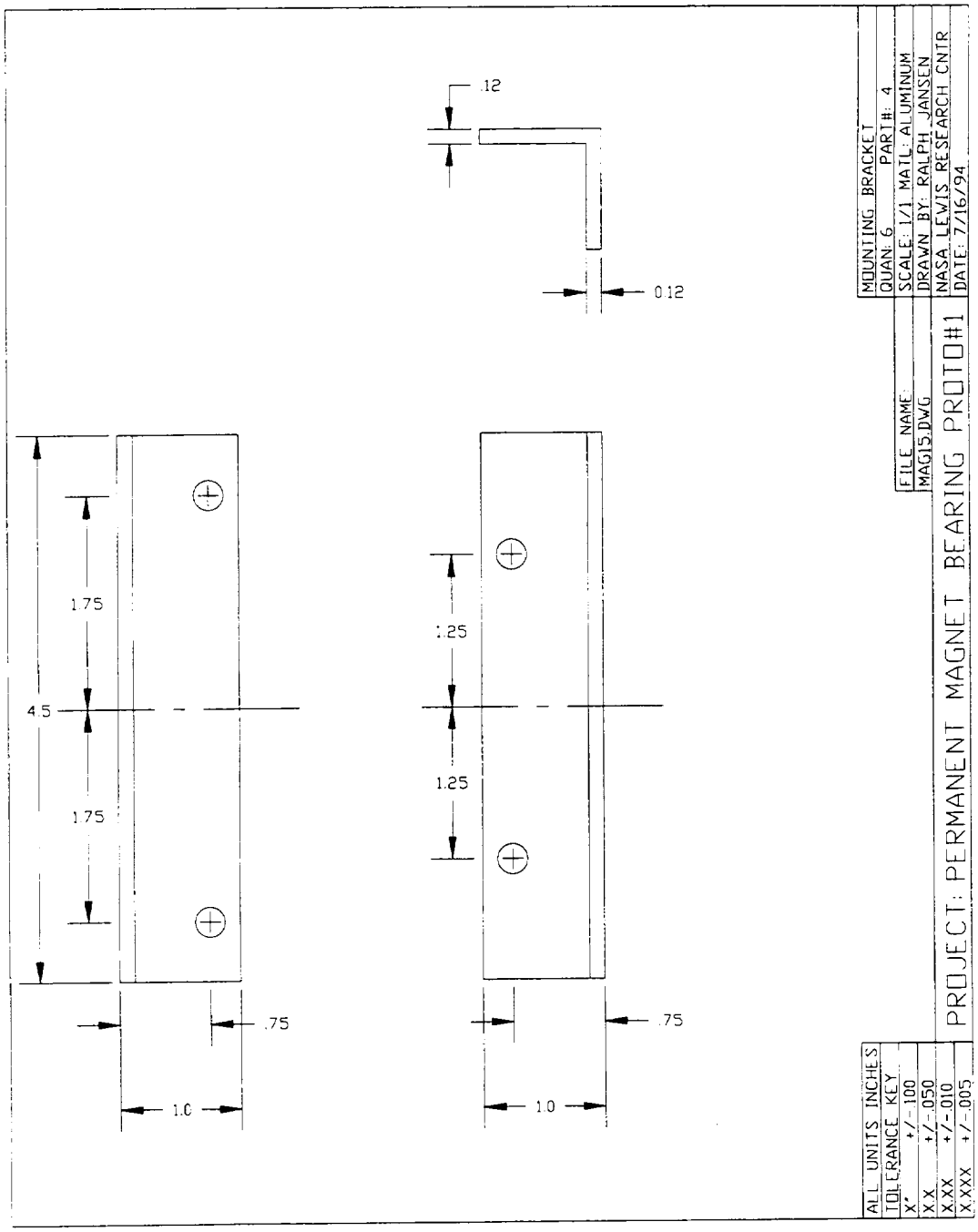

Figure C-5 - mounting bracket

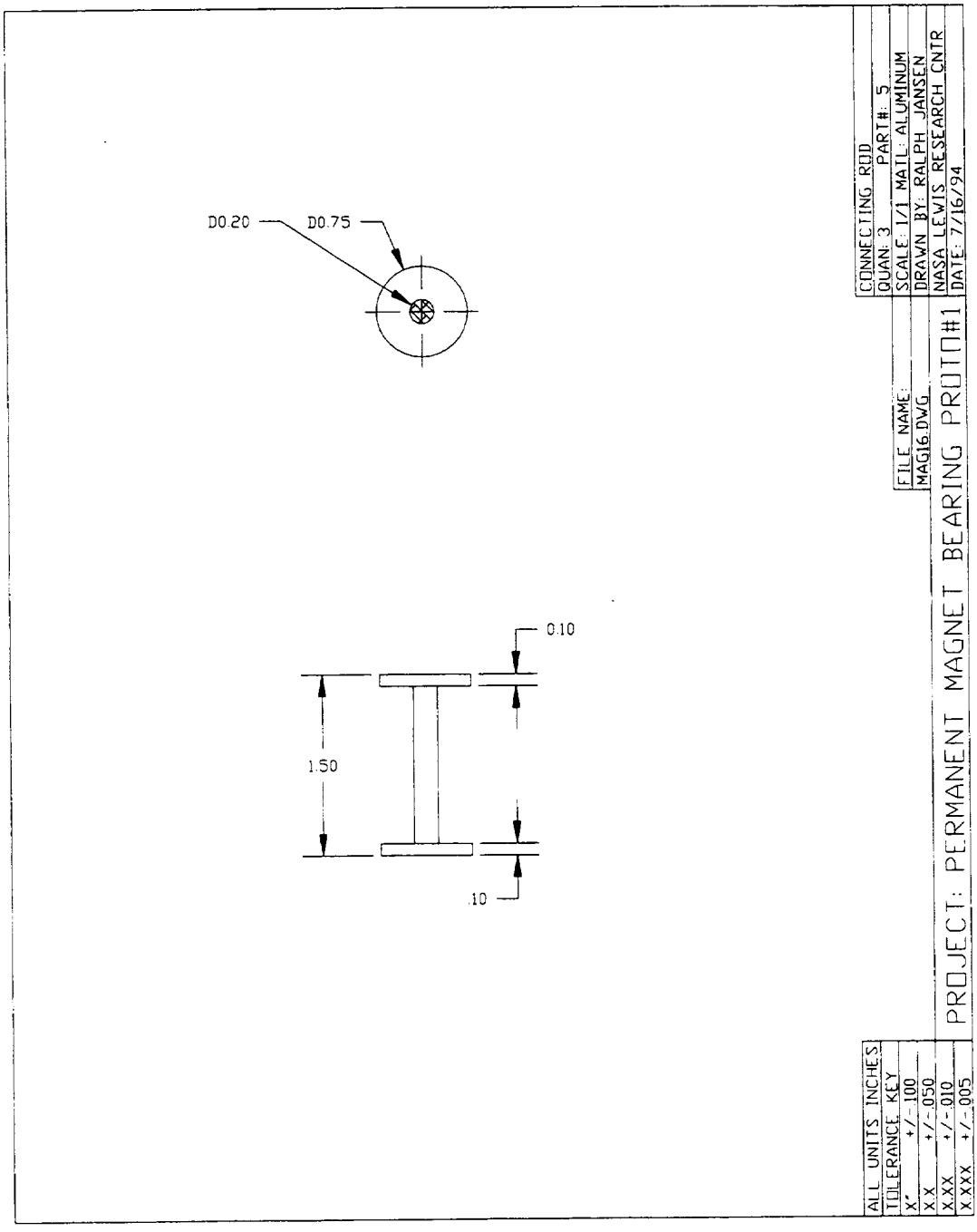

Figure C-6 - connecting rod

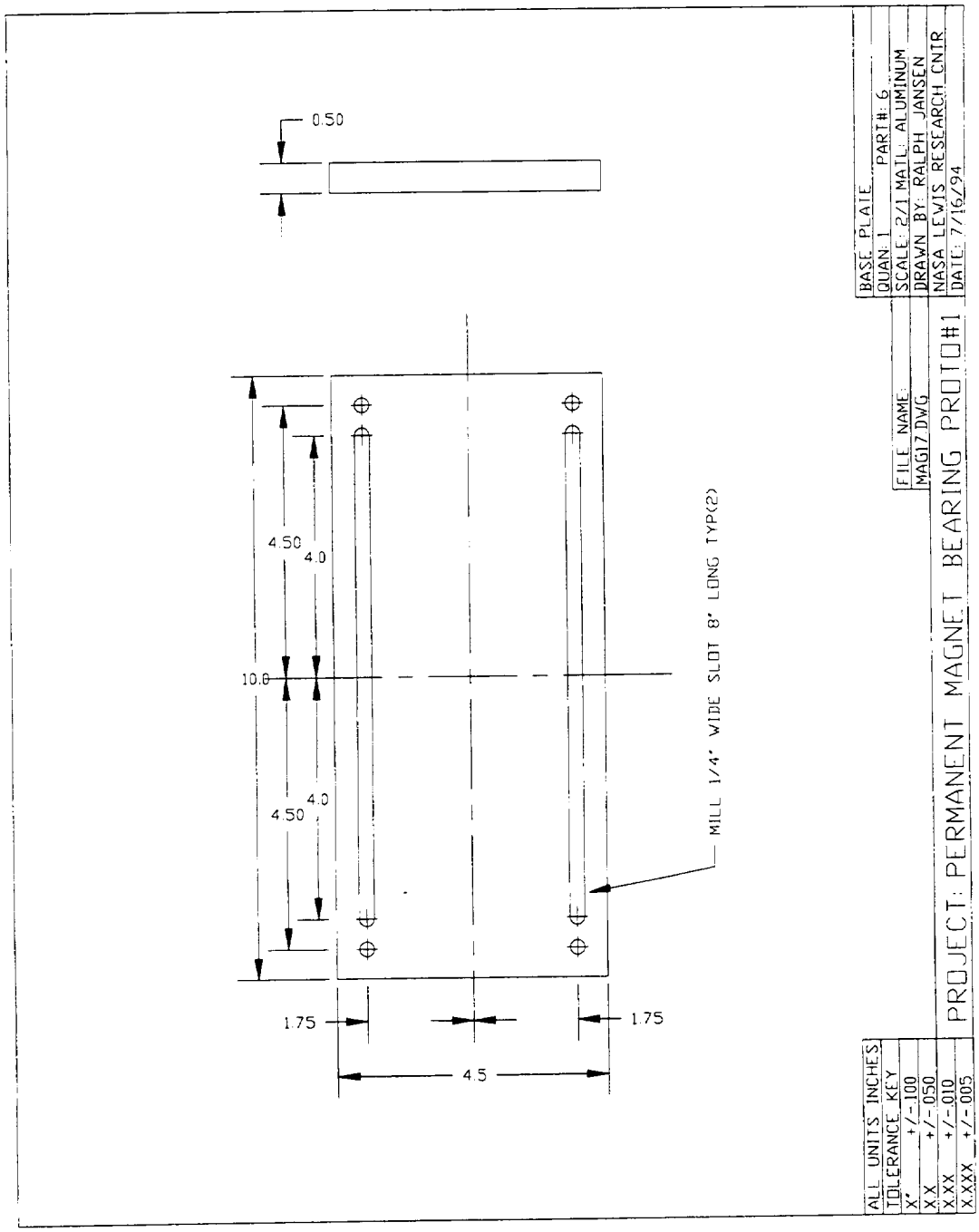

Figure C-7 - base plate

REPORT DOCUMENTATION PAGE

Form Approved
OMB No. 0704-0188

1. AGENCY USE ONLY (*Leave blank*)	2. REPORT DATE	3. REPORT TYPE AND DATES COVERED
	February 1996	Technical Memorandum

4. TITLE AND SUBTITLE
Passive Magnetic Bearing With Ferrofluid Stabilization

5. FUNDING NUMBERS
WU-505-63-5B

6. AUTHOR(S)
Ralph Jansen and Eliseo DiRusso

7. PERFORMING ORGANIZATION NAME(S) AND ADDRESS(ES)
National Aeronautics and Space Administration
Lewis Research Center
Cleveland, Ohio 44135-3191

8. PERFORMING ORGANIZATION REPORT NUMBER
E-10033

9. SPONSORING/MONITORING AGENCY NAME(S) AND ADDRESS(ES)
National Aeronautics and Space Administration
Washington, D.C. 20546-0001

10. SPONSORING/MONITORING AGENCY REPORT NUMBER
NASA TM-107154

11. SUPPLEMENTARY NOTES
Ralph Jansen, Ohio Aerospace Institute, 22800 Cedar Point Road, Brook Park, Ohio 44142 (work funded under NASA Cooperative Agreement NCC3-208); Eliseo DiRusso, NASA Lewis Research Center. This report was submitted by Ralph Jansen as a dissertation in partial fulfillment of the requirements for the degree Master of Science in Mechanical Engineering to Case Western Reserve University in 1995. Responsible person, Robert L. Fusaro, organization code 5230, (216) 433-6080

12a. DISTRIBUTION/AVAILABILITY STATEMENT
Unclassified - Unlimited
Subject Category 31

This publication is available from the NASA Center for Aerospace Information, (301) 621-0390.

12b. DISTRIBUTION CODE

13. ABSTRACT (*Maximum 200 words*)

A new class of magnetic bearings is shown to exist analytically and is demonstrated experimentally. The class of magnetic bearings utilize a ferrofluid/solid magnet interaction to stabilize the axial degree of freedom of a permanent magnet radial bearing. Twenty six permanent magnet bearing designs and twenty two ferrofluid stabilizer designs are evaluated. Two types of radial bearing designs are tested to determine their force and stiffness utilizing two methods. The first method is based on the use of frequency measurements to determine stiffness by utilizing an analytical model. The second method consisted of loading the system and measuring displacement in order to measure stiffness. Two ferrofluid stabilizers are tested and force displacement curves are measured. Two experimental test fixtures are designed and constructed in order to conduct the stiffness testing. Polynomial models of the data are generated and used to design the bearing prototype. The prototype was constructed and tested and shown to be stable. Further testing shows the possibility of using this technology for vibration isolation. The project successfully demonstrated the viability of the passive magnetic bearing with ferrofluid stabilization both experimentally and analytically.

14. SUBJECT TERMS
Magnetic bearing; Passive suspension; Ferrofluids

15. NUMBER OF PAGES
151

16. PRICE CODE
A08

17. SECURITY CLASSIFICATION OF REPORT	18. SECURITY CLASSIFICATION OF THIS PAGE	19. SECURITY CLASSIFICATION OF ABSTRACT	20. LIMITATION OF ABSTRACT
Unclassified	Unclassified	Unclassified	

National Aeronautics and
Space Administration

Lewis Research Center
21000 Brookpark Rd.
Cleveland, OH 44135-3191